POLYMER NETWORKS FOR THERMORESPONSIVE SHAPE STABILIZATION OF AN INORGANIC PHASE CHANGE MATERIAL

A Dissertation

by

PARVIN KARIMINEGHLANI

Submitted to the Office of Graduate and Professional Studies of
Texas A&M University
in partial fulfillment of the requirements for the degree of

DOCTOR OF PHILOSOPHY

Chair of Committee,	Svetlana A. Sukhishvili
Committee Members,	Terry Creasy
	Micah Green
	Jodie Lutkenhaus
Head of Department,	Ibrahim Karaman

August 2020

Major Subject: Materials Science and Engineering

ABSTRACT

Temperature responsive polymeric networks have been achieved for reversible shape stabilization of an inorganic salt hydrate phase change material (PCM). The unique feature of these networks is the capability to simultaneously provide shape stabilization of a liquid salt hydrate PCM at lower temperature, and to reversibly adjust its assembly strength in response to a temperature increase. Specifically, lithium nitrate tri-hydrate (LNH) as an inorganic ionic liquid (IL) and a high-latent-heat PCM was employed as a solvent for a neutral polymer, poly(vinyl alcohol), PVA. LNH solvent presents a water-salt medium with extremely high concentration of salt (~18 M).

Two distinct approaches for gelation − crosslinker-free and crosslinker-assisted − were explored. In the crosslinker-free case, addressing polymer solubility issues and understanding the nature of bonding that lead to gelation were the primary focus. In the second approach, gelation was facilitated by the addition of physical crosslinking molecules - poly (amidoamine) dendrimers. Strengthening of physical crosslinking in gels through dendrimers of various generations enhanced mechanical properties, enabled precise control of the gelation temperature, and afforded shapeable, self-healing materials. We showed that the activation energy for dissociation of dynamic crosslinks that are critical for self-healing was ≈130–140 kJ/mol, as determined by rheology and dynamic light scattering for different types of crosslinks (linear and branched). Finally, we aimed to understand correlations between gelation and solvation of polymer chains by studying dilute polymer solutions. Using Fourier transform infrared spectroscopy (FTIR),

fluorescence correlation spectroscopy (FCS) and viscometry, we showed that when LNH is used as a solvent instead of water, polymer chains are more expanded, less hydrated, and more permeable to a solvent. We argue that those features, taken together with binding of hydrated Li^+ ions to PVA chains revealed by ^7Li NMR spectroscopy, strongly contribute to distinct solubility and gelation properties of PVA in this inorganic IL. We believe that understanding solvation and ion-binding capability can offer crucial insights in designing polymer-based shape stabilization matrices for inorganic PCMs.

DEDICATION

I dedicate this dissertation to my family,

Reza – my husband and my love

For his unconditional support, love, and making me happy during hardships.

My mother and my father

For their absolute and beautiful love, endless support, and always encouraging.

&

Ryka – my beloved daughter

For coming to this world to bring joy to my life.

ACKNOWLEDGEMENTS

I am deeply grateful to my advisor, Dr. Svetlana Sukhishvili, for her motivation, guidance, and insightful feedback. Dr. Sukhishvili's ideas were integral to every phase of this dissertation and to the entire process leading up to it. She has taught me innumerable lessons and insights on my academic researches. Thanks to her, this journey was incredible experience for me.

I am thankful to my committee members, Drs. Creasy, Green, and Lutkenhaus for their guidance and support throughout the course of this research. I also thank Dr. Emily Pentzer for her time and feedback during my defense meeting.

I would like to thank Dr. Green again, and his student Smit Alkesh Shah for assisting us with setting up the rheological experiments at the early stage of this work. I also thank Dr. Patrick Shamberger from Texas A&M University for useful discussions during early stages of this project.

I would like to express my great appreciation to Dr.Yuhao Wang from Stevens Institute of Technology for his useful comments and help during labeling PVA experiments.

I thank Dr. Yan-Yan Hu and her student Jin Zheng, our collaborators from Florida State University, for their assistance in performing ^{7}Li NMR spectroscopy experiments.

I would especially like to thank Dr. Jack Douglas from National Institute of Standards and Technology for his useful comments and discussions.

Thanks also go to my friends, all lab members and colleagues and the department faculty and staff for making my time at Texas A&M University a great experience.

Finally, I would like to extend my heartfelt gratitude to my exceptional parents, and my supportive husband who always encouraged me throughout this long journey. This dissertation would not have been possible without their warm love and tremendous support.

CONTRIBUTORS AND FUNDING SOURCES

Contributors

This work was supervised by a dissertation committee consisting of Professor Svetlana Sukhishvili, as my chair, and Dr. Creasy of the Department of Materials Science and Engineering and Drs. Green and Lutkenhaus of the Department of Chemical Engineering.

The DSC data, shown in chapter 3, was provided by Emily Emmons of the Department of Materials Science and Engineering and were published in 2017. The dendrimer synthesis described in chapter 4 was conducted by Anbazhagan Palanisamy of the Department of Materials Science and Engineering and were published in 2018. ^{7}Li NMR spectroscopy results were performed by Jin Zheng of the Department of Chemistry and Biochemistry, Florida State University.

All other work conducted for the dissertation was completed by the student independently.

Funding Sources

This work was supported by TEES at Texas A&M University and in part by the NSF under Awards DMR-0906474 and DMR-1905535.

NOMENCLATURE

ATR-FTIR	Attenuated total reflection Fourier transform infrared spectroscopy
G_n (n=1,2,3)	Dendrimer, generation 1-3
D	Coefficient of transitional diffusion
DLS	Dynamic light scattering
DSC	Differential scanning calorimetry
DETA	Diethylenetriamine
E_a	Activation energy
FCS	Fluorescence correlation spectroscopy
FITC	Fluorescein isothiocyanate isomer I
G’	Storage modulus
G”	Loss modulus
GPC	Gel permeation chromatography
HIS	Inorganic hydrated salt
ICF	Intensity correlation function
IL	Ionic liquid
LND	Lithium nitrate tri-D_2O
LNH	Lithium nitrate trihydrate
^{7}Li NMR	^{7}Li nuclear magnetic resonance
PCM	Phase change material
PVA_{98}	Polyvinyl alcohol (98% hydrolyzed)

PVA_{87}	Polyvinyl alcohol (87% hydrolyzed)
PVA*	Fluorescently labeled PVA
R_H	Hydrodynamic radius
T_{gel}	Gelation temperature
WAXD	Wide-angle X-ray diffraction
γ_L	Linear viscoelastic regime

TABLE OF CONTENTS

Page

LIST OF FIGURES

Page

1. INTRODUCTION

With rising global energy crisis, the need for sustainable energy resources and the ways to minimize and recover wasted heat have been steadily increasing. Latent heat storage systems based on phase change materials (PCMs) present promising and inexpensive solutions in thermal energy storage applications.[1] By providing shape stabilization of liquid PCMs,[1-3] polymer gels and composites are beneficial in solar energy storage or waste heat recovery applications.[4] In contrast to organic PCMs, inorganic PCMs possess several advantages such as higher volumetric thermal storage density, good thermal conductivity, and low flammability.[5,6] However, one of the main drawbacks of inorganic PCMs, mostly salt hydrates, is leakage of low-viscosity PCMs within a heat-exchange module, leading to corrosion,[7,8] and resulting in high module replacement costs.[1,7-10]

Lithium nitrate trihydrate (LNH) – an inorganic ionic liquid (IL) –with a large specific heat of fusion of 287 ±7 J/g and a near-room temperature melting point (*i.e.* 30.1 °C), [11,12] is considered a promising PCM for energy storage applications. To overcome the leakage problem, we proposed designing a temperature-responsive polymer gel for shape stabilization of LNH. In contrast to chemically crosslinked matrices,[1,13-17] which are not designed to be easily replaceable with a new material, the temperature responsive polymeric networks can be constructed and deconstructed on-demand. A general schematic illustrating our main concept is shown in Figure 1-1.

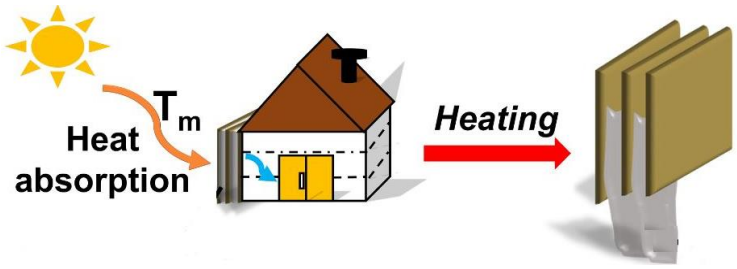

Figure 1-1. Schematic of a proposed application of a temperature-responsive polymer gel for reversible shape stabilization of PCMs. Reprinted from [10] with permission from the Royal Society of Chemistry.

This work explores two distinct approaches to designing thermoresponsive polymer networks, using crosslinker-free and crosslinker-assisted strategies. In both cases, we use a neutral polymer, poly (vinyl alcohol), PVA, which is commonly used in the preparation of hydrogels.[18-21] In the crosslinker-free case, we aimed to address polymer solubility issues and understand the nature of bonding that leads to gelation. The presence of high concentration of salt, *i.e.*~ 18 M, creates a strong competition for hydrating water between the ions and polymers and enables direct interaction of ions with functional groups of polymers.[22-24]

We first explore the crosslinker-free approach as the first step towards realization of PVA gelation in molten LNH. We found that unlike in water, PVA readily forms gels in LNH solutions, and that gelation does not require an extra step of cyclic freeze-thawing.[25-28] We focused on the mechanism by which salt environment affects the PVA gelation, which unlike polymer gelation in low salt

concentrations, [29-31] was rarely addressed in the literature. These results are presented in chapter 3 of this dissertation.

The second approach in this study was a crosslinker-based physical gelation for shape stabilization of LNH, with the goal of achieving tunable gelation temperature. In this step, gelation was facilitated by the addition of physical crosslinking molecules - poly (amidoamine) dendrimers. The cooperative hydrogen bonding between *–OH* groups of PVA and amino groups of dendrimers enhanced mechanical properties, enabled precise control of the gelation temperature through varying dendrimer generation number, and afforded shapeable, self-healing materials. This new category of gels, which formed in the molten salt as a solvent, was introduced as "salogels". We explored how the use of molten LNH as a solvent could support formation of physically cross-linked PVA network using dendrimers of various generations. Thermal behavior of PCM salogels and durability of the network over multiple heating/cooling cycles was also explored. These results are described in chapter 4.

In chapter 5, dissociation energy of dynamic bonds in phase change salogels was explored using rheology and dynamic light scattering (DLS). Both linear and branched types of amine-terminated molecules were used as hydrogen bond-forming crosslinkers. While rheology can give us good information about macroscopic relaxation time of the transient network[32-39], DLS can probe mobility of polymer clusters at the length scales comparable to q^{-1}, where q is the scattering vector.[40] A correlation has been demonstrated between stress relaxation shear modulus and the intensity correlation function (ICF) of the scattered light.[41-43] Additionally, the effect of crosslinker geometry (linear *vs*. branched)

on both the gelation temperature (T_{gel}) and the crosslinker-to-polymer ratio at which the gelation occurs, was explored.

The fact that PVA formed gel in a molten salt hydrate solution but not in the aqueous solution with the same concentration prompted a deeper fundamental study of interactions of PVA chains with LNH solvent. Understanding binding of lithium ions to polymer chain in dilute solutions and the resulting changes in the polymer chain conformation are the topics of chapter 6. Diffusion and expansion of PVA chains of different molecular weights in LNH were studied using fluorescence correlation spectroscopy (FCS). The molecular weight dependences of the diffusion coefficients of the fluorescently tagged polymer, as well as PVA overlap concentration (c*) were explored in LNH and compared to water. We argue that decreased hydration of the PVA chains in LNH as compared to that in water, as well as polymer chains solvation *via* binding of Li^+ ions as revealed by ^7Li NMR spectroscopy, both strongly contribute to distinct solubility and gelation properties of PVA chains in this inorganic IL. Understanding solvation and ion-binding capability can offer crucial insights in designing polymer-based shape stabilization matrices for inorganic PCMs.

2. MATERIALS AND METHODS

2.1. Materials

Anhydrous lithium nitrate (purity > 99%) and PVA (Mw 88-97 kg mol^{-1}, hydrolysis percentages 98% and 87%) were purchased from Alfa Aesar and used as received. For dendrimer synthesis, methanol, toluene, ethylene diamine, and methyl methacrylate were also purchased from Alfa Aesar and distilled prior to use. Dimethylformamide (DMF) used for gel permeation chromatography (GPC), deuterated chloroform ($CDCl_3$) used for ^1H NMR analysis, and deuterium oxide (D_2O) with 99.9 atom% D used for FTIR sample preparation were received from Sigma Aldrich.

The following materials were specifically used in chapter 6 experiments: Butanol, dimethyl sulfoxide (DMSO), and triethylamine were purchased from Alfa Aesar and used as received. The four PVA samples with the hydrolysis degree of 99% were synthesized using a previously described procedure.[44] Gel permeation chromatography (GPC) traces for the PVA samples are shown in Figure D-1. The molecular weights and PDIs are shown in Table 2-1. Fluorescein isothiocyanate isomer I (FITC) and dibutyltin dilaurate were obtained from Sigma Aldrich and used without further purification.

Table 2-1. Characteristics of PVA samples

Sample	M_w (g/mol)	PDI
PVA1	29,500	1.2
PVA2	69,700	1.39
PVA3	107,000	1.62
PVA4	135,200	1.54

2.2. Preparation of crosslinker-free PVA/LNH gels

Anhydrous lithium nitrate was mixed with stoichiometric amounts of deionized water to prepare LNH (56 wt%). Due to the highly hygroscopic nature of LNH, all chemicals were prepared and weighed in sealed vials under dry nitrogen atmosphere. Prior to adding PVA_{98}, LNH was heated above its melting temperature to create a homogenous liquid. As reported in the literature,[11] dynamic viscosity of liquid LNH is 5.34s mPa·s at 35 °C. Although this value is about 7-fold larger than viscosity of water at the same temperature, liquid LNH is still highly fluid at these temperatures. Anhydrous PVA_{98} was then added to liquid LNH to create 6, 10, and 15 wt% polymer concentrations in LNH. After adding PVA_{98} to liquid LNH, the solution was heated to 80 °C and subjected to slow stirring for 24 hours in a sealed container to promote homogeneity. The samples were then allowed to cool down to room temperature. Indeed, when PVA_{98}/LNH (15 wt%) mixtures were heated to ~ 80 °C and then slowly cooled down to 25 °C, clear gels were formed.

2.3. Preparation of physically crosslinked PVA/LNH gels

2.3.1. Dendrimer synthesis

Poly(amidoamine) dendrimers were synthesized *via* a two-step process involving exhaustive Michael addition and amidation reaction starting from ethylene diamine core as described elsewhere.[45] Methyl methacrylate and ethylene diamine were used alternatively in alkylation and amidation steps. The completion of the reaction was monitored by GPC performed with DMF solutions of the dendrimers, as well as by ^1H NMR spectroscopy of the reaction mixtures in $CDCl_3$. Briefly, to synthesize dendrimers

of the first, second and third generations (G1, G2 and G3, respectively), methanol solutions of ethylene diamine and methyl methacrylate were first allowed to react at 0 °C for 1 hr, and the reaction was then continued at room temperature for predetermined time intervals that were varied depending on dendrimer generation (3, 5 and 7 days for G1, G2 and G3 dendrimers, respectively). All reactions were conducted in argon inert atmosphere. Upon completion of the reactions, the solvent and excess of reagents were removed by azeotropic distillation in the presence of toluene at 40 °C using a rotary vacuum evaporator. The dendrimers were then dried overnight under vacuum and used for further experiments.

2.3.2. Preparation of gels

5 wt% PVA_{98} solutions in LNH were prepared by adding PVA_{98} powder to liquid LNH at 40 ^{o}C, followed by heating the mixture to 80 ^{o}C to complete dissolution. Gelation was induced by a simple addition of a small amount of dendrimer (a minimum of 0.75 wt% in the case of G3 dendrimer) to a PVA_{98}/LNH solution to achieve a total of 5 wt% of PVA_{98} in the system. For studies of the effect of dendrimer generation on PVA_{98} gelation, two sets of samples were prepared, in which G1, G2 or G3 were added either at matched overall molar concentrations of dendrimers or at concentrations required to achieve equal amount of $–NH_2$ groups in the systems. In addition, in order to explore tunability of the gelation temperature through varying the amount of G3 crosslinker, PVA_{98} gels were prepared with different concentrations of G3 (0.6, 0.75, 1, 1.5, 2, 2.5, 3, 7 and 10 wt%). The systems were stirred at 70 ^{o}C for 3 hours to ensure homogenous mixing of PVA_{98},

LNH, and dendrimer crosslinkers, and cooled down to the ambient temperature to induce gelation.

2.4. Fluorescent labeling of PVA

PVA was labeled with FITC by using the modified method of de Belder and Granath.[46] First, 150 mg of PVA were dissolved in 4 mL of DMSO by stirring and heating at 70 ^{o}C. Then, trimethylamine (25 µL), dibutyltin dilaurate (10 mg) and FITC (25 mg) were added consecutively to the polymer solution. The solution was stirred for 2 h at 95 ^{o}C to complete the reaction and purified from the unreacted dye by repeated precipitation in butanol. Fluorescently labeled PVA (PVA*) was then dried in the oven at 80 ^{o}C, dissolved in water and further purified from the unreacted FITC by extensive dialysis against water in a 5 L container for about a month. The water was refreshed daily during the first week, and then every 3 to 4 days. The external and internal solutions were periodically analyzed for the presence of free FITC, and the dialysis was terminated when no free fluorescent labels were detected in the internal or external solutions using FCS. The degree of labeling was determined by measuring the fluorescent intensities of 1 mg/ml PVA* aqueous solutions and comparing them against a calibration curve obtained with aqueous solutions of FITC of known concentrations (Figure D-2). This analysis yielded the labeling degree of approximately one label per 45 monomer units for PVA* of all molecular weights.

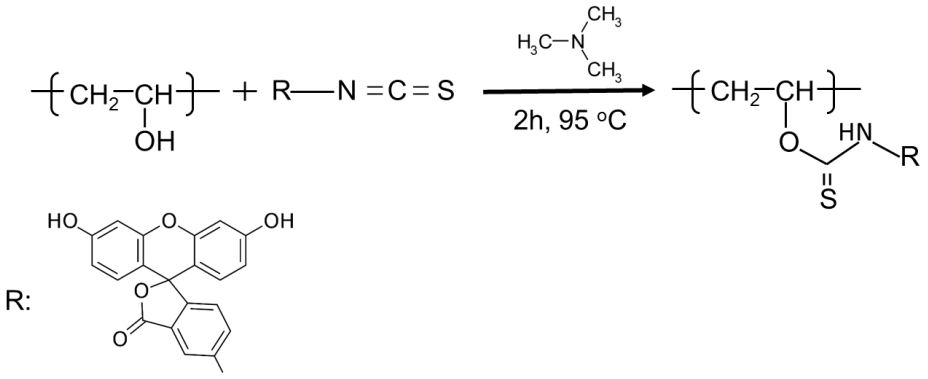

Figure 2-1. PVA labeling reaction.

2.5. Characterization methods

Attenuated total reflection Fourier transform infrared spectroscopy (ATR-FTIR). ATR−FTIR measurements were performed using a Nicolet 380 FTIR spectrometer, equipped with a single-reflection diamond ATR attachment. D_2O was used instead of H_2O in all systems to provide a spectroscopic window that enables the observation of vibrational bands associated with stretching vibrations of $-OH$ groups of PVA. Spectra were collected in the 400−4000 cm^{-1} range with a 4 cm^{-1} resolution using 64 scans. Deconvolution was performed by Origin 8.5 software assuming Gaussian band shapes and keeping the peak position fixed at the values previously reported in the literature.[47-49]

Thermal analysis. The melting temperatures and heat of fusion of PVA-based gels were determined by Differential scanning calorimetry (DSC) using a TA Instruments Q2000. Measurements were conducted at a 10 °C min^{-1} temperature ramp under nitrogen gas

purging at a flow rate of 50 ml min^{-1}. DSC samples were prepared by putting 10-20 mg of salogels into Tzero aluminium pans that were hermetically sealed prior to measurements.

Wide-angle X-ray diffraction (WAXD). The sample was placed in the sample holder of a two circle goniometer, enclosed in a radiation safety enclosure. The X-ray source was a 1 kW Cu X-ray tube, maintained at an operating current of 40 kV and 25 mA. The X-ray optics was the standard Bragg-Brentano para-focusing mode with the X-ray diverging from a DS slit (1 mm) at the tube to strike the sample and then converging at a position-sensitive X-ray detector (Lynx-Eye, Bruker-AXS). The two-circle 218-mm diameter goniometer was computer controlled with independent stepper motors and optical encoders for the θ and 2θ circles with the smallest angular step size of 0.0001^o 2θ.

Dynamic light scattering (DLS). DLS experiments were conducted with PVA/LNH gel in 12 mm × 12 mm cuvettes using a custom-made instrument. The laser light with the wavelength of 532 nm and the scattering angle was 90^o. The temperature was controlled by customizable Peltier-based temperature-controlled cuvette holder with four optical ports (Luma 40TM, Quantum Northwest). The tempeture control accuracy was ±0.2 °C. The sol–gel transition temperature was determined by performing sequential measurements in the temperature range between 55 °C and 19 °C starting from the highest temperature and allowing 20 minutes equilibration at each temperature. Hydrodynamic size measurements were also carried out by DLS. To that end, PVA/H2O and PVA/LNH mixtures at four different concentrations of 0.5, 0.75, 1 and 1.5 wt% were tested at 23 °C.

Rheological measurements. Rheological measurements were performed using an Anton Paar stress-controlled rheometer (MCR 301) equipped with a Peltier stage that enabled controlling the temperature within ±0.5 °C. All measurements, including viscosity measurements of high viscosity solutions, were performed using a parallel plate with a 50 mm diameter and the gap of 1 mm. For low viscosity solutions, the viscosity was measured using a double-gap geometry. The system was equipped with a solvent trap to prevent sample dehydration during measurements. To determine limits of the linear viscoelastic regime (γ_L), oscillation amplitude sweep tests were conducted at 25 °C within a strain range of 0.1-100 % using a frequency of 10 rad s^{-1}. For the temperature sweep experiments, the samples were equilibrated at 55 ^oC for 10 minutes to remove a prior thermal history before cooling down to lower temperatures. Chapter 5 measurements were performed by a TA rheometer (DHR-2) using a cone and plate geometry (cone angle = 2^o, diameter = 40 mm).

^{1}H-NMR, GPC and Mass spectroscopy. Dendrimers were characterized using ^{1}H-NMR (Varian Mercury 300 MHz), GPC and electrospray ionization mass spectrometry (EIS-MS, Thermo Scientific LCQ-DECA). Agilent GPC equipped with two liner Styragel HR 4 columns at a flow rate of 0.2 mL min^{-1} and a temperature of 30 ^oC was used for GPC characterizations. The formation of full generation dendrimers by amidation reaction was confirmed by the disappearance of ester signal around 3.6 ppm in the ^{1}H-NMR spectra.[50] G1, G2 and G3 dendrimers contained 4, 8 and 16 amino groups, were 1.5, 2.2 and 2.9 nm

in diameter, respectively,[51,52] and had polydispersities of 1.09, 1.15 and 1.08, as measured by GPC in this work. The molecular weights of G1, G2 and G3 dendrimers determined using a positive-ion-mode ESI-MS technique were 517, 1756 and 3831 g mol^{-1}. These values are within <10% deviation from the theoretical molecular weights of 572, 1598 and 3705 g mol^{-1} for these dendrimers, respectively.[51,53]

Fluorescence correlation spectroscopy (FCS). FCS experiments were conducted using a custom-made setup which includes a World Star Tech laser, TECBL-488. A 488-nm beam was reflected from a mirror after filtering with Thorlabs NE10B and passing through an attenuator. Upon reflection, laser irradiated the back aperture of an Olympus 60× oil immersion objective, N.A. 1.45 to reach to the sample. The emission was collected after filtering with a Semlock 474/25 narrow-band filter and sent to an Excelitas SPCM-AQRH-14-FC photon detection counting module. A custom-made glass cell was used to hold sample solutions. Time fluctuations of intensity were collected for 30 minutes for each sample, and results were averaged over three repeated measurements. In FCS, diffusion coefficients of the fluorescently-labeled molecules are determined from the intensity correlation function (ICF), which is defined as:[54,55]

$$G(\tau) = \frac{\langle \delta I(t) \quad \delta I(t+\tau) \rangle}{\langle I(t) \rangle^2} \tag{2-1}$$

where τ is the decay time, and $\delta I(t) = I(t) - \langle I \rangle_t$ where $\langle I \rangle_t$ is the time-averaged intensity. In the case of translational diffusion of monodispersed fluorescent species, the ICF is related with the diffusion coefficient through the following equation:[56]

$$G(t) = \frac{1}{N}\left(1+\frac{4Dt}{\omega_{xy}^2}\right)^{-1}\left(1+\frac{4Dt}{\omega_z^2}\right)^{-1/2} \quad (2\text{-}2)$$

where ω_{xy} and ω_z are the radii of the laser excitation volume in xy and z directions, *N* is the average number of fluorescent particles in the excitation volume and *D* is the coefficient of transitional diffusion. Calibration of the FCS setup was performed by measuring the diffusion time of a fluorescent dye with known *D*. FITC dye with *D* ~ 425-490 $\mu m^2/s$ at 22 ^oC [57-58] for calibration gave a beam waist (ω_{xy}) of 0.323 μm (Figure D-3).

^{7}Li Nuclear Magnetic Resonance (NMR) Spectroscopy. ^{7}Li NMR experiments were acquired at room temperature (22 ^oC) on a Bruker Avance III spectrometer at a field of 11.7 T with the ^{7}Li Larmor frequency of 194.4 MHz. The 90° pulse length was 2 μs. The recycling delay was 10 s. ^{7}Li chemical shift was referenced to 1M LiCl at 0 ppm. Spectra were processed and analyzed using Topspin 4.0.5.

3. A TEMPERATURE-RESPONSIVE POLY (VINYL ALCOHOL) GEL FOR CONTROLLING FLUIDITY OF AN INORGANIC PHASE CHANGE MATERIAL[1]

3.1. Introduction

With the developing global energy crisis, the search for sustainable energy resources and ways to minimize and recover waste heat become increasingly important. Latent heat storage systems based on phase change materials (PCMs) present an attractive way of storing solar thermal energy or recovering industrial waste heat. In order to be used in efficient and practical energy storage devices, PCMs generally require a high heat storage density and a narrow temperature range for the phase transition (typically melting and freezing).[4,59]

Several inorganic hydrated salts (IHSs) meet these requirements.[4,60-62] In particular, lithium nitrate trihydrate (LNH), with a large specific heat of fusion of 287 ±7 J/g and a near-room temperature melting point (*i.e.* 30.1 °C) is considered a promising PCM for a number of energy storage and thermal management applications. However, as a PCM, LNH also suffers from fairly large volume change upon melting/freezing ($\Delta V/V$ ~ 10%) and high fluidity after melting that may lead to redistribution within a heat exchanger module.[7,60-62] Therefore, shape stabilization of inorganic PCMs could offer significant practical advantages.

---

[1] Reprinted with permission from "A temperature-responsive poly (vinyl alcohol) gel for controlling fluidity of an inorganic phase change material" by Parvin Karimineghlani, Emily Emmons, Micah Green, Patrick Shamberger, and Svetlana A. Sukhishvili, 2017 Journal of Materials Chemistry A, 5, 12474-12482, Copyright 2017 by Royal Society of Chemistry.

Incorporating PCMs inside 3D networks has recently been explored to overcome the leakage of PCM during phase transition and protect it from the environment.[13,63,64] Several types of materials, such as a silica matrix[4,15,17,65-67] or polymers,[1,13,64] including block copolymers[13,14] have been used for thickening and shape stabilization of PCMs. While these materials provide shape stabilization, and in some cases such as a silica gel matrix, also increase thermal conductivity of organic PCMs,[66] they are not designed to be environmentally responsive, easily fillable and removable from a used PCM device in order to be replaced with a new material. To allow for such a material property, a new functionality should be introduced in the material, which enables on-demand construction and destruction of 3D matrices for PCMs. This work presents the first step towards realization of such a function in an inorganic PCM.

Specifically, we explore the use of a physical polymeric gel as a temperature-responsive matrix for LNH. Similar to other matrices for PCMs, such a gel should incorporate LNH salt during melting and crystallization, prevent leakage of melted LNH and protect it from the environment. However, in contrast to other PCM matrices, the gel should be easily filled in a heat-exchange module, reversibly decomposed in order for a PCM to be removed by heating and replaced with a new material after the PCM becomes unusable.

The realization of such a behavior with polymer gels in high-salt aqueous environments is challenging. Most known polymer systems form physical gels in water upon an increase rather than a decrease in temperature. One well-known example of this category is the systems in which sol-gel transitions correlate with

their lower critical solution temperature (LCST).[68,69] However, the presence of high concentration of salt, *i.e.*~ 55 wt% calculated for polymer-free LNH, drastically changes the temperature response of aqueous polymer systems.[70] In particular, several reports describe the loss gelation if the inorganic salt content is high.[71-73] The strong effect of inorganic ions on polymer gelation stems from competition between ions and polymers for water in the hydration shell and/or direct interaction of ions with functional groups of polymers, among other factors.[22-24] For example, salt-induced dehydration and precipitation of polymer chains included in the micellar coronae suppress-polymer gelation which is driven by the formation of micellar networks. In this extreme salinity explored in this work, a competition for hydration water occurs between salt ions and polymer chain, resulting in a dramatic effect of salt on the polymer solubility and gelation. This work addresses, to our knowledge for the first time, the temperature-responsive gelation of polymers in high-salinity environment of inorganic PCMs.

Here, we focus on poly (vinyl alcohol) (PVA) - a nontoxic, biocompatible polymer which is commonly used in the preparation of hydrogels.[18-21] Given that PVA is prepared from the polymerization of vinyl acetate, the final product possesses a portion of hydrophobic acetate groups. Hydrolysis percent determines the extent of -*OH* groups in the PVA backbone. In its highly hydrolyzed form, water prevents formation of physical gels even at high concentration of the polymer, and an additional step of cyclic freeze-thaw process is required to produce strong PVA gels.[27,28] By this method, PVA gels are formed through water-crystallization-

enhanced intermolecular hydrogen bonding between PVA chains which is further strengthened by the PVA micro crystalline domains.[25,26]

In this study, temperature-responsive gelation of PVA in hydrated salt is explored. Salt-induced polymer gelation has been extensively studied in other systems[29-31] but never in the extreme salinity environment provided by LNH. We explore expansion of PVA chains in LNH solutions, gelation and the sol-gel transition in this system, and focus on the mechanism by which salt environment affects the formation and temperature-triggered destruction of the PVA physical network.

3.2. Results and Discussion

3.2.1. Gel formation

Figure 3-1a shows that while PVA_{98} aqueous solutions (15 wt%) easily flowed at 25 °C, PVA_{98}/LNH samples gelled. While the melting temperature of LNH is 31 °C, no crystallization of salt is observed in LNH solution (Figure 3-1a, right) because of the supercooling effect (crystallization temperature normally observed with LNH salt in the absence of nucleating agent is ~ -10 °C). Indeed, when PVA_{98}/LNH (15 wt%) mixtures were heated to ~ 80 °C and then slowly cooled down to 25 °C, clear gels were formed. Rheological experiments were performed to better understand the behavior of PVA_{98} in aqueous and LNH media. Prior to oscillatory shear experiments, the strain sweep at a frequency of 10 rad/s was carried out to determine the linear viscoelastic regime. The maximum value of strain at which the storage modulus remains independent of the strain rate was determined as γ_L and kept constant for all further experiments. The strain sweep

data are presented in Figure A-1. Figure 3-1b shows the oscillation shear measurements for PVA_{98}/H_2O and PVA_{98}/LNH systems. The logarithmic plots of dynamic storage modulus (G') and loss modulus (G") as a function of angular frequency are shown in Figure 3-1b. PVA_{98} aqueous solutions at 25 °C demonstrate predominantly liquid-like behavior with G" exceeding G' over the whole range of frequencies. In contrast, PVA_{98}/LNH system exhibits larger and closer values of G' and G". The proximity of G' and G" indicates that the gel is close to the sol-gel transition temperature.[74]

We then aimed to explore the effect of polymer concentration and the hydrolysis percentage of PVA on gelation of PVA/LNH solutions. Figure 3-2a shows the oscillatory shear results for PVA_{98}/LNH system containing 6, 10 and 15 wt% of the polymer. It is seen that at PVA_{98} concentrations below 10 wt%, the system exhibited liquid-like behavior (G" > G'). In the concentration range between 10 and 15 wt% of PVA, the PVA/LNH system showed a crossover between G' and G" over the frequency sweep which is characteristic of viscoelastic fluid. Starting from 15 wt% of PVA_{98} in LNH at room temperature, the polymer gelation occurred as indicated by the absence of flow of the materials using the tilting method (Figure 3-1a, right). Previously, physical gels of PVA were reported for aqueous solutions only when the intermolecular hydrogen bonding between *–OH* groups of PVA and crystallization of PVA were enhanced by the freeze-thaw technique.[25] Additional insights into the role of *-OH* functional groups in the PVA gel formation were obtained in the experiments with varied degree of hydrolysis. Figure 3-2b shows that PVA_{98}/LNH and PVA_{87}/LNH systems containing 15 wt% of PVA exhibited significant differences in rheological behavior. While PVA_{98}/LNH system

becomes more elastic at higher frequencies, PVA_{87}/LNH samples remain viscous, with G" exceeding G' over the whole frequency range. In addition, values of G' were higher in the PVA_{98}/LNH system than those in PVA_{87}/LNH system. These results are consistent with our initial hypothesis that -*OH* functional groups play a major role in the gelation of PVA, and an increase in the density of –*OH* groups within a polymer chain increases the probability of the gel formation.

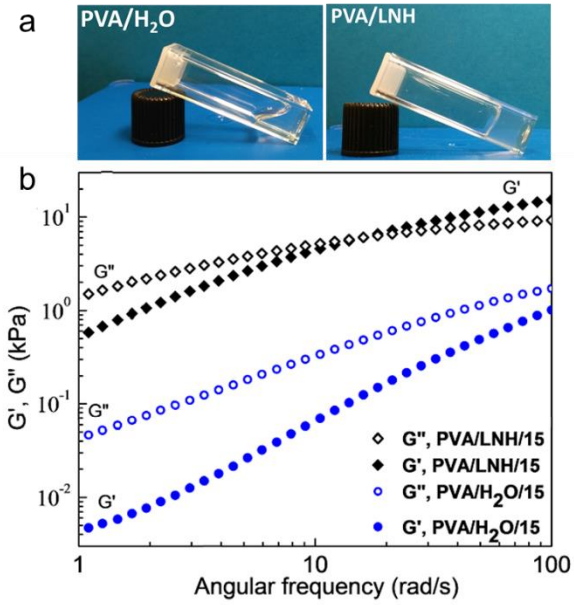

Figure 3-1. (a) Photographs of 15 wt% PVA_{98} solutions in H_2O and LNH; (b) and frequency dependence of G' and G" in the PVA_{98}/H_2O and PVA_{98}/LNH systems (15 wt%) at 25°C. The measurement was performed at γ_L = 5%. Reprinted from [10] with permission from the Royal Society of Chemistry.

Figure 3-2b additionally shows that complex viscosity decreased with frequency for both PVA/LNH samples, indicating non-Newtonian and shear thinning behavior. The complex viscosity substantially decreases with the frequency, reflecting structural

breakdown at higher angular frequencies. Importantly, for more hydrolyzed PVA, both the magnitude and the slope of the complex viscosity during shear thinning experiments were higher than that for less hydrolyzed PVA, indicating formation of a stronger physical network in the former case. While a similar trend was reported for viscosity of PVA of varied hydrolysis degrees in aqueous solution,[75] this work provides first insights on gelation of PVA in LNH as a solvent.

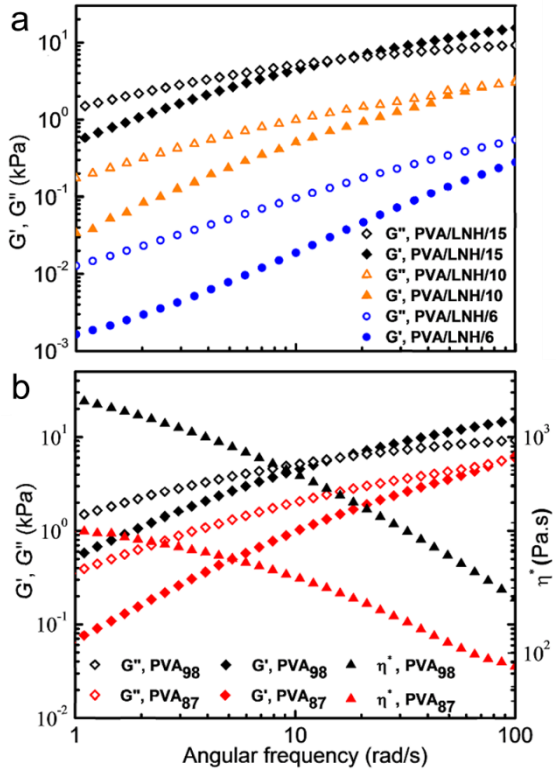

Figure 3-2. Frequency dependencies of G' and G" in (a) PVA_{98} /LNH system at selected polymer concentrations, and in (b) PVA_{98}/LNH and PVA_{87}/LNH systems containing 15% wt% of PVA of varied degrees of hydrolysis, with $\eta^*(\omega)$ also shown on the second axis. Temperature was 25 °C. The measurement was performed at γ_L = 1%. The data for additional polymer concentrations are shown in Figure A-2. Reprinted from [10] with permission from the Royal Society of Chemistry.

3.2.2. Effect of LNH on PVA hydrodynamic size

It has been reported experimentally that the onset of physical gelation concentration for polymeric gels correlates with the overlap concentration of polymer in the solvent.[76,77] Therefore, we aimed to determine the overlap concentration in solutions of PVA in LNH and compare these data with those measured in aqueous solutions of the polymer. These experiments have been performed with PVA_{98} dissolved at varied concentrations in LNH and water. In order to find C^*, the viscosity of polymer solutions was measured using double gap and parallel plate geometries when used with low- and high-viscosity solutions, respectively. A log-log plot of specific viscosity *versus* PVA_{98} concentration (Figure 3-3a) clearly exhibits two regions with slopes of 1.5 and 3.5 that are in good agreement with those reported for aqueous solutions of a different polymer, *i.e.* polyacrylamide-butyl methacrylate copolymer.[78] The cross-section of the linear curves indicates the transition between dilute and semi-dilute solution, *i.e.* the onset of the polymer chain overlap (C^*).[79] The value of C^* was significantly lower for PVA_{98} in LNH than in water (1.25 wt% vs. 2.5 wt%, respectively), indicating a significant expansion of PVA_{98} chains in LNH as compared to water which has been reported to be a good solvent for highly hydrolyzed PVA_{98}.[80] DLS data conducted with PVA_{98} concentrations lower than C^* (Figure 3-3b) confirm PVA chain expansion in the presence of salt. The hydrodynamic diameter of PVA_{98} coils in water was ~ 20 nm, which is in good agreement with the value previously reported for PVA of similar molecular weight.[81] An increase of hydrodynamic diameter of PVA coils to ~ 30 nm occurred in LNH solutions.

Expansion of PVA chains in LNH could be explained by coordination of lithium ions with PVA –*OH* groups that was reported earlier.[82-84] If one assumes such a scenario, chain expansion is analogous to the well-known salting-in effect, *i.e.*, an increase of polymer solubility in the presence of salts.[85] Further evidence of Li^+ ion complex formation with –*OH* groups will be discussed later in this manuscript.

Taken together, these results show that LNH is a better solvent than water for PVA chains. The LNH-induced chain expansion can contribute to an enhanced gelation of PVA in LNH solutions observed at high PVA concentrations.

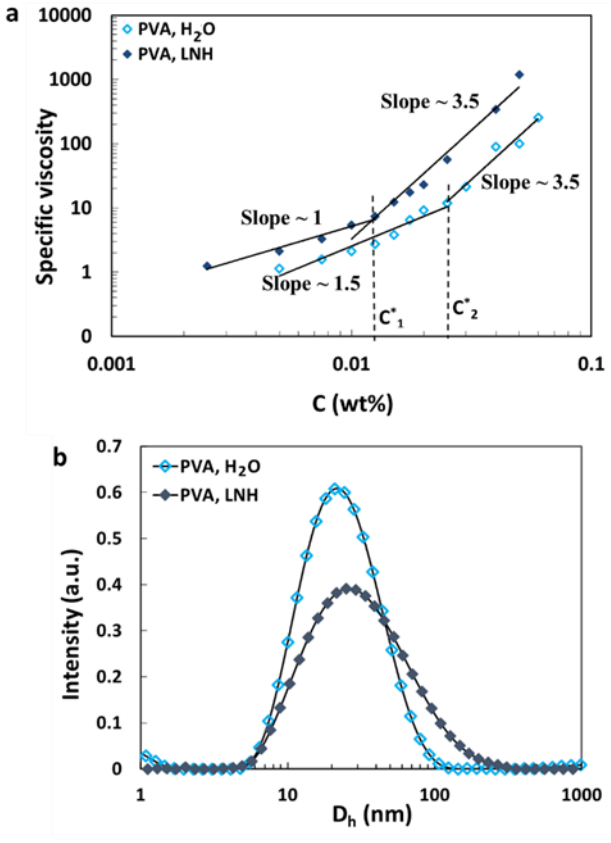

Figure 3-3. (a) Specific viscosity in PVA_{98}/LNH solutions as a function of PVA concentration; (b) hydrodynamic diameter as determined by DLS in dilute solutions of PVA_{98} (0.5, 0.75, and 1 wt%) in LNH and water at 23 °C. Reprinted from [10] with permission from the Royal Society of Chemistry.

3.2.3. Gelation mechanism

ATR-FTIR spectroscopy was applied to probe the effect of a hydrated salt solvent on the PVA chains interactions at the molecular level. To avoid spectral overlap of vibrational modes of hydroxyl groups of PVA with those of water, D_2O rather than H_2O was used in these studies. PVA_{98} solutions (15 wt%) were prepared using D_2O and lithium nitrate tri-deuterium (LND) at three different D_2O-to-LND mass ratios of 23/1, 4/1, and 1.5/1.

Figure 3-4a shows infrared spectra of PVA_{98} dissolved in D_2O/LND mixtures of varied composition. A broad peak at 3000-3600 cm^{-1} occurs due to the stretching vibrations of -*OH* groups of PVA, while the one at 2000-2800 cm^{-1} is associated with the -*OD* stretching and bending vibrations of D_2O. In the spectrum of LND, a strong vibration band occurs at 1328 cm^{-1} due to antisymmetric stretching vibrations of nitrate ions.[86,87] The spectral position of this band is not significantly affected by the addition of PVA. The most pronounced trend observed in the series of these experiments is that with a gradual increase of the content of LND, the peak associated with -*OH* stretching vibration in PVA is shifted to higher values. This shift was obvious in the 3000-3600 cm^{-1} range (Figure 3-4a, inset). When comparing the absorption peaks for PVA dissolved in D_2O and LND, a large shift of 40 cm^{-1} of the -*OH* band of PVA was observed (Figure 3-4b). This shift is likely due to disruption of hydrogen bonding between -*OH* band of PVA and water molecules in the polymer hydration shell.[88] In the case of solvent-free PVA, a similar blue shift in the -*OH* stretching vibrational band was observed as a result of binding of Li^+ ions

with lone electron pair of oxygen in -*OH* groups in PVA.[83] In our system, the -*OH* groups of PVA are hydrogen-bonded with D_2O in the hydration shell, exhibiting a band at 3390 cm^{-1}. Upon gradual addition of LND, a competition for the scarce amount of water between LND and PVA chains occurs, resulting in significant dehydration of PVA chains, disruption of hydrogen bonds with water and the corresponding blue shift of PVA's –*OH* stretching vibrational band to 3430 cm^{-1} (Figure 3-4b). An increase in the asymmetry of the -*OH* absorption band in LND-rich solutions might be due to residual hydration of PVA chains.

Figure 3-4c,d show enlarged spectral features in the 2000-2800 cm-1 D_2O vibrational region. Spectral deconvolution using Origin 8.5 software was applied in this region; Gaussian band shapes were assumed. The peak positions were fixed at 2395, 2479 and 2587 cm^{-1} corresponding to bending (δ), symmetric (ν_1) and non-symmetric (ν_2) stretching vibrations in D_2O, respectively.[2] The positions and the relative intensities (symmetry) of contributing D_2O bands drastically differed for D_2O and LND solutions. The presence of PVA in either D_2O or LND did not significantly affect the vibrational spectra of D_2O. However, lithium nitrate drastically changed vibrational features of D_2O as a result of onset of D_2O binding with lithium nitrate species. These interactions caused a remarkable changes in asymmetry of the D_2O vibrational band and a shift of a ν_1 stretching vibrational frequency of -*OD* groups from 2497 to 2505 cm^{-1}. Taken together, the above results suggest that the mechanism of PVA gelation in LNH can be due to a combined effect of dehydration of PVA chains and lithium ion coordination. Unlike its

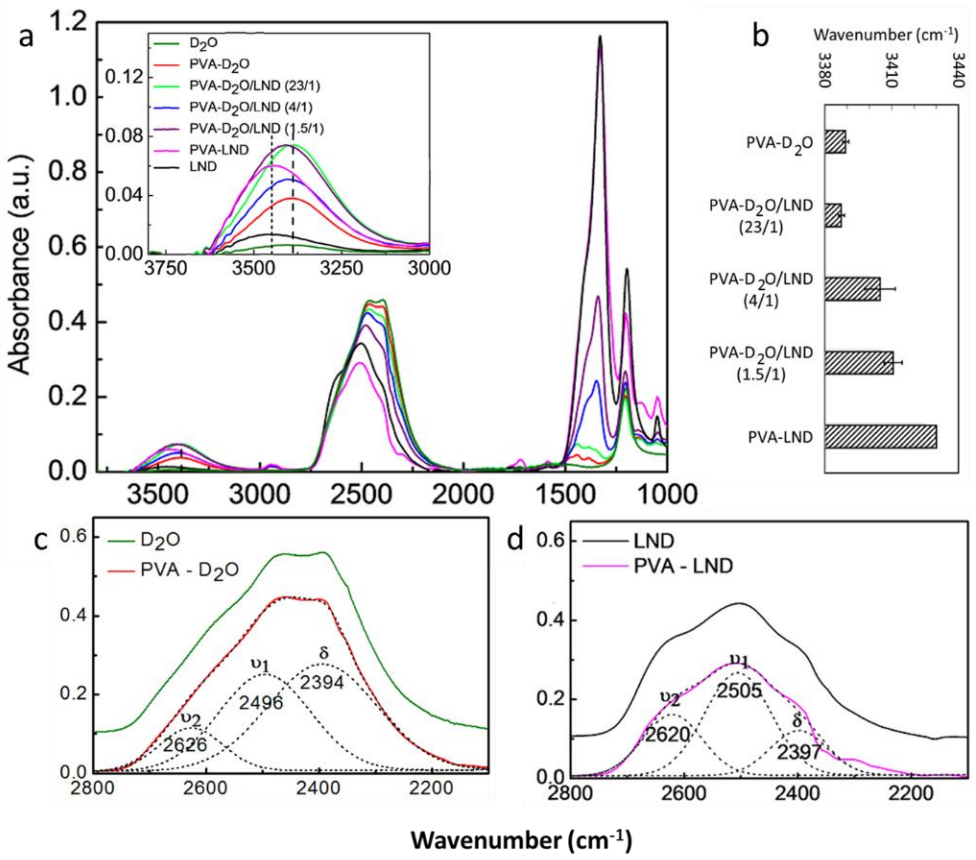

Figure 3-4. (a) ATR-FTIR spectra of 15 wt% PVA_{98} in D_2O, LND and their mixtures. Inset shows changes in the *–OH* region of PVA; (b) Wavenumber of the maximum of the *–OH* vibrational band of PVA in various solvents (c), (d) Enlarged -*OD* vibrational region of PVA_{98} in D_2O and LND, respectively. Reprinted from [10] with permission from the Royal Society of Chemistry.

aqueous solution, dehydrated PVA is capable of forming intermolecular hydrogen bonds.[89] In addition, Li^+ ion is capable of coordinating with four *–OH* groups[90] and therefore can bridge between PVA chains. Figure 3-5 summarizes the proposed mechanism for PVA gelation in LNH.

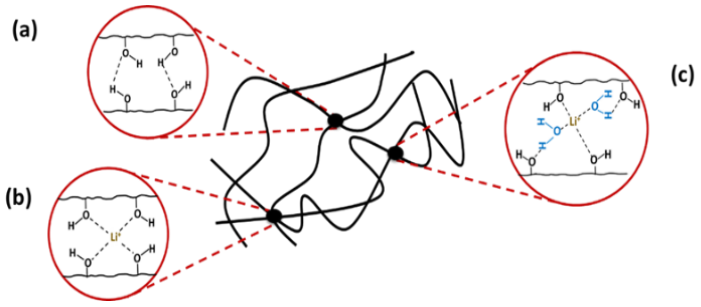

Figure 3-5. Schematic illustration of gelation in PVA/LNH system that involves PVA intermolecular association through hydrogen bonding between -*OH* groups (a), coordination of Li^+ ions with PVA's -*OH* groups without or with the involvement of water molecules (b and c, respectively). Reprinted from [10] with permission from the Royal Society of Chemistry.

3.2.4. Gelation as a function of temperature

Temperature is expected to affect the secondary molecular interactions by modulating the strength of intermolecular interactions. To test the hypothesis that gelation of PVA is primarily driven by the hydrogen bonding between hydroxyl groups of PVA, we aimed to explore temperature dependence of PVA_{98} gelation in LNH. To that end, we have employed rheological and DLS techniques which have been widely used to monitor the viscoelastic and chains dynamic properties during sol-gel transition, respectively.[91-95] These techniques have obvious advantages over the tube tilting method [74,96-98] as they are capable of probing macro-, micro- and molecular-scale, structural and dynamic events that accompany sol-gel transitions.

Figure 3-5a shows oscillation shear measurements performed with PVA_{98}/LNH gels over the temperature range of 10 to 30 °C in a heating-to-cooling thermal cycle. Upon

heating to temperatures above 25 °C, the storage modulus (G') became smaller than the loss modulus (G"), indicating a liquid-like state. A hysteresis of about 3 °C was observed upon cooling, and the crossover between G' and G" occurred at ~ 20 °C, indicating the sol-gel transition.[98-102] Note that the simple tilting technique gave a similar transition temperature of 21 ± 1 °C (Figure 3-5a, inset).

While rheological experiments unravel the "macroscopic" gel point, DLS probes gelation at a microscopic level. The use of DLS to determine the gelation points is based on the fact that gelation substantially affects dynamics of system. During gelation, fractal-like hierarchical structures can form and transitional diffusion of clusters can be suppressed, affecting the shape of the intensity correlation function (ICF) (where τ is the decay time and q is the wave vector).[93] Specifically, a transition from exponential to power law ICF is correlated with the onset of gelation.[93] In the sol phase, fast diffusion of clusters gives rise to the exponential form of ICF (Eq.3-1):[93-95]

$$\boldsymbol{S(q,\tau) \approx A \exp(-\tau/\tau_c) + B} \tag{3-1}$$

where A is the amplitude of correlation function, and B and τ_c are the intercept and characteristic decay time of the correlation function, respectively. However, in the gel state, the following power law function with no characteristic decay time describes dynamics of the system:[94]

$$\boldsymbol{S(q,\tau) \approx \tau^{-(1-u)}} \tag{3-2}$$

where u is the fractal dimension of ICF.

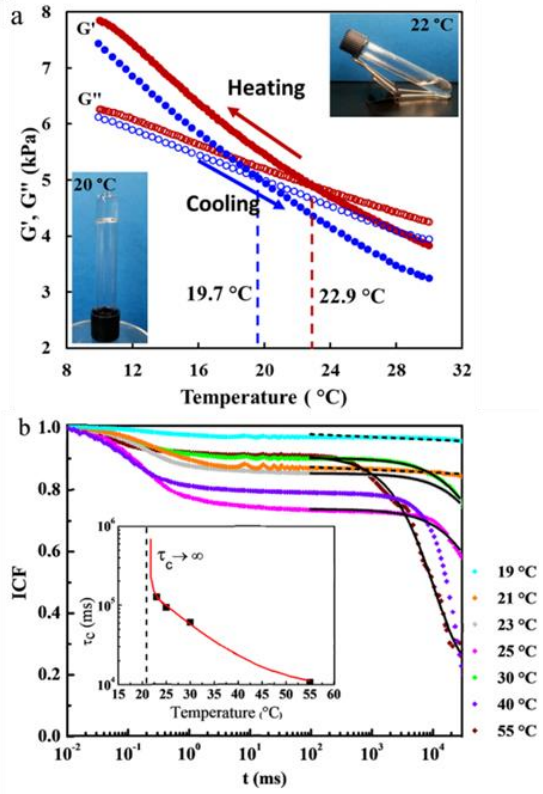

Figure 3-6. (a) Temperature-dependent G′ and G” of PVA_{98}/LNH gel measured at an angular frequency of 10 rad/s, γ_L= 10%, and a heating-cooling rate of ±1 °C/min. Images show PVA_{98}/LNH (15 wt% of polymer) system above and below the gel transition temperature. (b) Temperature-dependent ICFs of PVA_{98}/LNH gels measured by DLS during gelation process at the scattering angle of 90°. Inset shows the characteristic decay time of the slow mode *versus* temperature. Reprinted from [10] with permission from the Royal Society of Chemistry.

In order to obtain the microscopic sol-gel transition temperature for PVA_{98}/LNH gels, DLS measurements have been performed at varied temperatures when the sample was gradually cooled from 55 °C. Figure 3-5b shows that both slow and fast relaxation modes are seen in the data. The fast mode corresponding to the β relaxation, *i.e.* side group and other localized motions of PVA chains, were observed at temperatures between 21 and 55 °C. The slow mode (α relaxation), which corresponds to motions of the entire

polymer chain,[103] was analyzed to determine the sol-gel transition temperature. The characteristic decay time (τ_c) calculated after fitting the data with Eq. 1, increased at lower temperatures diverging to infinity at about 20 °C (inset in Figure 3-5b). The fact that the data could be well fitted with the exponential function (Eq. 1) at all temperatures exceeding 21 °C, and with the power law function at 21 and 19 °C was used to determine the sol-gel transition temperature of 20 ± 1 °C. This value is in good agreement with the gelation point of ~20 °C determined by rheology (Figure 3-5a). Similar agreement between these two techniques in determining the gelation temperature was found in other systems.[95,104] Thus, in this system, the gelation point is slightly below the equilibrium melting point of pure LNH (30.1 °C).

3.2.5. Stability of PVA/LNH gel

Finally, we have assessed PVA/LNH gels from the standpoint of LNH performance during multiple cycles of heating/cooling. Figure 3-6 shows the DSC analysis to study thermal stability of PVA/LNH gels during phase change transition in the temperature range of (-30 to 50) °C. While large undercooling (about 35 °C) occurs in both systems with comparable ΔT, we did not aim to reduce its magnitude by adding inorganic nucleators,[5] but rather aimed to explore thermal stability of PVA gels. Importantly, the melting and crystallization temperatures were highly reproducible during 10 cycles of melting/crystallization of LNH salt. A decrease in the LNH latent heat from 287 J/g for polymer-free LNH to 215 J/g for LNH entrapped within 15 wt% PVA matrix comprises a 25% reduction. Such an effect cannot be explained solely by the contribution

of the weight of PVA to the PVA/LNH sample, and is likely to contain contributions from binding of Li^+ ions and water molecules to *–OH* groups on PVA backbone. Association of Li^+ ions with PVA also resulted in broadening of melting transition and lowering the T_m of LNH. These processes could also interfere with crystallization of the inorganic hydrated salt. This kind of reduction has been previously observed for hydrated salts incorporated inside silica composites.[63] Figure 3-7 demonstrates the LNH salt melting with and without any polymeric matrix. The melting process was tracked at different times on a hot plate

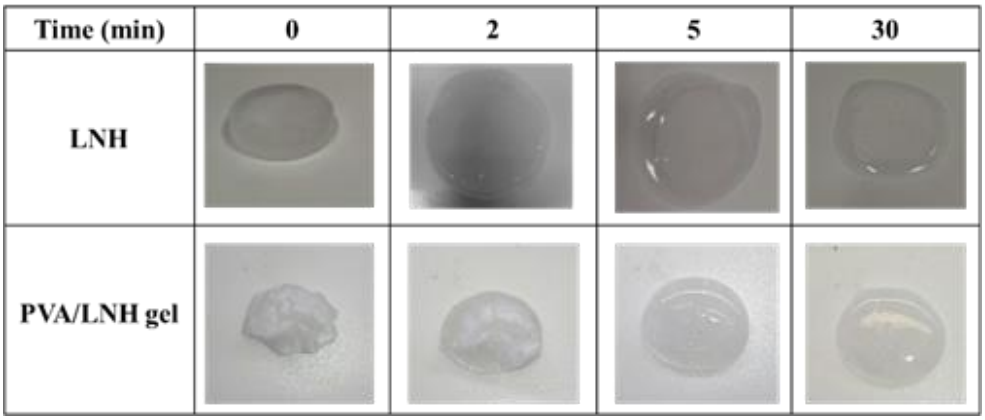

Figure 3-7. Melting behavior of LNH and PVA/LNH gel (15 wt% of polymer) on the heater kept at 35 °C. Images were taken during melting process at different time scales. Reprinted from [10] with permission from the Royal Society of Chemistry.

keeping at 35 °C. Figure 3-7 clearly shows that LNH was melted after 30 min and it totally became liquid and LNH spreads onto the hot plate surface. However, PVA networks are highly viscous at this temperature and obviously the polymer matrix could inhibit salt

fluidity after melting and no water leakage was observed around the gels. This means that PVA/LNH gel keeps good form-stable performance. The complex viscosity of this gel also was measured during LNH melting (Figure A-3). It was shown that at 50 °C, the gel vsicosity is about 300 Pa.s which is ~ 75,000 times of LNH viscosity reported at this temperature (3.96 mPa.s).[11] It is important to note that in the PVA/LNH system, the observed gelation point of ~ 20 °C falls near the onset of melting of the system (20.5 °C). Thus, this point represents a transition from a metastable liquid to a metastable gel.

3.3. Conclusion

We have demonstrated that PVA is a promising thermoreversible matrix for shape stabilization of an inorganic PCM. LNH was found to be a good solvent for PVA chains, which resulted in polymer chain expansion. Moreover, the solvent induced dramatic dehydration of PVA chains, promoting PVA gelation due to direct hydrogen bonding between hydroxyl groups of PVA and/or additional Li^+ ion-induced crosslinking between PVA chains. DLS and rheology consistently indicated the occurrence of sol-gel transition in this system, and DSC showed high robustness of salt phase transitions in the PVA-LNH shape-stabilizing matrix during repetitive heating-cooling cycles. This study is the first step towards designing efficient temperature-controlled matrices for high-heat-storage-density inorganic phase change materials.

4. SELF-HEALING PHASE CHANGE SALOGELS WITH TUNABLE GELATION TEMPERATURE[2]

4.1. Introduction

Hydrogels[105-107] and organogels[108,109] are important classes of soft materials that entrap large amounts of water and organic solvents, respectively, whose tunable mechanical properties make them attractive for a variety of applications. In contrast, this work is focused on a new category of gels, salogels, which include fluid inorganic salt hydrates as the solvent. In general, gelation occurs when super-molecular networks are formed as a result of either physical or chemical interactions. Contrary to chemically crosslinked gels, which have permanent networks of irreversible chemical bonds,[110] physical gels can reconfigure through dissociation of prior and formation of new secondary bonds. Various secondary interactions such as van der Waals, hydrophobic, hydrogen bonding, Columbic, and dipole-dipole can act individually or jointly to form physical networks.[105] Reversibility of the secondary bonds provides an important property of physical gels to self-heal the damaged areas.[111] Moreover, in certain cases non-covalent crosslinks can be formed and dissociated on demand in response to external stimuli such as temperature,[112] ionic strength,[113] pH,[114] solvent type,[115] or light.[116] As reconfigurable

[2] Reprinted with permission from "Self-healing phase change salogels with tunable gelation temperature" by Parvin Karimineghlani, Anbazhagan Palanisamy, and Svetlana A. Sukhishvili, 2018. ACS Applied Materials & Interfaces, 10, 14786-14795, Copyright 2018 by American Chemical Society.

materials, physical gels find applications in tissue engineering, drug delivery and sensing.[117,118]

Polymer gels and composites are also beneficial in solar energy storage or industrial waste heat recovery applications, where they provide shape stabilization of phase change materials (PCMs) [1,3,13] above their melting point.[4] In these cases, polymers are exposed to a medium quite different from that in hydrogels, *i.e.* instead of water, they are dissolved in organic (often liquid paraffin)[119] or inorganic (typically in inorganic salt hydrates) solvents.[10] In comparison to their organic counterparts, inorganic PCMs possess higher volumetric thermal storage density, good thermal conductivity, and low flammability.[5,6] Lithium nitrate trihydrate (LNH) is one of the most promising types of inorganic phase change materials. Specifically, LNH's low melting point of 30.1 °C and high volumetric latent heat storage capacity (≈ 400 $MJ \cdot m^{-3}$) which is twice as high as that of organic PCMs (128-200 $MJ \cdot m^{-3}$),[11,12] make this inorganic PCM a promising candidate for the use in energy storage and thermal management systems, especially as compact thermal buffers in the aerospace applications. [11,120,121] However, the use of inorganic PCMs, including LNH, in heat-exchange device applications is largely aggravated by leakage of highly fluid molten salt hydrates from the heat exchanger modules, leading to corrosion[1] and high maintenance costs. [1,7-10] Specifically, viscosity of molten LNH is ~ 5 mPa·s at 35 ^{o}C, which is only 7-fold higher than that of water at the same temperature. To overcome the leakage problem, several types of inorganic matrices[15-17] and polymer networks[1,13,14,122] have been developed. However, these permanently crosslinked materials

do not enable easy replacement of used PCMs within heat exchange modules, specifically in those designed to have a small gap (<1 mm) in between thermally conductive fins.

In a recent paper, we introduced the use of temperature-responsive polymer network as a thermo-reversible decomposable matrix for shape stabilization of LNH.[10] The network was formed by polyvinyl alcohol (PVA) dissolved at high polymer concentrations in LNH (≥ 15 wt%). However, the previously reported gels exhibited a relatively low gel-sol transition temperature (20 ^{o}C) that was below LNH melting point (30.1 °C) and were weak, *i.e.* did not possess sufficient mechanical strength to maintain their shape when liquid LNH was trapped within these matrices.[11] In this study, we report on a new type of salogels with shapeable and self-healing capabilities with the precise control of the gelation temperature achieved by the use of amine-terminated dendrimers as versatile physical crosslinkers. Self-healing capability of PCM is desired since it provides easy curing of possible defects in a PCM material confined within the heat-exchange device and thus improves the PCM life cycle. This problem is specifically relevant for LNH that suffers from a fairly large volume change upon melting/freezing ($\Delta V/V \sim 10\%$) and prone to the subsequent damage caused by the induced strains. [27-28, 123] We found that the use of molten LNH as a solvent provides a unique environment that obstructs hydration of PVA chains and favors hydrogen bonding between polymer chains and the crosslinkers. The cooperative hydrogen bonding between *–OH* groups of PVA and amino groups of dendrimers yielded strong yet reversible binding of crosslinkers with the polymer network. As a result, salogels were able to maintain their macroscopic shape, but at the same time exhibited robust self-healing behavior and could be reversibly

decomposed by an increase in temperature. Most importantly, we demonstrated that the gel-sol transition temperature can be precisely tuned within a range between 35 and 62 °C by controlling the crosslinker binding energy and density enabled through selection of different generations and concentrations of dendrimers. To our knowledge, this is the first report of self-healing physical gels with highly controlled gelation temperature formed in the high salinity (17.3 M of $LiNO_3$) environment.

4.2. Results and Discussion

4.2.1. PVA/dendrimer gelation in a liquid salt hydrate

A series of physically crosslinked PVA gels can be prepared by a facile addition of a certain amount of dendrimers (G1, G2, or G3, Figure 4-1a) to a PVA solution in LNH by mixing at 70 ^{o}C for 3 hrs. Figure 4-1b illustrates that the procedure resulted in the formation of robust gels with strong capability of holding the liquid salt hydrate. These gels are reminiscent of much better known hydrogels[106,107] and organogels,[124,125] but retain the liquid salt hydrate rather than water or organic solvents. LNH is composed of 56 wt% of inorganic ions, which supply extremely high (~17.3 M) concentration of inorganic ions in water. In such a high-salinity environment, solvation water is scarce, and solubility and gelation of polymers will be largely determined by interaction of salt with polymer chains and polymer-salt competition for the hydration water. We then were seeking to better understand the solvation state of PVA chains in LNH as an unusual solvent, and relate the overlap of the polymer chain with the formation of PVA/dendrimer/LNH salogels. While

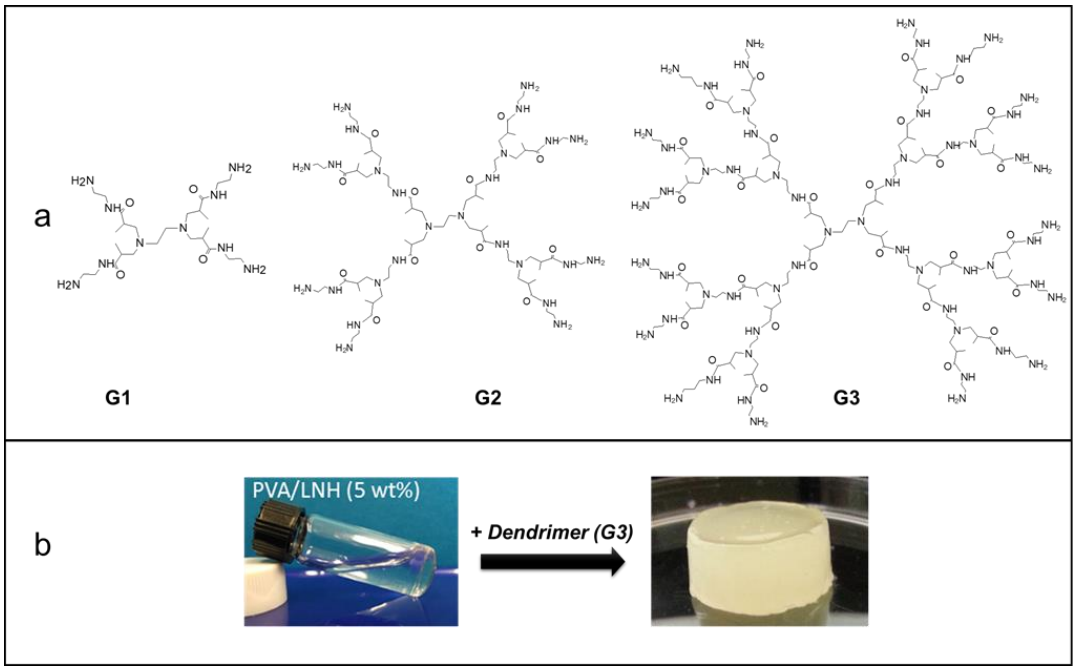

Figure 4-1. (a) Chemical structures of G1, G2 and G3 dendrimers; (b) Illustration of gelation in PVA/LNH system induced by the addition of G3 dendrimer at 70 ºC. Reprinted from [185] with permission from American Chemical Society.

physical gelation usually occurs above the critical overlap concentration (c^*) of the polymer chains,[126] further increase to the critical polymer entanglement concentration (c_e) results in an improved mechanical strength of physical networks.[127,128] Figure B-1, appendix B, shows the log-log plot of specific viscosity *versus* PVA concentration measured in LNH solutions at 23 °C. The distinct slopes in the curve suggest the existence of three different solution regimes, corresponding to the dilute ($c < c^*$), semi-dilute ($c^* < c < c_e$), and the highly entangled solutions ($c > c_e$).[129] The concentration for the onset of entanglements in PVA/LNH solutions, c_e, as determined from Figure B-1, was ~ 3.5 ± 0.5

wt%. Therefore, a concentration of PVA of 5 wt%, *i.e*. above the onset of PVA entanglements was chosen and used in all further experiments.

It is important to note that the salogels shown in Figure 4-1b formed exclusively in LNH rather than aqueous environment. In a control experiment, gelation was attempted using the same ratio of PVA and dendrimer as used for salogels shown in Figure 4-1b, but with water rather than LNH as a solvent. No gelation occurred in these conditions, and PVA/dendrimer/water system remained fluid at room temperature, as followed from both visual observations and measurements of the oscillation shear moduli which revealed that loss modulus (*G"*) exceeded storage modulus (*G'*) over a wide range of frequencies ω (Figure B-2). In addition to LNH, the presence of a dendrimer as a crosslinker was central to the efficient gelation in PVA/LNH solutions. Inset *b* in Figure B-2 shows that in the absence of dendrimers, PVA/LNH solutions also remained highly fluid, exhibiting the scaling of the elastic and loss moduli with the angular frequency which is typical for a viscous fluid ($G' \sim \omega^2$ and $G'' \sim \omega$, respectively).[130]

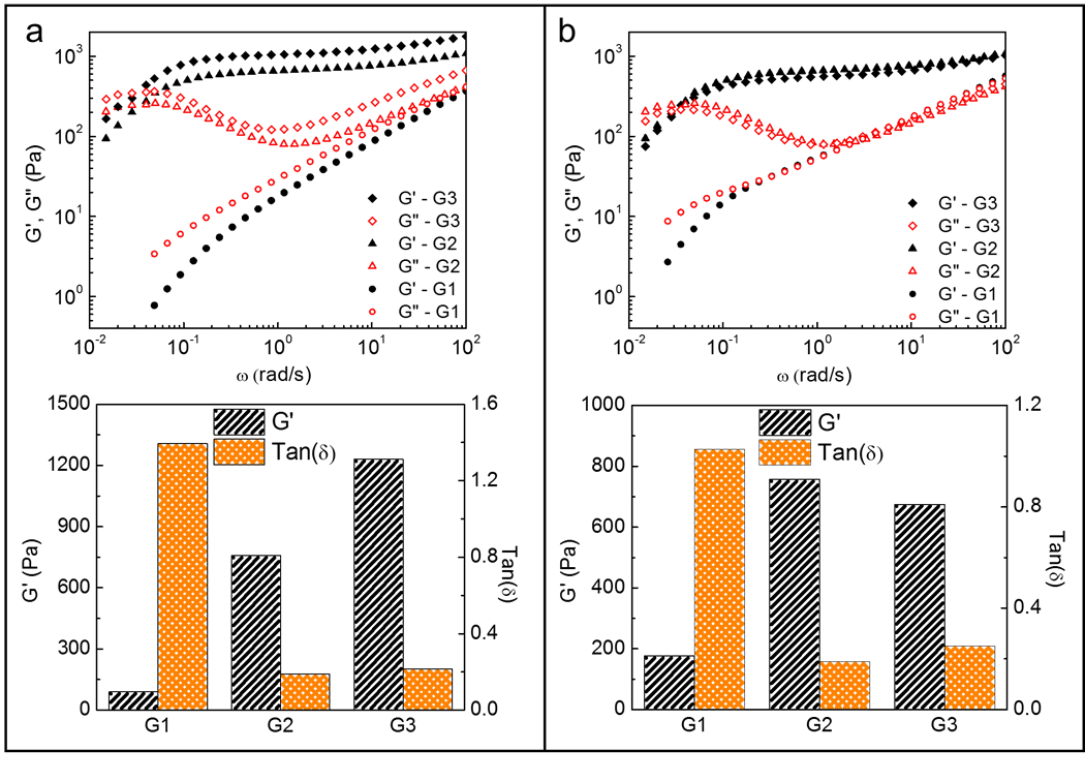

Figure 4-2. The frequency dependencies of *G'* and *G"* of PVA/GX/LNH salogels containing (a) equal number of GX molecules or (b) equal number of *–NH₂* groups in the system. Measurements were performed at 1.5 wt% concentration of G2 dendrimers and a temperature of 25 °C. The bar charts illustrate the oscillatory rheological properties achieved for the above systems at a constant frequency ω of 10 rad s^{-1} and a strain γ_L of 5%. Reprinted from [185] with permission from American Chemical Society.

The role of dendrimers in the formation of salogels was further explored in the experiments with various generations of dendrimers. In two series of experiments, either molar concentration of dendrimers or total number of *–NH₂* groups were matched and compared for different dendrimer generations. Viscoelastic behavior of these two systems was studied in rheological measurements under oscillatory shear mode. Figure 4-2a and b show that in both cases, *G'* increased with dendrimer generation number. However, an

increase in number of amino groups from 4 to 8 and 16 in G1, G2, and G3, respectively at a constant number of dendrimer crosslinks (Figure 4-2a) did not cause a proportional increase in the elastic and loss moduli. Specifically, samples prepared with G1 did not form salogels, exhibiting the typical viscous fluid behavior (*G" > G'*), while G2 and G3 dendrimers lead to the formation of salogels with similar viscoelastic properties, possibly because not all G3 amino groups participate in hydrogen bonding with PVA. Moreover, G1 crosslinkers were not able to form robust salogels and exhibited the incipient behavior (*G' = G"*) in a wide range of frequencies (Figure 4-2b) even when their concentration was significantly increased to match number of $-NH_2$ groups in G2- and G3-containing salogels. The dramatic differences in the behavior of G1 *versus* G2 and G3 crosslinkers can be attributed to the differences in the dendrimers binding energy and/or size. The average binding energy per crosslinker (proportional to number of amino groups in individual dendrimers) should reach a critical value in order to provide efficient binding between polymer chains and support elastic behavior of PVA networks. This critical binding energy was exceeded for G2 and G3, but not for G1 dendrimers. Another possible explanation is that the size of dendrimer is also a critical parameter for bridging between the polymer chains. If the polymer chains in 5 wt% PVA solutions are considered to be rod-shaped, the average interchain distance of ~ 2 nm would be larger than the diameter of G1 of ~ 1.5 nm, but comparable with diameters of G2 and G3 (~ 2.2 nm and ~ 2.9 nm, respectively).[51,52] Therefore, for these purely geometric reasons, G1 might not be efficient in binding PVA chains within a continuous network. The viscoelastic properties of

PVA/LNH system with G1, G2 or G3 crosslinkers at a constant frequency of 10 rad $s^{-1}$are also compared in Figure 4-2a and b, bottom panels.

We were then seeking to better understand molecular origin of gelation, *i.e.* identify the roles of hydration of PVA and ions in $LiNO_3$ medium, as well as explore the competitive hydrogen bonding between polymers, dendrimers, and water molecules. To that end, an ATR-FTIR spectroscopy was used. As mentioned in the Experimental Section, to enable separate observation of *–OH* groups in PVA and water molecules, D_2O was used in place of H_2O. This strategy has allowed us to prevent an overlap of spectral bands associated with stretching vibrations of *–OH* groups in water molecules with the ones in PVA. A deuterated analogue of LNH prepared by mixing D_2O and anhydrous lithium nitrate at a 3:1 molar ratio is abbreviated as LND. This salt was further diluted with D_2O and used as a solvent to study the effect of salt ions at different concentrations. In addition, dendrimer-free PVA/LND and PVA aqueous solutions were prepared as controls. Figure B-3 shows a set of infrared spectra of PVA/G2/D_2O/LND system in a wide range of wavenumbers. Vibrational features of PVA in the *–OH* stretching region for various compositions of PVA/dendrimer/solvent compositions, when the solvent was systematically varied from LND to D_2O, are shown in Figure 4-3a and b.

In these experiments, concentrations of PVA and G2 were fixed at 5 wt% and 1 wt%, respectively. As seen in Figure 4-3, complete replacement of LND with D_2O caused a large, ~ 63 cm^{-1} shift of the *–OH* stretching band of PVA to lower wavenumbers. The large red shift in the *–OH* stretching band of PVA is attributed to the formation of the

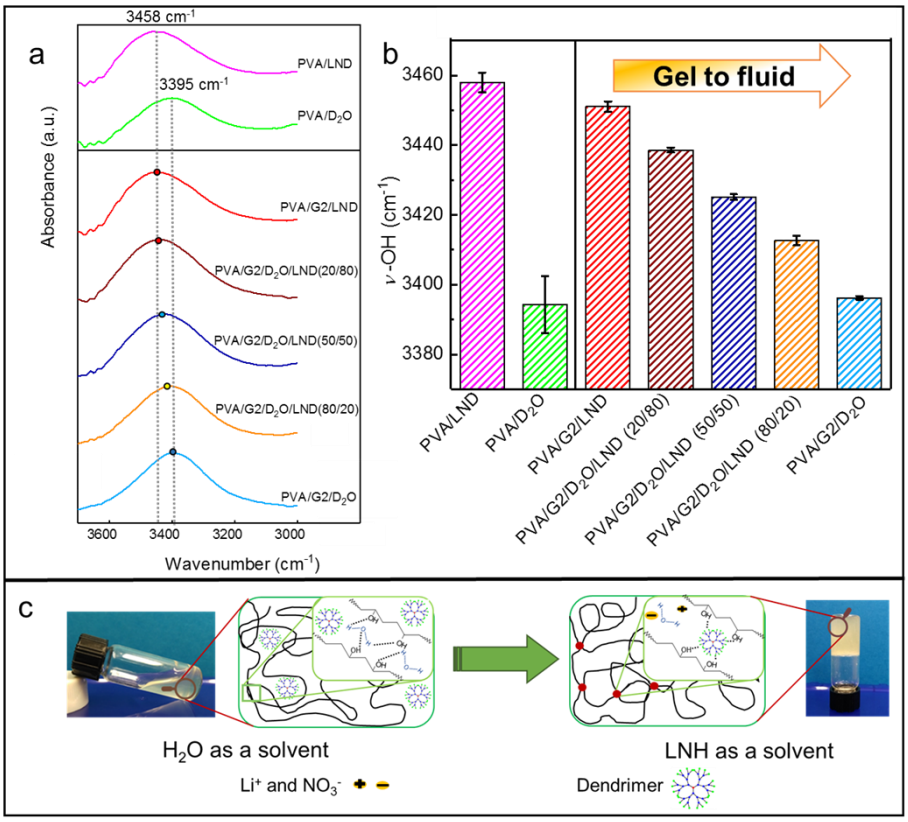

Figure 4-3. (a) ATR-FTIR spectra in the region of *–OH* stretching vibrational bands and (b) spectral shifts of the *–OH* vibrational bands for PVA in D_2O, LND, or LND/D_2O with or without the addition of a dendrimer crosslinker. (c) Schematic representation of the dendrimer-assisted gelation of PVA in LNH. Numbers in the abbreviations indicate molar percentages of D_2O and LND, respectively. Reprinted from [185] with permission from American Chemical Society.

hydration shell of PVA in D_2O thorough hydrogen bonding between *–OH* groups of PVA and *–OD* groups of heavy water, and a dramatic dehydration of PVA when LND used as a solvent. This observation is reminiscent of the previously reported blue shifts of the *–OH* band of PVA when the polymer became gradually dehydrated upon drying.[88] Li^+ is a strongly water-binding cation, which is usually solvated by four or five water

molecules.[131] In $LiNO_3$ hydrate melt, solvation water is scarce and water molecules are preferably coordinated with the salt, leaving PVA largely dehydrated.

The addition of a dendrimer to PVA/LND solution (see Figure 4-3c for illustration of gelation), caused a significant shift of *–OH* vibrational band of PVA from 3458 to 3452 cm^{-1}, suggesting formation of hydrogen bonds between PVA and the dendrimer. However, as the content of D_2O in the solvent increased above that supplied by LND, PVA chains became increasingly hydrated by the extra water, and hydrogen bonds were formed between *–OH* of PVA and D_2O. The vibrational frequencies of the PVA *–OH* band gradually decreased, reflecting the enhanced PVA hydration. Figure 4-3c illustrates that such a replacement of LNH with water molecules was accompanied by solvation of PVA chains and loss of gelation ability. This schematic clearly shows the crucial rule of molten salt hydrate as a solvent in the salogel formation.

4.2.2. Thermal behavior of shape-stabilized LNH

For realistic applications of the developed PVA/GX/LNH salogels, it is important to assess the performance of these matrices during multiple melting/freezing cycles. DSC analysis of PVA/G3/LNH salogels in the temperature range between -30 and 50 °C is shown in Figure 4-4a and b. DSC is known as one of the most sensitive indicators for the chemical purity of the system[11,132] and has been earlier applied to detect interactions of other types of PCM materials with stabilizing matrices.[133] Comparison of the thermal performance of LNH entrapped within the salogel with that of the pure LNH shows that the presence of polymer/dendrimer matrix had only a slight effect on the overall thermal

performance of LNH, and that the performance was highly repeatable for at least 10 melting/freezing cycles. A ~ 3 °C lowering of the melting temperature of LNH trapped within the polymer/dendrimer matrix and a change in the shape of LNH melting peak all point toward a possibility of interactions of LNH with the polymer matrix. An analogy can be driven with the earlier reports on interaction of Li^+ ions with the *–OH* groups of PVA[134] and binding of *–OH* groups of silica matrices with Na^+ of hydrated salts crystal ($Na_2SO_4 \cdot 10H_2O$, a commonly used inorganic PCM). The effect of polymer matrix has also manifested itself in lowering the crystallization temperature of LNH confined within salogels as compared to pristine LNH (Figure B-4).

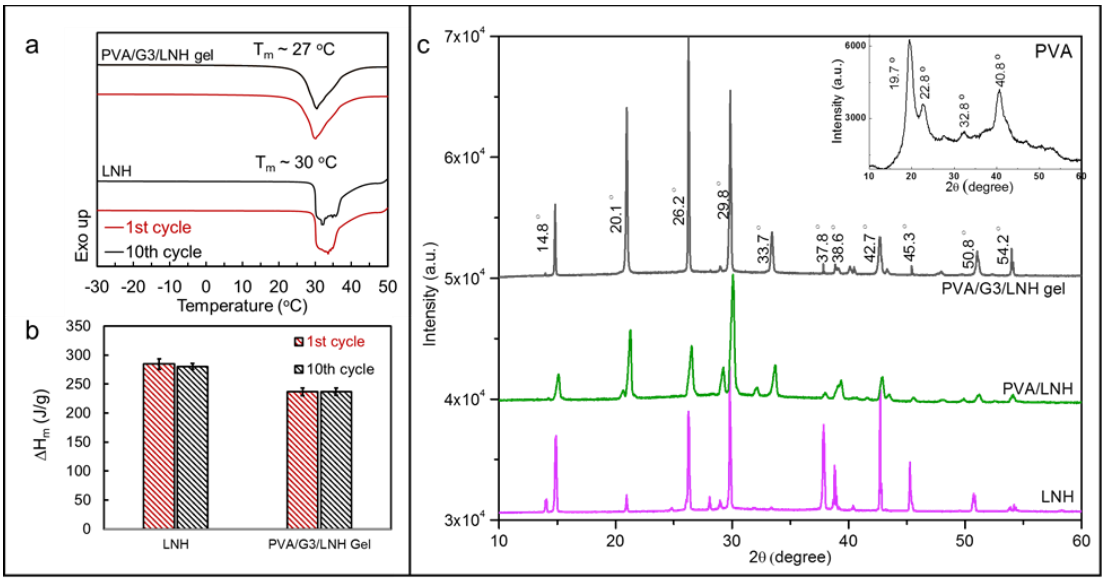

Figure 4-4. (a, b) DSC studies of the temperature transitions in PVA/G3/LNH salogel upon heating at a rate of 10 °C min^{-1} under a nitrogen atmosphere. (c) WAXD patterns of crystallized LNH within PVA/G3/LNH matrix, as well as those for control PVA/LNH and pure LNH samples at 20 °C. Concentrations of PVA and G3 were 5 and 1 wt%, respectively. Reprinted from [185] with permission from American Chemical Society.

Crystallization of LNH within polymer/dendrimer matrices induced by low temperatures was confirmed by X-ray diffraction (XRD) studies. Figure 4-4c shows the main characteristic peaks of crystalline LNH, PVA/LNH, and PVA/G3/LNH salogel as well as pure PVA powder (the inset). The characteristic sharp diffraction peaks observed for LNH are clearly visible in the PVA/G3/LNH diffraction patterns confirming the native crystalline nature of LNH after inclusion in the polymer matrix. Note that a new peak at $2\theta = 33.7°$ appeared in the salogel and PVA/LNH samples that was not observed in pure LNH. This peak, also observed earlier by others,[135] is seen in the WAXD data of the PVA powder (inset in Figure 4-4c) and indicates the presence of crystalline domains of PVA in PVA/G3/LNH matrix.

4.2.3. Controlling gelation temperature of salogels

For an efficient control of fluidity of LNH and on-demand destruction of the polymer matrix for its replacement, the gel-sol transition temperature (T_{gel}) of the polymer matrices should be higher than the melting point of LNH (30.1 ºC), and should be programmable to a desired temperature for easy replacement of a PCM matrix. In the case of hydrogels and organogels, either polymer [136,137] or crosslinker concentration[138] can be used to tune the gelation temperature. In this work, we were concerned with preserving the large latent heat storage capacity of LNH in the shape-stabilized PCM, and therefore aimed to keep the polymer concentration low. The lower limit of PVA concentration was determined by the onset of entanglements that assisted in enhancing the salogel

mechanical strength. Therefore, the amount of G3 dendrimer was varied at a fixed (5 wt%) concentration of PVA in LNH.

To determine the 'true' gelation temperature, temperature sweep rheological measurements were conducted at different frequencies. T_{gel} was chosen as a temperature point at which the loss tangent, *tan* δ (G''/G') became frequency-independent. This approach, introduced by Winter *et al.*[139] as the robust way to define the gelation temperature.[74,140,141] It considers the following power law relationships between the oscillation moduli and frequency at the gelation point (Equation 4-1), with the equality between the elastic and viscous moduli achieved when the relaxation exponent (n) is equal to 0.5 (Equation 4-2):[141]

$$G' \sim G'' \sim \omega^n, (0 < n < 1) \quad (4\text{-}1)$$

$$G''/G' = \tan\delta = \tan(n\pi/2), \quad (4\text{-}2)$$

where δ is the phase angle between stress and strain. The value of n is dependent on the molecular structure of the system and an exponent of n = 0.5 can be found only in few systems such as stoichiometrically balanced networks. In other systems, the G'- G'' crossover is frequency dependent and does not allow exact determination of the gelation point.[141]

Figure 4-5 shows the dependences of *tan* δ *vs.* temperature for several frequencies in PVA/G3/LNH system. The loss tangent decreased in the entire temperature range upon cooling for all the frequencies, reflecting an increased dominance of the elastic modulus

as the system was cooled. The crossover points of these dependences for frequencies of 3, 6 and 10 rad s^{-1} gave the reliable crossover points indicative of T_{gel}. The value of n was estimated from log-log plots of *G'* and *G" vs*. frequency at the gel point (insets in Figure 4-5). The relaxation exponent was close to 0.5 for all concentrations of the dendrimers, demonstrating insensitivity of the gel structure to the crosslinker concentration. Therefore, in this salogel system, the gelation points could be simply determined from the crossover of *G'* and *G"* measured at a single frequency of 10 rad s^{-1} as illustrated in Figure B-5. The frequency sweep experiments at the gelation temperature confirmed this conclusion, showing the relaxation exponents n = 0.5 for salogels prepared with varied dendrimer content (Figure B-5, inset).

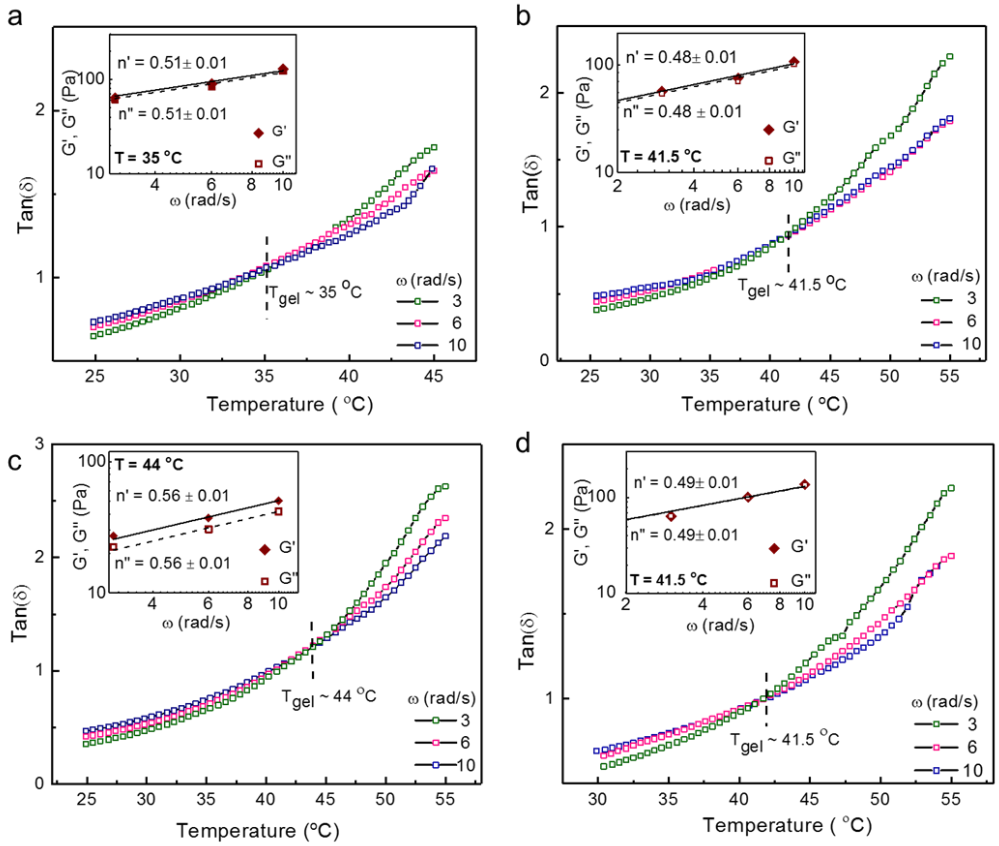

Figure 4-5. The temperature sweep experiments in PVA/G3/LNH system at multiple frequencies performed with a temperature ramp of ±1 °C min^{-1} and a strain amplitude γ_L of 10%. Concentrations of G3 were (a) 0.75%, (b) 1%, (c) 3%, and (d) 10%. Insets show the oscillation shear moduli versus frequency at the gelation point. Reprinted from [185] with permission from American Chemical Society.

Figure 4-6 shows the dependence of T_{gel} *versus* G3 for the low content of dendrimer (≤ 2 wt%) in PVA/G3/LND system. An increase in G3 concentration up to 2 wt% results in a linear increase in the gelation temperature. Thus, the gelation transition can be efficiently controlled in a wide temperature range between 35 and 62 °C by a facile increase in the concentration of G3. The linear dependence was observed till the ratio of number of $-NH_2$ groups in the dendrimers to $-OH$ groups in PVA increased from 1:100

to 1:10 at 0.5 and 2 wt% of G3, respectively. Note that at higher G3 concentrations, a decrease in the gelation temperature occurred (Figure B-6), probably due to a transition from random distribution of the crosslinking molecules to crosslinker clustering, as was also observed with other physical gels.[142-145]

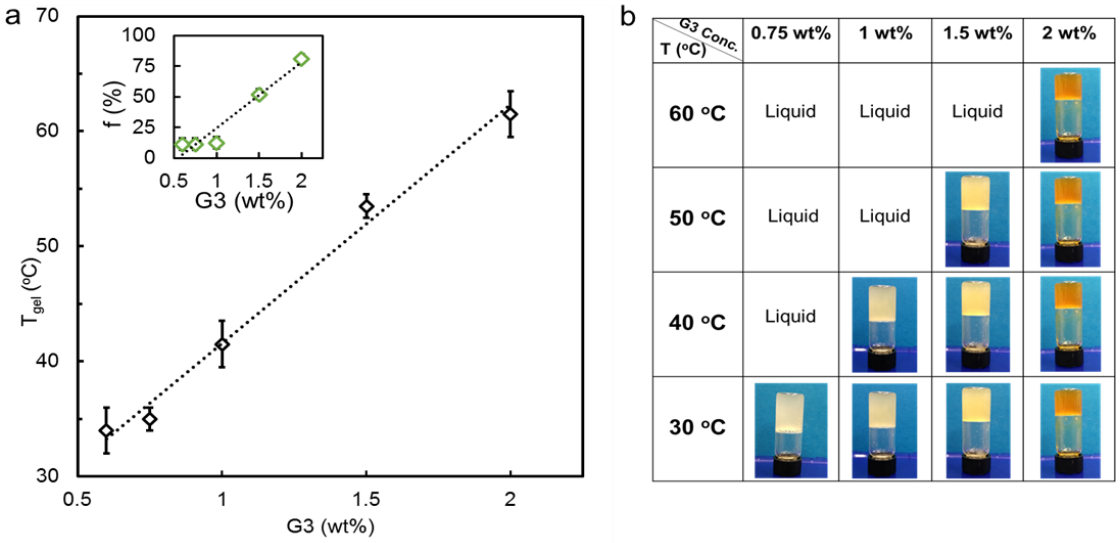

Figure 4-6. (a) The effect of G3 concentration on the gelation temperature (main panel) and the fraction of elastically effective chains (inset) in PVA/G3/LNH salogels, as determined from the rheological experiments conducted at 25 °C and a frequency of 10 rad s^{-1}. (b) Tunability of gelation in PVA/G3/LNH system containing varied amount of G3. Reprinted from [185] with permission from American Chemical Society.

An analogy with a chemically crosslinked network was then drawn, and *G'* values were used with the classical rubber elasticity theory developed by Flory[146] to estimate number of elastically effective chains ν as $G = \nu RT$, where R is the gas constant, and T is the absolute temperature. The fraction of elastically effective chains *f* can be then

determined from the experimental measurements of *G'* by dividing *v* to the chain molar density. The calculated fraction of elastically active chains as a function of G3 concentration is shown in inset in Figure 4-6a. Figure 4-6b shows that the transition temperature was highly tunable and could be precisely controlled by the fraction of hydrogen-bonding dendrimer crosslinkers.

Figure 4-7 demonstrates that PVA/G3/LNH matrix efficiently entrapped molten LNH, completely inhibiting its leakage at 35 ºC. In comparison, pure LNH is highly fluid in its molten state due to its low viscosity (only seven times higher than that of water).[11] The robust entrapping of LNH and retention of the salogel shape persisted within the temperature range between the melting temperature of LNH (30.1 ºC) and the gelation temperature of the salogels (41 ºC for the system shown in Figure 4-7). When further heated to higher temperatures, the system exhibited plastic flow, highly desirable for removal of these matrices from the heat-exchange devices after PCM becomes unusable.

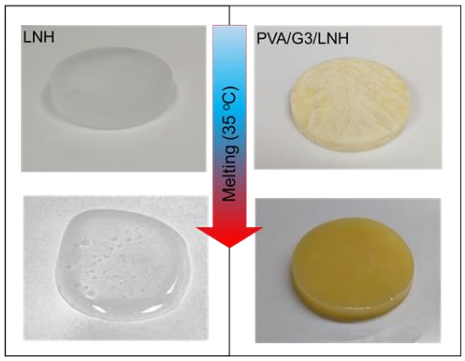

Figure 4-7. Melting of LNH as pure salt hydrate or after entrapping within PVA/G3/LNH salogel (3 wt% of G3) when heated to 35 °C for 2 hours on a hot plate. Reprinted from [185] with permission from American Chemical Society.

4.2.4. Self-healing of salogels

The ability to self-heal is an intrinsic property of physical gels that arises from the transient nature of reversible crosslinks.[111,147-150] To explore whether dendrimer-crosslinker salogels exhibit self-healing properties, rheological experiments on recovery of mechanical properties after network rupture were performed. First, a simple strain amplitude test was conducted on PVA/G3/LNH gels to find the highest and the lowest strain magnitude limits for the network breaking and recovery, respectively (Figure 4-8a). Then step-strain measurements were performed between 10% and 300% strain (*i.e.* far beyond the linear viscoelastic regime) to explore the rupture and recovery of the shear moduli of the salogels (Figure 3-8b). Figure 4-8c illustrates rapid and complete recovery of viscoelastic properties of the PVA/G3/LNH salogels after three cycles of network breaking and recovery.

The results of similar experiments conducted with PVA/GX/LNH systems prepared with G1 and G2 with equal total number of -NH_2 groups of dendrimers are shown in Figure B-7. The gels prepared with G1 crosslinkers were significantly weaker, and showed faster recovery time as compared with G2- and G3-containing systems. For all the systems, the recovery of the viscoelastic properties occurred just within 10-15 seconds after breaking, and was repeatable within at least three cycles of step-strain measurements, confirming the robust dynamic nature of salogels. The highly dynamic, reconfigurable nature of the hydrogen-bonded PVA/GX/LNH networks could be further visualized in a simple experiment shown in Figure 4-8d-f. In good agreement with rheological studies in

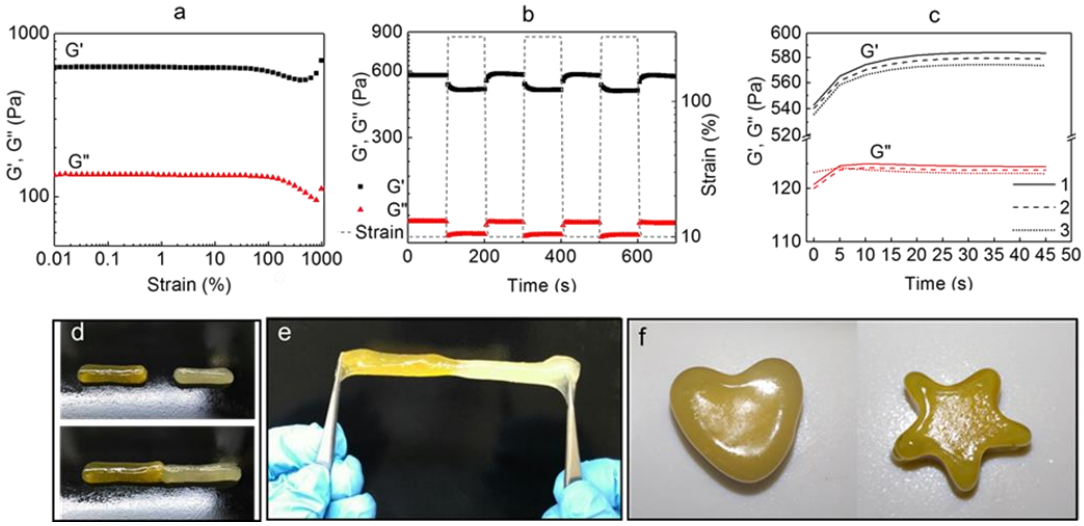

Figure 4-8. Self-healing and shapeability of PVA/G3/LNH salogels: (a, b) strain amplitude sweep (ω =10 rad s^{-1}) and step-strain measurements; (c) the recovery rate of *G'* and *G''* over three cycles of braking and recovery; (d-f) illustration of self-healing and shapeability of the salogels at ambient temperature. In (d), the salogels were held together side by side for 2 minutes prior to stretching. Temperature was 25 °C. Reprinted from [185] with permission from American Chemical Society.

Figure 4-8a-c, PVA/G3/LNH salogels were able to heal within 2 min at ambient temperature, exhibiting a strong healed interface when stretched up to ~ 200 %.

The rate and extent of recovery reflect the reversible and robust nature of the physically crosslinked salogels. Self-healing behavior of the salogels is likely related to dynamic nature of hydrogen bonds between hydroxyl groups of PVA and amine groups of dendrimers. Upon breaking of PVA-dendrimer bonds, free dendrimer molecules can diffuse in the material and form hydrogen bonds with new PVA chains. In the PVA/G1/LNH system which had the lowest G' and T_{gel} values among all the salogels, the

low activation energy associated with breaking of these hydrogen bonds enabled faster molecular diffusion and self-healing rates.

While the self-healing properties of PVA-based hydrogels have been reported in the literature,[151-153] this is the first demonstration of the self-healing capability of shape-stabilized salogels containing an inorganic PCM.

4.3. Conclusion

In summary, temperature-responsive, shapeable, and self-healing salogels were demonstrated for reversible shape stabilization of a molten inorganic salt hydrate PCM, LNH. The salogels are based on physical networks of PVA enhanced by hydrogel-bonding dendrimer crosslinkers and function exclusively in a high-salinity environment (17.3 M) created by liquid LNH. These thermoresponsive salogels enable on-demand removal and replacement of the PCM from the heat exchange devices, and offer a capability of programming the gel-sol transition temperature within a wide range above the LNH melting point. In addition, the self-healing capability of PCM matrices can improve its life cycle *via* curing defects that might occur during multiple phase change cycles. This work explored the unique features of molten LNH as a solvent, and showed that the low degree of PVA hydration in the water-scarce LNH environment is critical for establishing strong hydrogen bonding network with dendrimer molecules. This insight provides a guideline for future design of environmentally-responsive matrices for a broad range of inorganic PCMs. Importantly, strong gelation capability in this system allows minimizing the amount of organic components in order to preserve the high latent heat performance of

LNH. The straightforward method of the salogel preparation leading to unprecedented, temperature-controlled shape retention capability makes this systems promising for applications in solar thermal energy storage or recovering industrial waste heat devices. Furthermore, tunability of viscoelastic properties above the melting temperature of LNH might be useful for the development of shape-conformable energy storage consumer products, such as thermo-regulating packs and pillows. Future work focused on improving the heat conductivity of the salogels matrices and addressing the supercooling issue can further advance performance of these materials.

5. ACTIVATION ENERGY FOR DISSOCIATION OF HYDROGEN-BONDING CROSSLINKERS IN PHASE-CHANGE SALOGELS: DYNAMIC LIGHT SCATTERING VS. RHEOLOGICAL STUDIES[3]

5.1. Introduction

Physical gels present an important class of polymer networks which are formed *via* noncovalent binding, such as hydrophobic[154,155] and/or van der Waals interactions,[156] metal-ion coordination,[157,158] or hydrogen bonding.[159,160] In contrast to permanent chemical crosslinks, physical bonds are dynamic and can be dissociated under the influence of increased thermal energy or a mechanical force. It is widely accepted that dissociation energy of dynamic bonds can be probed in rheological experiments by measuring the terminal relaxation time.[161]

Determining the activation energy of dissociation of physical bonds can be a challenging task, however, because of the multiple hierarchical length and time scales involved in the polymer chain relaxation, as well as diverse contributions of crosslinkers of varying functionality and binding strength to network dynamics.[162-167]

Rheology has been proven to be a powerful technique that is uniquely suited for studying viscoelasticity and dynamic bonding in physical gels. Specifically, in rheological studies, temperature dependences of the time-temperature shift factor[161,168,169], zero-shear

[3] Reprinted with permission from "Activation energy for dissociation of hydrogen-bonding crosslinkers in phase change salogels: dynamic light scattering versus rheological studies" by Parvin Karimineghlani and Svetlana A. Sukhishvili, 2019. Macromolecular Chemistry and Physics, 220, 1900329, Copyright 2019 by Wiley.

viscosity[170,171], and macroscopic relaxation time of the transient network[38,39]-[32-37] have been all used to calculate a flow activation energy (E_a). Dynamic light scattering (DLS) is another useful technique for probing different relaxations, which detects fluctuations in concentration or mobility of polymer clusters at the length scales comparable to q^{-1}, where q is the scattering vector.[40] This technique can probe a variety of molecular motions of polymer chains including transitional, rotational diffusion and/or intermolecular relaxation. DLS relaxation spectra of dynamic networks typically include two dominant – fast and slow – relaxation modes.[172] It is generally accepted that the fast mode emerges as a result of cooperative diffusion of network strands at the time scale at which the whole network can be assumed to be immobile.[173] The origin of the slow mode, however, is still a subject of a scientific debate, [174] with some theories suggesting its origin in the relaxation of the elastic stress generated by viscoelastic network deformation caused by concentration fluctuations. [41,172,175,176]

Correlating rheological and DLS data on polymer chain dynamics has been a focus of several studies.[43,172,177-179] In concentrated solutions and physical gels, relaxation processes observed by DLS and rheology could be related to the same fundamental phenomena of disentanglement and bond dissociations.[180] Tanaka *et. al* studied thermally excited displacement fluctuations in polyacrylamide gels using quasi-elastic light scattering and developed a theory that relates the intensity correlation function (ICF) of the scattered light with viscoelastic properties of the gels.[41] In particular, it has been shown that ICF and the stress relaxation shear modulus are related *via* a cooperative diffusion coefficient and longitudinal bulk modulus of a polymer network. [41-43]

While there is a sizable body of literature on the rheology-based studies of the flow activation energy, [160,162,163,166,169,181] only a few studies assessed the activation energy of dissociation of physical networks from the temperature dependence of the DLS slow mode.[182-184] This study aims to explore the role of the hydrogen-bonding crosslinkers of varied functionality on gelation of a new family of physical gels – phase change salogels, recently developed in our group.[185] The specific focus is on making a head-to-head comparison of the flow activation energies in these systems as independently determined by rheology and DLS. Phase change salogels are formed by a physically crosslinked polymer, *i.e.* PVA, which shape-stabilizes a liquid inorganic phase change material (PCM) – lithium nitrate tri-hydrate (LNH). [185] Salogel networks can be strengthened by the use of a physical crosslinker whose amine groups form hydrogen bonds with *–OH* groups of PVA.[185] In LNH, hydration of PVA chains was suppressed and *–OH* groups were available for hydrogen bonding with a crosslinker. From the application perspective, entrapping a molten salt hydrate PCM within a thermo-responsive polymeric matrix prevents leakage of molten LNH and enables easy replacement of used PCMs within heat exchange modules. [185]

5.2. Results and Discussion

PVA salogels were prepared with two crosslinkers of varied molecular architecture, *i.e.* with linear DETA and an 8-arm G2 dendrimer. T_{gel} was first determined to quantify and compare the gelation strength of these physical crosslinkers and enable measurements of the activation energy of the salogels at $T < T_{gel}$. For a constant PVA

concentration of 0.1g/ml, a crosslinker concentration was gradually increased, and T_{gel} was determined in rheological experiments. Figure 5-1 shows the dependencies of T_{gel} on the molar concentration of crosslinkers for DETA, G2, as well as for a 16-arm G3 crosslinker explored in our previous publication.[185] To find T_{gel}, we followed the Winter-Chambon's theory.[139] According to this theory, T_{gel} is characterized by the frequency-independent tan δ and can be determined from the crossover point of G' and G" in the temperature sweep experiments, providing that the relaxation exponent is equal to 0.5. Because of the earlier confirmed ~ 0.5 value of the relaxation exponent for the salogels prepared with dendrimers, [185] and also determined for DETA-based salogels in this work (data shown in Figure 5-2), a simple crossover of G' and G" in the temperature sweep experiments yielded reliable values of T_{gel}.

In all cases, the dependencies are bell-shaped with a maximum in T_{gel}, which likely corresponds to the optimum number of physical crosslinks in the network. Suppression of T_{gel} at higher than optimal crosslinker contents is likely attributed to the overloading PVA with crosslinker molecules. In the case of G2 and G3, T_{gel} is higher and gelation occurred at almost two orders of magnitude lower content of crosslinker molecules as compared to DETA-induced gelation. We attribute these observations to multiplicity of binding sites and geometry of dendritic crosslinkers as compared to the linear one. In particular, each G2 molecule carries 4 times more primary amino groups (which are mainly responsible for hydrogen bonding with PVA) than DETA. Interestingly, in the case of DETA, gelation occurs only when the molar ratio of crosslinker to PVA chains, X, exceeded 200, suggesting relatively weak binding of this crosslinker to polymer chains. It is possible that

the earlier suggested crosslinker clustering [160,181] occurring upon increased DETA content was required to induce gelation in this system. A higher number of amino groups in dendritic G2 and G3 crosslinkers dramatically changed this scenario and enabled gelation when X was as low as ~ 2-5. Interestingly, T_{gel} values overlapped between X = 2 and X = 10 for G2 and G3, suggesting that even though G3 crosslinkers carry twice more amino groups than G2 (16 *vs*. 8, respectively), not every additional amino group efficiently contributed to binding with PVA. This is probably due to backfolding of functional groups, which was earlier reported for dendrimers of high generations. [186]

Figure 5-1 also shows a clear trend of a decrease in T_{gel} with a decrease in number of amino groups in a crosslinker, with an especially large difference between G2 and DETA. This finding is a direct effect of the increased binding energy of dendritic crosslinkers, which provided a larger number of hydrogen bonds with PVA chains. The higher affinity of branched crosslinkers to polymer chains in physical gels has been previously reported by several groups including ours.[185,187,188] The sol-gel transition temperature is thermodynamically controlled, [187] with a competition between favorable enthalpy-driven hydrogen-bonding between polymer chains and crosslinkers, and an unfavorable entropy loss associated with immobilization of crosslinkers within the network. The observed trend in T_{gel} is indicative of a higher propensity of the branched crosslinkers for gel formation in comparison to the linear ones.

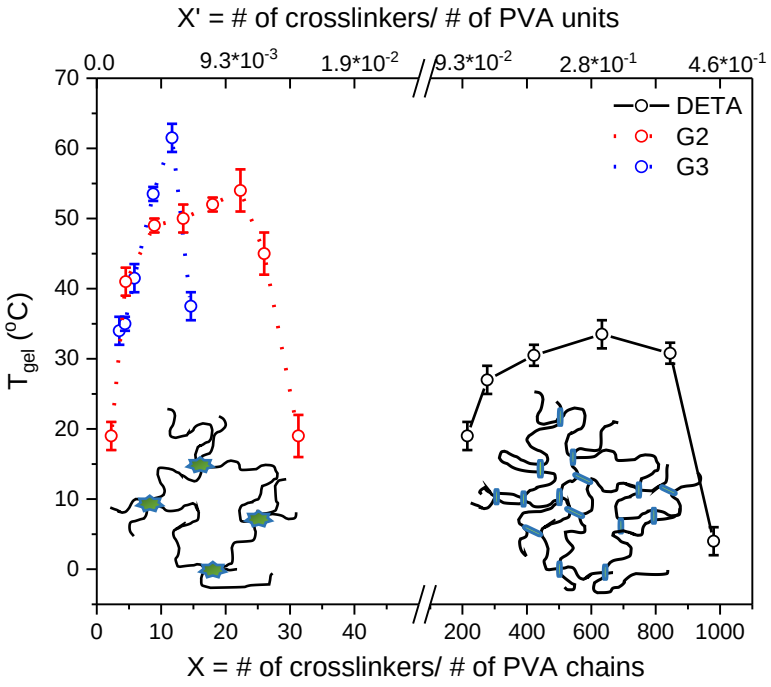

Figure 5-1. Variation of T_{gel} for linear and dendritic crosslinkers as a function of molar ratio of a crosslinker to PVA chains or units, *X or X'*, respectively. The data for G3-based salogels are replotted using the data in our previous publication [185] and are shown for comparison. Reprinted from [205] with permission from the Wiley.

To gain deeper insight into salogel network dynamics, we investigated the activation energy of the network crosslinking dissociation using two independent techniques of DLS and rheology. First, DETA-based salogels with the maximum T_{gel} ($X \cong 600$, $X' \cong 0.3$) were chosen to measure the polymer/crosslinker dissociation activation energy using DLS. Our setup is able to probe the sample dynamics on length scales of $1/q \approx 35$ nm. The outcome of DLS results is shown by ICF, which is defined as: [189]

$$g(q,\tau)=\frac{\langle I(q,t)I(q,t+\tau)\rangle}{\langle I(q,t)\rangle^2} \tag{5-1}$$

where τ is the decay time, and *I(q,t)* is the scattering intensity at time *t*.

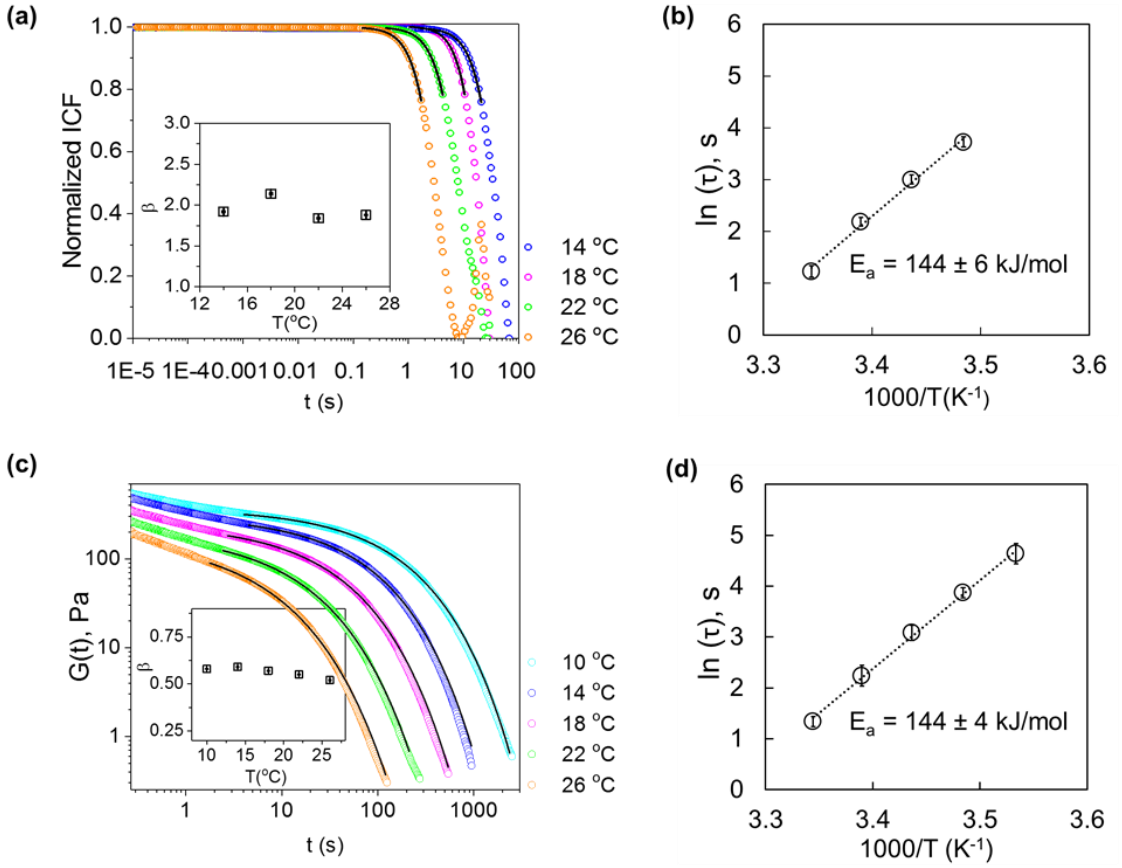

Figure 5-2. DLS intensity correlation functions, ICFs (a), and rheology stress relaxation data (c) performed at different temperatures in DETA-based salogels ($X\cong 600$ in Figure 5-1), along with Arrhenius plots of DLS slow mode characteristic time (b) and stress relaxation time (d). ICF decay exponents and stress relaxation exponents as a function of temperature are shown in insets of (a) and (c), respectively. Reprinted from [205] with permission from the Wiley.

The ICF shows a plateau region at $t < 0.1$ s, suggesting that no detectable dynamics existed at the length scale of our experiments (Figure 5-2a). However, at longer times (t > 0.1 s), a noticeable and steep decay of ICF was observed, indicating significant microscopic rearrangement and chain relaxation occurring at this time scale. Note that while ICFs for the salogels in Figure 5-2 showed only the slow decay modes, both fast and slow decays were observed for weaker salogels prepared with < 0.5% concentrations of DETA (Figure C-1, appendix C).

For the data in Figure 5-2a, by a decrease in temperature, the onset of the ICF decay shifted to the longer times. To quantify the relaxation kinetics, the decay regions of ICFs were fitted with the following function (Equation 5-2):

$$g_1(t) = A\exp[-(t/\tau)^{\beta}],\ \beta > 1 \qquad (5\text{-}2)$$

where A, β and τ are the amplitude, the relaxation exponent and the decay time, respectively.

Figure 5-2b shows the dependence of the decay time determined from the fit on the inverse temperature, following the Arrhenius behavior. The plot yielded the activation energy (E_a) of ~144 ± 6 kJ/mol. This value is about one order of magnitude higher than the activation energy for dissociation of hydrogen bonds in water of ~ 13 kJ/mol,[190] and likely suggests the formation of crosslinker clusters also observed by others in hydrogen bonding hydrogels.[160,181]

Similar experiments on the temperature dependence of the relaxation time were then performed by rheology (Figure 5-2c). For physical gels, stress relaxes through breaking and reforming of physical bonds.[191,192] The data on the stress relaxation at

different temperatures were fitted using the Kohlrausch's stretched exponential relaxation model (Equation 5-3):[193,194]

$$G(t) = G_o \exp[-(t/\tau)^{\beta}],\ 0 < \beta < 1 \tag{5-3}$$

where τ is the characteristic relaxation time, G_o is the plateau modulus and β is the relaxation exponent. The results show that the stress relaxation time followed the Arrhenius behavior (Figure 5-1d) with E_a of ~144 ± 4 kJ/mol as calculated using the following equation:

$$\ln[\tau(T)] = \ln \tau_o + \frac{E_a}{kT} \tag{5-4}$$

Thus, the activation energies obtained in DLS and rheology studies are in good agreement. It is worth noting that the activation energies, determined by both techniques are in fact the apparent activation energy, since they only reflect the temperature dependence of τ rather than τ/τ_o.[195] The apparent values of the activation energies obtained by rheology can be corrected by subtraction of the activation energy of LNH of ~16 kJ/mol from rheology activation energy to obtain the true value of the rheological activation energy of ~128 kJ/mol (Figure C-2). However, determination of the solvent activation energy using DLS was not possible because of the insufficient sensitivity and lack of scattering contrast. Therefore, this manuscript compares the apparent activation energies obtained by the two techniques. Our finding is consistent with the theories that draw a correlation between the DLS slow mode decay time and the macroscopic relaxation time of viscoelastic networks. While this correlation has been previously reported,[196,197] there

is only one report on a temperature dependence for relaxation time obtained by these two techniques, with no attempts to quantify the activation energy of network dissociation.[198] It should be also noted that the relaxation exponents plotted for DLS and rheology data in insets of Figure 5-2a,c, respectively, showed no temperature dependence, but varied between the two techniques. The β value of DLS decay was found to be unusually large, ~1.8-2, possibly due to light-induced heating which lead to acceleration of slow decay time during scattering. A similarly high relaxation exponent >1 has been previously found in DLS studies of physical gels by Ramos *et al*.[178] At the same time, the relaxation exponent of ~ 0.5-0.6 measured by rheology was close to those previously reported by others and our group for PVA-based gels.[185,199-201]

A similar comparison of the activation energy obtained by DLS and rheology was also performed for G2-based salogels (Figure 5-3). With the G2-based salogels at $X \cong 20$ (see Figure 5-1), the apparent activation energies using DLS and rheology were ~ 129 ± 5 and 129 ± 2 kJ/mol, respectively. Similar to DETA-based salogels, the relaxation exponents for this salogel, shown in insets of Figure 5-3a, c, were $\beta \cong 0.5$, and 2 for rheology and DLS, respectively. It is important that the activation energies for dissociation of G2- and DETA-based salogels were very close in spite of dramatic differences seen in Figure 5-1 in gelation in these systems. These results confirm that for both types of salogels, the activation energy is likely associated with dissociation of -NH_2...*PVA* individual bonds rather than with dissociation of an entire crosslinker molecule.

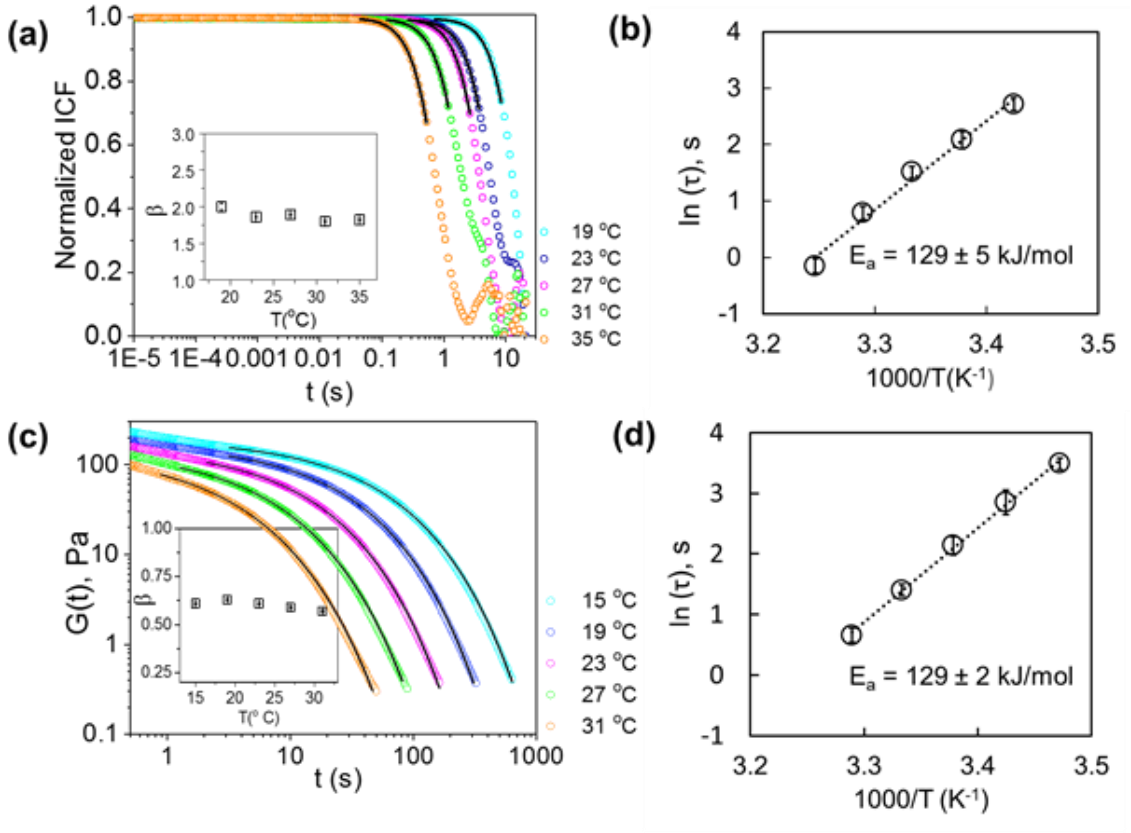

Figure 5-3. DLS intensity correlation functions, ICFs (a), and rheology stress relaxation data (c) performed at different temperatures in G2-based salogels (X≅20 in Figure 5-1), along with the Arrhenius plots of DLS slow decay time (b) and stress relaxation time (d). ICF decay exponents and stress relaxation exponents as a function of temperature are shown in insets of (a) and (c), respectively. Reprinted from [205] with permission from the Wiley.

5.3. Conclusion

We have explored and compared the activation energies of physically crosslinked salogels formed with linear and branched crosslinkers using two different complementary techniques. We observed a higher affinity for branched crosslinkers in comparison to linear ones for hydrogen bonding with polymer chains, which manifested itself as gelation

within a wider temperature range caused by a smaller concentration of a crosslinker. To our knowledge, for the first time, we demonstrated that the apparent values of the network dissociation activation energies determined by DLS and rheology are in very good agreement. This result was valid for both linear and dendritic crosslinker geometries. We believe that this finding can significantly contribute to a better understanding of relaxation phenomena and chain dynamics in thermo-responsive physical networks.

6. SOLVATION AND DIFFUSION OF POLY (VINYL ALCOHOL) CHAINS IN A HYDRATED INORGANIC IONIC LIQUID

6.1. Introduction

Phase change materials (PCMs) possess the unique capability for absorbing/releasing large amounts of energy over a narrow temperature range associated with a phase transition and thus present promising and inexpensive solutions in thermal energy storage applications.[202] In comparison to widely used organic PCMs, such as paraffins, inorganic PCMs offer several unique properties, including nonflammability and high levels of thermal conductivity and volumetric latent heat capacity.[203,204] One specific representative of inorganic PCMs – lithium nitrate trihydrate (LNH) – is considered promising for energy storage applications because of its close-to-ambient melting temperature (≈ 30 ^{o}C) and high specific heat of fusion (≈ 290 J/g).[11] However, because of the high fluidity of LNH in its molten state (viscosity as low as 5.71 mPa.s at 30 ^{o}C), incorporation of this material within a shape-stabilizing matrix is required to efficiently harness its thermal storage properties. In our prior work, we have introduced poly (vinyl alcohol), PVA, gel matrices – called 'salogels' – as an efficient means to provide such shape stabilization, and then to remove and replace the used LNH after multiple heating/cooling cycles by a temperature-triggered dissolution of the salogel matrix. We also explored the role of physical crosslinkers in gelation and studied the viscoelasticity of shape-stabilized salogels.[185,205] However, the factors that contribute to the gelation of PVA in LNH, as opposed to water remain unexplored.

In salt-free aqueous PVA solutions, polymer chains are fully solubilized as individual coils. Gelation can be induced, however, through intermolecular polymer-polymer hydrogen bonding between crystallized PVA domains that emerge as a result of freeze-thawing, or can be mediated by multivalent organic[206] or inorganic salt ions, such as borate[207-209] or vanadate.[210] Binding of multivalent ions with polymer chains was identified as the main reason for gelation in moderate ion concentrations. An increase in ion concentration beyond a certain value (~ 40 mM for borax), however, resulted in the emergence of a strong charge on PVA chains, a significant decrease in the number of crosslinks, and suppressed gelation.[209]

Gelation of PVA occurs much more readily when water is replaced with a different solvent − a hydrated inorganic ionic liquid (IL), which also is used as a PCM. Unlike common ILs which are composed entirely of ions, these new solvents are made of salt ions which are hydrated by water molecules supplied by the crystalline frameworks of the hydrates. Little is known, however, about behavior of polymer chains in hydrated inorganic ILs. In contrast, much more is known about properties of polymer coils in organic ILs because of the relevance of these systems for applications in solar cells and lithium batteries.[211-213] Simulations predicted, for example, an expansion of poly (ethylene oxide), (PEO), coils in an imidazolium-based IL and a scaling of the radius of gyration with molecular weight consistent with strong polymer-solvent interactions.[214] Experimentally, altering anion basicity and cation alkyl length of ILs (*e.g.* 1,3-dialkylimidazolium tetrafluoroborate) had a significant impact on PEO coil dimensions.[212] Strong interactions between polymer units and organic IL were also shown to affect the

sol-to-gel transition of poly (N-isopropylacrylamide), PNIPAM,[215] as well as improve the thermal stability of PVA.[216] However, liquid LNH is a different kind of solvent with no organic ions and an extremely high (≈18M) concentration of inorganic ions. In such a solvent, water is scarce and largely utilized for solvation of ions, and polymer chains simultaneously compete with salt ions for solvating water.

This work aims to understand the solvation of PVA chains in LNH solvent and compare it with what is observed in aqueous solutions. Polymer chain solvation and ion binding are important to understand physical gelation, in which polymer-polymer interactions are mediated by these parameters.[217] At the same time, solvation of polymer chains also influences excluded volume and hydrodynamic interactions within the polymer coil and thus affects the degree to which polymer chains are permeable to a solvent. The simplest model of polymer chains with strong hydrodynamic interactions was often used to interpret the results of hydrodynamic measurements in polymer solutions. Specifically, the scaling of hydrodynamic radius, diffusion coefficient, intrinsic viscosity and sedimentation coefficient with polymer molecular weight was used to evaluate solvent quality based on the value of the mass scaling exponents associated with these properties.[218-221] For polymer chains with increased excluded volume interactions, however, draining of polymer coils was theoretically predicted.[222-225] These models were further developed and experimentally tested for the case of rigid-chain polymers, such as DNA dissolved in water having a significant concentration of salt so that charge interactions are largely screened.[226] The effects of IL solvents on the hydrodynamics of polymers chains remain largely unexplored, however. In particular, it is unclear if the

Flory exponents are the same for polymers having long range dipolar interactions and it is unclear how strong solvation might alter the strength of polymer-polymer hydrodynamic interactions. Here, we investigate the hydrodynamic solution properties of polar flexible polymers in ILs to compare with the well-established phenomenology of neutral polymers in non-associating organic solvents.

Among experimental techniques capable of validating the earlier polymer diffusion models and relating them to chain solvation, fluorescence correlation spectroscopy (FCS) is one of the most suitable ones. This technique has an extremely high, single-molecule sensitivity that allows easy access to extremely dilute solutions, where chain diffusivity becomes concentration-independent.[227] At the same time, through using mixtures of fluorescently labeled and unlabeled polymer chains, FCS enables studies of chain motions in solutions at higher polymer concentrations. So far, applications of FCS to dilute aqueous polymer solutions generated sets of results that were consistent with the traditional model of non-draining polymer coils.[218,228,229] Here, we explore the diffusion of PVA chains and the overlap concentration (c*) in a molten inorganic IL, LNH, and demonstrate that strong chain solvation results in an emergence of draining of polymer coils in this solvent. Finally, we show that enhanced solvation of the polar PVA polymer chains in LNH involves binding of Li^+ ions to polymer chains and suggest that such binding also contributes to the increased propensity of PVA to physical gelation in this solvent.

6.2. Results and Discussion

Figure 6-1 illustrates the effect of a solvent (LNH *vs*. water) on gelation and rheology of PVA solutions. While gelation occurred in 15 wt% PVA solutions in LNH, aqueous solutions with the same concentration of the polymer had a significantly lower viscosity and easily flowed (Figure 6-1a). Figure 6-1b shows that while the relative viscosity of aqueous PVA solutions was weakly dependent on the shear rate − a behavior close to that of a Newtonian fluid − the gelled samples exhibited strong shear-thinning behavior, typical of associating liquids. Note that LNH did not crystallize at room temperature due to the supercooling effect, enanbling us to use it as a solvent without rising the temperature.[11]

Physical gelation in polymer solutions is often related to poor solvation of polymer chains at the crosslink points, such as, for example, the association between PVA chains induced by freeze-thawing.[25] However, polymers of all molecular weights studied here were readily soluble in LNH. To understand the nature of the gelation of PVA in LNH, we aimed to study the intricate details of the solvation of PVA chains and their interactions with the abundant LNH ionic species.

Molten LNH salt is an unusual solvent, which presents an ≈18M aqueous solution of lithium nitrate salt. When compared to other organic ILs,[230] LNH is unique in its role as a high-heat-capacity PCM. Water molecules in the high-salt environment of LNH are scarce and extensively used to solvate Li^+ and NO_3^- ions. In such a solvent, the effects of ion solvation on the solution properties – an effect only recently been developed theoretically for other systems[231] – should be especially strong. The intricate solvation

structure of the LNH can be revealed through FTIR analysis of vibrational bands associated with different types of noncovalent intermolecular bonding.

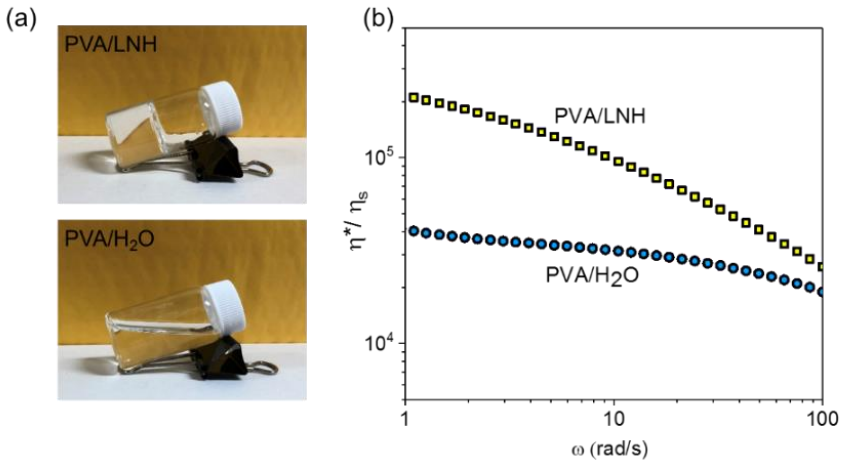

Figure 6-1. Digital images (a) and frequency dependence of the relative shear viscosities (b) of 15% PVA3 solutions in LNH and water at T = 22 ^{o}C.

In the ATR-FTIR spectroscopy studies, replacing H_2O with D_2O has enabled us to avoid the overlap of -*OH* vibrational bands originating from PVA and LNH. Specifically, the use of fully deuterated lithium nitrate (LND) and D_2O enabled the selective observation of -*OD* stretching vibrations in the 2000-2800 cm^{-1} region. The 3000-3300 cm^{-1} -*OH* stretching region was examined in our previous paper, and a significant blue shift in the –*OH* vibrational frequencies of PVA was observed upon increasing salt concentration in aqueous solutions. This change indicated a weakening of hydrogen bonding between –*OH* groups of PVA and water when the concentration of salt ions was increased. We hypothesize here that lower hydration of PVA results from strong binding

of water within the solvation shell of Li^+ and NO_3^- ions. Similarly, lower hydration of PVA and chitosan was also reported for organic ILs, which can bind with water stronger than with polymer units.[232,233] To better understand the binding of water with salt ions in LNH, we focused here on the *–OD* stretching (2000-2800 cm^{-1}) vibration region which is sensitive to hydrogen bonding and structure formation in heavy water.

Figure 6-2 shows that dramatic changes occurred in the overall peak shape in the *–OD* stretching vibrational region as D_2O was gradually replaced with LND. Mixed solutions are abbreviated as D_2O/LND (x/y), where x/y is the volume ratio of D_2O to LND. In water, there exist a broad range of water-water hydrogen-bonded configurations that vary in both their energy and the binding angle between the donor (D) and acceptor (A) moieties of water molecules, but all can be grouped within two main types of weakly and strongly hydrogen-bonded water.[234,235] In this work, we based the deconvolution procedure on the theoretical prediction of the existence of two additional sub-peaks of strongly and weakly hydrogen-bonded water.[47,236] The peaks centered at 2336 cm^{-1}, 2383 cm^{-1}, 2493 cm^{-1}, 2580 cm^{-1}, and 2648 cm^{-1} are assigned to *–OD* vibrations involved in the strongest DAA (single donor and double acceptor, symmetric stretching vibration) hydrogen-bonding, strong DDAA (double donor – double acceptor, symmetric stretching vibration) tetrahedral hydrogen bonding, weak DA (single donor–single acceptor, bending vibration) and another weak DDA (double donor–single acceptor, antisymmetric stretching vibration) hydrogen bonds, as well as to stretching vibrations of free *–OD* groups, respectively. For D_2O, the wavenumbers of the contributing deconvoluted bands and their intensities were consistent with prior theoretical and experimental results.[47-49]

Deconvolution of the absorbance bands (see Experimental section for details) revealed significant changes in both positions and relative intensities of the contributing *–OD* bands. With increasing salt concentration, the positions of all the peaks shifted to higher wavenumbers (Figure 6-2, b), suggesting weakening of water-water hydrogen bonding in solutions with high concentrations of Li^+ and NO_3^- ions. At the same time, the fractional intensities of weaker H-bonds (DA and DDA) increased at the expense of intensities of the stronger DAA and DDAA hydrogen bonds (Figure 6-2, c). These results suggest that Li^+ and NO_3^- ions drastically changed the energy and structure of hydrogen-bonding networks of water molecules in the aqueous environment. Strong competition of inorganic ions and water-water hydrogen bonding occurred because of the scarcity of water in LNH, with only three water molecules being available for a pair of Li^+-NO_3^- ions. The data in Figure 6-2, therefore, illustrate breaking of the water-water hydrogen bonds which are abundant in salt-free water and emergence of weaker hydrogen-bonded water, which is included in solvation shells of Li^+ and NO_3^- ions.

Weaker hydration of PVA chains, resulting from competition for water between the polymer chains and LNH, reduced the number of hydrogen bonds between *-OH* groups of PVA and water. One can suggest that this could facilitate the formation of polymer-polymer hydrogen bonding and thus contributing to gelation. Alternatively, gelation can

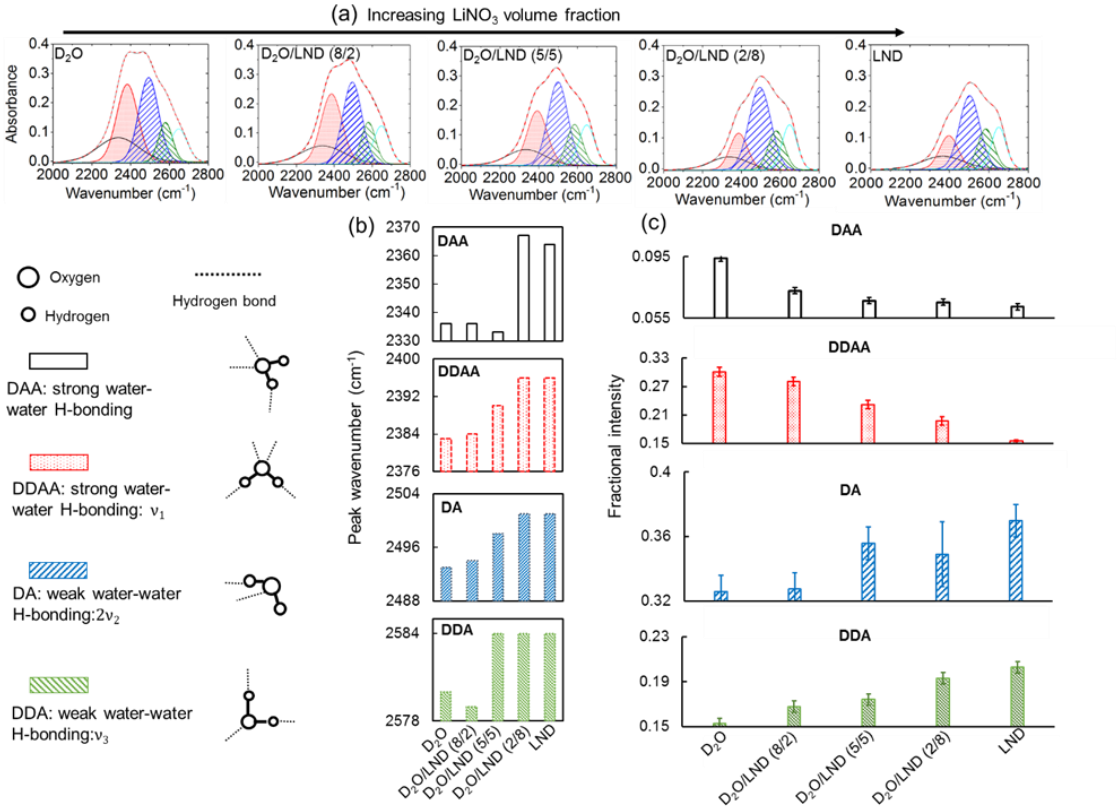

Figure 6-2. FTIR analysis of 2000-2800 cm^{-1} –OD vibrational region in LND, D_2O, and D_2O/LND mixed solvents (a), peak wavenumber (b) and fractional intensity (c) changes corresponding to the deconvoluted peaks of DAA, DDAA, DA, and DDA vibrations upon gradual transition from D_2O to LND.

be mediated through the binding of solvated inorganic ions. Li^+ ions are known to coordinate with high-electron-density species, such as sulfur or oxygen atoms; [237,238] thus we hypothesized that Li^+ ions can bind with -*OH* groups of PVA. To test this hypothesis, we have performed ^7Li NMR studies of the mobility of Li^+ ions in PVA-free and PVA-containing LNH solutions.

^{7}Li NMR spectra of LNH and PVA3/LNH solutions are displayed in Figure D-4. The ^{7}Li NMR resonance of PVA3/LNH is significantly broadened compared to polymer-free LNH, owing to the reduced Li^{+} ion mobility in the viscous PVA3 polymer matrix. To further investigate the effects of PVA on Li^{+} ion mobility, we performed ^{7}Li NMR spin-lattice relaxation time (T_1) measurements which provide important clues in ion dynamics.[239] Figure 6-3 shows that the initial ^{7}Li NMR T_1 in LNH of 3.6 s gradually decreases upon addition of PVA, reaching a value of 1.2 s in 15% PVA3/LNH solution. Spin-lattice relaxation is generally described by the Bloembergen, Purcell, and Pound (BPP) model[240]:

$$\frac{1}{T_1} \propto \frac{\tau_c}{1+(\omega_0\tau_c)^2} \tag{6-1}$$

where τ_c is the correlation time and ω_0 is the Larmor frequency.

For smaller molecules at room temperature, such as LNH, ion dynamics falls in the fast-motion region, where $\omega_0\tau_c << 1$. Under these conditions, a decrease in T_1 indicates slowing down of ionic motions, [241] which in our system most likely occurred due to increased interactions between Li^{+} ion and PVA chains.

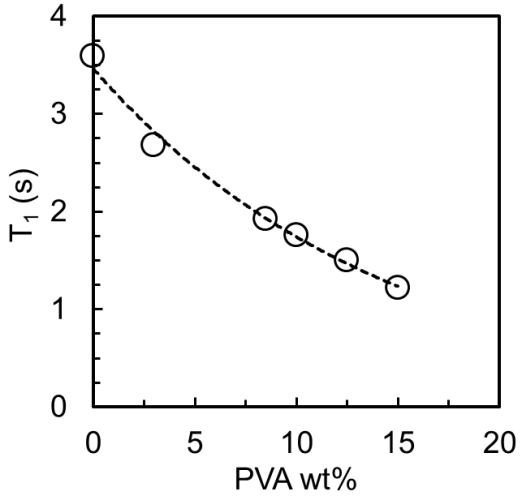

Figure 6-3. ^{7}Li spin-lattice relaxation time (T_1) as a function of PVA3 concentration in LNH measured at 22 °C.

After demonstrating strong solvation of inorganic ions in LNH and binding of Li^+ ions with PVA, we sought to explore the effect of these interactions on hydrodynamic properties of the polymer coils. To that end, we employed the FCS technique that is capable of probing polymer dynamics with single-molecule sensitivity (see Experimental section for details). Using fluorescently tagged PVA* chains of four different molecular weights with relatively narrow molecular weight distributions (Table 2-1), we first explored hydrodynamic properties of PVA coils in the dilute regime using LNH and water as solvents. In the dilute regime, polymer chains do not overlap, and hydrodynamic radius (R_H) of the polymer coils can be determined using the Stokes-Einstein equation, $D = k_B T / 6\pi\eta R_H$. This equation applies regardless of the strength of the hydrodynamic interaction, but the "non-draining" limit of strong hydrodynamic polymer-polymer interactions mediated by the solvent is often assumed.

Figure 6-4 a,b show the diffusion coefficients (D) and R_H of PVA* calculated using the Stokes-Einstein equation as a function of polymer molecular weight. Representative intensity correlation functions (ICFs) for the diffusion of PVA4* in aqueous and LNH solutions are shown in Figure D-5. For flexible chains in theta and good solvents, diffusion coefficients for non-draining polymer coils are expected to scale as $D \sim M^{-1/2}$ and $D \sim M^{-3/5}$, respectively.[146,242] Here, for solutions of PVA* in LNH and water, the diffusion mass scaling exponents were 0.6 ± 0.1 and 0.45 ± 0.10, respectively (Figure 6-4a, b). No strong conclusions with regard to solvent quality can be made here, considering the relatively narrow range of molecular weights, moderate polydispersity of the samples, and the experimental error of the measurements. Prior publications by others have also advised caution in interpreting the mass scaling exponents as direct measures of the equilibrium size of polymer chains in solution.[211]

More instructive were unexpectedly low values of the hydrodynamic radii of PVA* chains in LNH as compared to those in water, which were consistently observed for polymers of all molecular weights. At the same time, the hydrodynamic sizes of aqueous PVA* solutions agreed well with prior reports and can be interpreted using the non-draining polymer coil model.[243] The smaller hydrodynamic diameters of the polymer chains in the PVA/LNH system were also confirmed by the measurements of intrinsic viscosity with 2 to 10 mg/ml PVA solutions (Figure 6-4c). These concentrations fell within the dilute solution regime (Figure D-6), considering that a c* of 17.3 mg/ml was determined for PVA with molecular weight of 166,000 g/mol,[244] which is higher than all the molecular weights of PVA studied here (see Table 2-1). One explanation for a smaller

hydrodynamic sizes of PVA chains in LNH could indicate partial collapse of the polymer coils in a solvent, but this explanation is inconsistent with the high exponents in the molecular mass dependences of D, R_H and intrinsic viscosity of PVA in LNH (Figure 6-4). The lower calculated hydrodynamic size of polymer coils, taking together with the higher values of diffusion and intrinsic viscosity mass scaling exponents of PVA in LNH as compared to those in water indicate likely draining of PVA coils in the LNH solvent.

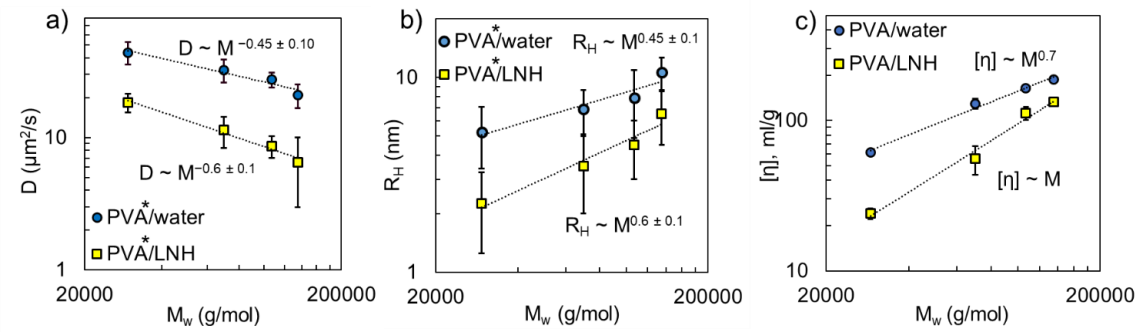

Figure 6-4. Molecular weight dependences of FCS diffusion coefficients (a) and hydrodynamic radii (b) of PVA* measured in 10^{-4} mg/ml aqueous or LNH solutions at 22 ^{o}C, as well as intrinsic viscosities of PVA in aqueous and LNH solutions at 35 ^{o}C as a function of polymer molecular weight (c).

Note that earlier models by Flory[245] and Kirkwood and Riseman[246] already took into account the possibility of draining of polymer chains, for example by introducing the partial draining parameter h. Draining of a solvent through the polymer coils was also suggested by experiments performed with rigid chains in a good solvent, which showed deviation from the impermeable sphere model.[226,247-249] More recently, Mansfield *et al.* performed hydrodynamic modeling of a biological molecule – duplex DNA – and found

evidence of weak hydrodynamic interactions and significant draining of DNA coils for this semi-flexible polymer, consistent with extensive measurements of transport properties in DNA solutions.[226] While DNA molecules are highly charged, the measurements described here are performed for polymer chains in a solvent with extremely high salt concentrations for which the charge interactions have been largely neutralized. Yet the DNA solutions resemble the PVA solutions of the present work in that the polymer chains are highly solvated so it is perhaps unsurprising that they exhibit a similar pattern in the solution hydrodynamic properties in which hydrodynamic interaction strength is relatively weak.

Finally, assessing the chain overlap concentration value c* in these two solvents and comparing these values with the hydrodynamic size measurements can provide another piece of evidence related to the draining of solvent through polymer coils. The value of c* separates the dilute and semidilute solution regimes of polymer solutions and indicates the onset of the physical overlap of the polymer coils determined by their R_g. The transition can be probed by measuring polymer dynamics in a wide range of solution concentrations. When polymer concentrations exceed c*, chain diffusivity is slowed by the surrounding molecules.[227] In this work, this transition was explored by FCS measurements of diffusion of PVA* chains in solutions containing increasing concentrations of unlabeled PVA molecules. These experiments were performed using PVA2 polymer with the average molecular weight M_w of 69,700 g/mol and polydispersity of 1.39. Figure 6-5 a,c show the representative fluorescence intensity correlation functions and the diffusion coefficients obtained for fluorescent PVA* chains which were added in

ultra-low concentrations to solutions of unlabeled PVA solutions which were 4-6 orders of magnitude higher that of the fluorescing species. An obvious shift of ICFs for diffusing PVA* to longer diffusion times was observed at high PVA concentrations. Figure 6-5b, d summarize the diffusion coefficients for PVA* in a wide concentration range of PVA for the two solvents. The region of a nearly constant *D* at low polymer concentrations is followed by a strong decrease in PVA* mobility above the overlap concentration c*. The independence of the diffusion coefficients on polymer concentration in the dilute regime ($c << c^*$) is expected because of separation of individual polymer coils in this regime.[242,250] Above the overlap concentration, the scaling of *D* vs. $c^{-1/2}$ was predicted for $c^* < c < c_e$ (the Rouse-like regime),[251] where c_e is the entanglement transition concentration. The data in Figure 6-5 b,d yielded the scaling exponents of 0.55 ± 0.15 and 0.7 ± 0.1 above the overlap concentration for water and LNH, respectively. Most importantly, the PVA chain overlap occurred at twice higher concentration in water as compared to LNH (20 *vs* 10 mg/ml, respectively), suggesting ~25% larger radial and ~ two-fold volume chain expansion of PVA in LNH solvent. Taken together with hydrodynamic measurements discussed above in the paper, the extension of physical chain dimensions of PVA in LNH with a simultaneous decrease of hydrodynamic dimensions as compared to water are suggestive of increased draining of polymer chains in the hydrated inorganic IL solvent.

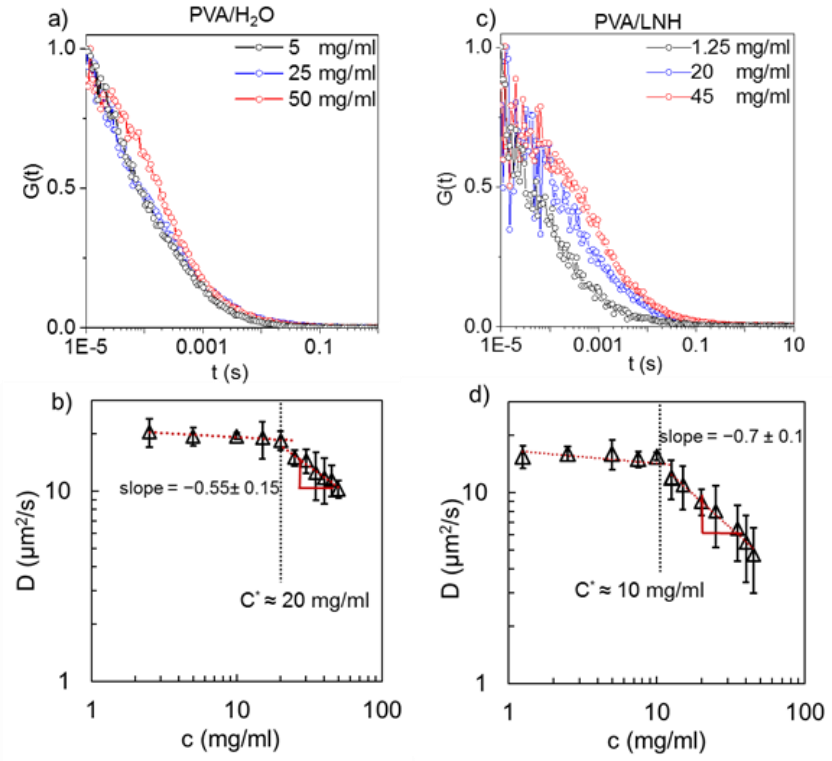

Figure 6-5. FCS autocorrelation functions and diffusion coefficients in 10^{-4} mg/ml PVA2* solutions in water (a,b) and LNH (c, d), which also contained increasing amounts of unlabeled PVA2 with M_w of 69,000 g/mol. Temperature was 22 ºC.

6.3. Conclusion

In summary, here we explored the behavior of a neutral polar polymer in a hydrated inorganic IL, LNH, and found that binding of components of this solvent with PVA chains led to increased chain rigidification and decreased hydrodynamic interaction strength, resulting in draining of polymer coils. To the best of our knowledge, the draining of polymer coils caused by a hydrated inorganic IL has not been previously reported and can be a compelling subject for further studies. The intricate details of interactions of ions and water molecules with hydrophilic polymer chains in the water-scarce environment of LNH

raise new fundamental questions about the role of competitive hydration of polymers in ion-rich solutions. At the same time, these studies shed light on the mechanism of gelation of polymers in the highly ionic environments of LNH – a high-performance inorganic PCM whose applications demand controlled and efficient shape stabilization. We believe that an understanding of expansion and solvation of polymer chains in hydrated inorganic ILs can facilitate the development of new types of shape-stabilizing salogels for thermal storage applications.

7. CONCLUSIONS

In this work, we have demonstrated that PVA-based physical gels are promising thermoreversible matrices for shape stabilization of an inorganic salt hydrate PCM. We explored two different approaches for development of these physical gels. First, we demonstrated crosslinker-free gelation of PVA in molten salt hydrate, *i.e.* LNH. Our experimental results confirmed that dramatic dehydration of PVA chains in the molten salt hydrate promoted PVA gelation due to either direct hydrogen bonding between hydroxyl groups of PVA and/or additional binding through Li^+ ion.

Secondly, we developed the temperature-responsive, shapeable, and self-healing gels based on PVA networks whose strength has been enhanced by incorporation of hydrogen-bonding dendrimer crosslinkers. The existence of hydrogen bonding and the importance of low-hydration state of PVA for the efficient gelation were experimentally confirmed. We demonstrated that in this system, the gel-sol transition temperature could be precisely controlled within a range of temperatures above LNH melting point by the choice of dendrimer generation and their concentration. The thermal behavior of PCM salogels was highly reversible and repeatable during multiple heating/cooling cycles. Using two complementary techniques − rheology and DLS – we determine the crosslinker dissociation activation energy for these networks, and show that the results obtained by both techniques are in good agreement for salogels with both linear and dendritic crosslinkers.

To more explore the underlying reasons of PVA gelation in the high-salinity environment created by liquid LNH (~18 M), expansion and diffusion of PVA chains in a

very dilute solution of LNH was studied using FCS. The molecular weight dependences of the diffusion coefficients of the fluorescently tagged polymer revealed a larger value of the Flory exponent and lower hydrodynamic radii for PVA chains in LNH as compared to water, suggesting possible draining of polymer coils in LNH. A low overlap concentration (c*) of PVA in LNH measured by FCS, taken together with the intrinsic viscosity results, suggest expansion of polymer coils and weakened hydrodynamic interactions in this solvent.

We believe that understanding solvation and ion-binding capability can offer crucial insights in designing polymer-based shape stabilization matrices for inorganic PCMs. Importantly, strong gelation capability in the crosslinker-based gel system allows minimizing the amount of organic components in order to preserve the high latent heat performance of PCM. Adding conductive nanoparticles to the system can improve the heat conductivity of these PCM materials, further enhancing their performance and making them suitable for of the use in heat exchangers. The facile method of the gel preparation leading to unprecedented, temperature-controlled shape retention makes these systems promising for applications in solar thermal energy storage or recovering industrial waste heat devices. Furthermore, the new feature of tunability of the viscoelastic properties of shape-stabilized salogels above the melting temperature of PCM offers new opportunities for the development of thermo-regulating consumer products, such as packs and pillows, of tunable softness.

REFERENCES

(1) Wang, L.; Meng, D. Fatty acid eutectic/polymethyl methacrylate composite as form-stable phase change material for thermal energy storage. *Applied Energy* **2010**, *87*, 2660-2665.

(2) De Marco, L.; Carpenter, W.; Liu, H.; Biswas, R.; Bowman, J. M.; Tokmakoff, A. Differences in the Vibrational Dynamics of H2O and D2O: Observation of Symmetric and Antisymmetric Stretching Vibrations in Heavy Water. *The Journal of Physical Chemistry Letters* **2016**, *7*, 1769-1774.

(3) Zhang, Y.; Xiu, J.; Tang, B.; Lu, R.; Zhang, S. Novel semi-interpenetrating network structural phase change composites with high phase change enthalpy. *AIChE Journal* **2018**, *64*, 688-696.

(4) Farid, M. M.; Khudhair, A. M.; Razack, S. A. K.; Al-Hallaj, S. A review on phase change energy storage: materials and applications. *Energy Conversion and Management* **2004**, *45*, 1597-1615.

(5) Zalba, B.; Marín, J. M.; Cabeza, L. F.; Mehling, H. Review on thermal energy storage with phase change: materials, heat transfer analysis and applications. *Applied thermal engineering* **2003**, *23*, 251-283.

(6) Liu, C.; Li, F.; Ma, L. P.; Cheng, H. M. Advanced materials for energy storage. *Advanced materials* **2010**, *22*.

(7) Wu, D.; Ni, B.; Liu, Y.; Chen, S.; Zhang, H. Preparation and characterization of side-chain liquid crystal polymer/paraffin composites as form-stable phase change materials. *Journal of Materials Chemistry A* **2015**, *3*, 9645-9657.

(8) Shamberger, P. J.; O'Malley, M. J. Heterogeneous nucleation of thermal storage material LiNO 3· 3H 2 O from stable lattice-matched nucleation catalysts. *Acta Materialia* **2015**, *84*, 265-274.

(9) Tyagi, V. V.; Kaushik, S. C.; Tyagi, S. K.; Akiyama, T. Development of phase change materials based microencapsulated technology for buildings: A review. *Renewable and Sustainable Energy Reviews* **2011**, *15*, 1373-1391.

(10) Karimineghlani, P.; Emmons, E.; Green, M.; Shamberger, P.; Sukhishvili, S. A Temperature-Responsive Poly (vinyl alcohol) Gel for Controlling Fluidity of an Inorganic Phase Change Material. *Journal of Materials Chemistry A* **2017**.

(11) Shamberger, P. J.; Reid, T. Thermophysical Properties of Lithium Nitrate Trihydrate from (253 to 353) K. *Journal of Chemical & Engineering Data* **2012**, *57*, 1404-1411.

(12) Sharma, A.; Tyagi, V. V.; Chen, C.; Buddhi, D. Review on thermal energy storage with phase change materials and applications. *Renewable and Sustainable energy reviews* **2009**, *13*, 318-345.

(13) Liu, Y.; Yang, Y.; Li, S. Graphene oxide modified hydrate salt hydrogels: form-stable phase change materials for smart thermal management. *Journal of Materials Chemistry A* **2016**, *4*, 18134-18143.

(14) Xiao, M.; Feng, B.; Gong, K. Preparation and performance of shape stabilized phase change thermal storage materials with high thermal conductivity. *Energy Conversion and Management* **2002**, *43*, 103-108.

(15) Wu, Y.; Wang, T. The dependence of phase change enthalpy on the pore structure and interfacial groups in hydrated salts/silica composites via sol–gel. *Journal of Colloid and Interface Science* **2015**, *448*, 100-105.

(16) Tang, B.; Cui, J.; Wang, Y.; Jia, C.; Zhang, S. Facile synthesis and performances of PEG/SiO 2 composite form-stable phase change materials. *Solar Energy* **2013**, *97*, 484-492.

(17) Fang, G.; Li, H.; Liu, X. Preparation and properties of lauric acid/silicon dioxide composites as form-stable phase change materials for thermal energy storage. *Materials Chemistry and Physics* **2010**, *122*, 533-536.

(18) Stammen, J. A.; Williams, S.; Ku, D. N.; Guldberg, R. E. Mechanical properties of a novel PVA hydrogel in shear and unconfined compression. *Biomaterials* **2001**, *22*, 799-806.

(19) Hyon, S.-H.; Cha, W.-I.; Ikada, Y. Preparation of transparent poly (vinyl alcohol) hydrogel. *Polymer bulletin* **1989**, *22*, 119-122.

(20) Jiang, S.; Liu, S.; Feng, W. PVA hydrogel properties for biomedical application. *Journal of the mechanical behavior of biomedical materials* **2011**, *4*, 1228-1233.

(21) Muratoglu, O. K.; Spiegelberg, S. H.; Ruberti, J. W.; Abt, N.: PVA hydrogel. Google Patents, 2007.

(22) Alexandridis, P.; Holzwarth, J. F. Differential Scanning Calorimetry Investigation of the Effect of Salts on Aqueous Solution Properties of an Amphiphilic Block Copolymer (Poloxamer). *Langmuir* **1997**, *13*, 6074-6082.

(23) Bahadur, P.; Pandya, K.; Almgren, M.; Li, P.; Stilbs, P. Effect of inorganic salts on the micellar behaviour of ethylene oxide-propylene oxide block copolymers in aqueous solution. *Colloid and Polymer Science* **1993**, *271*, 657-667.

(24) Lee, S. B.; Song, S.-C.; Jin, J.-I.; Sohn, Y. S. A New Class of Biodegradable Thermosensitive Polymers. 2. Hydrolytic Properties and Salt Effect on the Lower Critical Solution Temperature of Poly(organophosphazenes) with Methoxypoly(ethylene glycol) and Amino Acid Esters as Side Groups. *Macromolecules* **1999**, *32*, 7820-7827.

(25) Hassan, C. M.; Peppas, N. A. Structure and morphology of freeze/thawed PVA hydrogels. *Macromolecules* **2000**, *33*, 2472-2479.

(26) Hassan, C. M.; Peppas, N. A.: Structure and applications of poly (vinyl alcohol) hydrogels produced by conventional crosslinking or by freezing/thawing methods. In *Biopolymers· PVA Hydrogels, Anionic Polymerisation Nanocomposites*; Springer, 2000; pp 37-65.

(27) Peppas, N. A.; Merrill, E. W. Development of semicrystalline poly (vinyl alcohol) hydrogels for biomedical applications. *Journal of Biomedical Materials Research* **1977**, *11*, 423-434.

(28) Peppas, N. A.; Stauffer, S. R. Reinforced uncrosslinked poly (vinyl alcohol) gels produced by cyclic freezing-thawing processes: a short review. *Journal of Controlled Release* **1991**, *16*, 305-310.

(29) Ikeda, S.; Morris, V. J.; Nishinari, K. Microstructure of Aggregated and Nonaggregated κ-Carrageenan Helices Visualized by Atomic Force Microscopy. *Biomacromolecules* **2001**, *2*, 1331-1337.

(30) Watase, M.; Nishinari, K. Effect of alkali metal ions on the viscoelasticity of concentrated kappa-carrageenan and agarose gels. *Rheologica Acta* **1982**, *21*, 318-324.

(31) Viebke, C.; Borgström, J.; Carlsson, I.; Piculell, L.; Williams, P. A differential scanning calorimetry study of κ-carrageenan in the NaCl/NaI/CsI/CsCl systems and analysis by Poisson-Boltzmann calculations. *Macromolecules* **1998**, *31*, 1833-1841.

(32) Li, Q.; Barrett, D. G.; Messersmith, P. B.; Holten-Andersen, N. Controlling hydrogel mechanics via bio-inspired polymer–nanoparticle bond dynamics. *ACS nano* **2016**, *10*, 1317-1324.

(33) Schultz, R. K.; Myers, R. R. The chemorheology of poly (vinyl alcohol)-borate gels. *Macromolecules* **1969**, *2*, 281-285.

(34) Watase, M.; Arakawa, K. Rheological properties of hydrogels of agar-agar. III. Stress relaxation of agarose gels. *Bulletin of the Chemical Society of Japan* **1968**, *41*, 1830-1834.

(35) Arakawa, K. Rheological properties of thermo-reversible gels. *Bulletin of the Chemical Society of Japan* **1962**, *35*, 309-312.

(36) Fumagalli, M.; Belal, K.; Guo, H.; Stoffelbach, F.; Cooke, G.; Marcellan, A.; Woisel, P.; Hourdet, D. Supramolecular polymer hydrogels induced by host–guest interactions with di-[cyclobis (paraquat-p-phenylene)] cross-linkers: from molecular complexation to viscoelastic properties. *Soft matter* **2017**, *13*, 5269-5282.

(37) Tan, C. S. Y.; Agmon, G.; Liu, J.; Hoogland, D.; Janeček, E.-R.; Appel, E. A.; Scherman, O. A. Distinguishing relaxation dynamics in transiently crosslinked polymeric networks. *Polymer Chemistry* **2017**, *8*, 5336-5343.

(38) Zhang, Z.; Huang, C.; Weiss, R.; Chen, Q. Association energy in strongly associative polymers. *Journal of Rheology* **2017**, *61*, 1199-1207.

(39) Chen, Q.; Tudryn, G. J.; Colby, R. H. Ionomer dynamics and the sticky Rouse model. *Journal of Rheology* **2013**, *57*, 1441-1462.

(40) Bohdan, M.; Sprakel, J.; Van Der Gucht, J. Multiple relaxation modes in associative polymer networks with varying connectivity. *Physical Review E* **2016**, *94*, 032507.

(41) Tanaka, T.; Hocker, L. O.; Benedek, G. B. Spectrum of light scattered from a viscoelastic gel. *The Journal of Chemical Physics* **1973**, *59*, 5151-5159.

(42) Candau, S.; Bastide, J.; Delsanti, M.: Structural, elastic, and dynamic properties of swollen polymer networks. In *Polymer Networks*; Springer, 1982; pp 27-71.

(43) Nystroem, B.; Lindman, B. Dynamic and viscoelastic properties during the thermal gelation process of a nonionic cellulose ether dissolved in water in the presence of ionic surfactants. *Macromolecules* **1995**, *28*, 967-974.

(44) Debuigne, A.; Detrembleur, C.; Bryaskova, R.; Caille, J.-R.; Jérôme, R.: Cobalt-mediated radical polymerization of vinyl acetate: a new tool for macromolecular engineering. ACS Publications, 2006.

(45) Tomalia, D. A.; Baker, H.; Dewald, J.; Hall, M.; Kallos, G.; Martin, S.; Roeck, J.; Ryder, J.; Smith, P. A New Class of Polymers: Starburst-Dendritic Macromolecules. *Polym J* **1985**, *17*, 117-132.

(46) de Belder, A. N.; Granath, K. Preparation and properties of fluorescein-labelled dextrans. *Carbohydrate Research* **1973**, *30*, 375-378.

(47) Sun, Q.; Guo, Y. Vibrational sum frequency generation spectroscopy of the air/water interface. *Journal of Molecular Liquids* **2016**, *213*, 28-32.

(48) Choe, C.; Lademann, J.; Darvin, M. E. Depth profiles of hydrogen bound water molecule types and their relation to lipid and protein interaction in the human stratum corneum in vivo. *Analyst* **2016**, *141*, 6329-6337.

(49) Max, J.-J.; Larouche, P.; Chapados, C. Orthogonalyzed H2O and D2O species obtained from infrared spectra of liquid water at several temperatures. *Journal of Molecular Structure* **2017**, *1149*, 457-472.

(50) Lam, S. J.; Sulistio, A.; Ladewig, K.; Wong, E. H. H.; Blencowe, A.; Qiao, G. G. Peptide-Based Star Polymers as Potential siRNA Carriers*. *Australian Journal of Chemistry* **2014**, *67*, 592-597.

(51) Müller, R.; Laschober, C.; Szymanski, W. W.; Allmaier, G. Determination of Molecular Weight, Particle Size, and Density of High Number Generation PAMAM

Dendrimers Using MALDI−TOF−MS and nES−GEMMA. *Macromolecules* **2007**, *40*, 5599-5605.

(52) Tomalia, D. A.; Naylor, A. M.; Goddard, W. A. Starburst Dendrimers: Molecular-Level Control of Size, Shape, Surface Chemistry, Topology, and Flexibility from Atoms to Macroscopic Matter. *Angewandte Chemie International Edition in English* **1990**, *29*, 138-175.

(53) Schwartz, B. L.; Rockwood, A. L.; Smith, R. D.; Tomalia, D. A.; Spindler, R. Detection of high molecular weight starburst dendrimers by electrospray ionization mass spectometry. *Rapid Communications in Mass Spectrometry* **1995**, *9*, 1552-1555.

(54) Hess, S. T.; Webb, W. W. Focal volume optics and experimental artifacts in confocal fluorescence correlation spectroscopy. *Biophysical journal* **2002**, *83*, 2300-2317.

(55) Krichevsky, O.; Bonnet, G. Fluorescence correlation spectroscopy: the technique and its applications. *Reports on Progress in Physics* **2002**, *65*, 251.

(56) Aragon, S.; Pecora, R. Fluorescence correlation spectroscopy as a probe of molecular dynamics. *The Journal of Chemical Physics* **1976**, *64*, 1791-1803.

(57) Rani, S. A.; Pitts, B.; Stewart, P. S. Rapid diffusion of fluorescent tracers into Staphylococcus epidermidis biofilms visualized by time lapse microscopy. *Antimicrobial agents and chemotherapy* **2005**, *49*, 728-732.

(58) Culbertson, C. T.; Jacobson, S. C.; Michael Ramsey, J. Diffusion coefficient measurements in microfluidic devices. *Talanta* **2002**, *56*, 365-373.

(59) Ryu, H. W.; Woo, S. W.; Shin, B. C.; Kim, S. D. Prevention of supercooling and stabilization of inorganic salt hydrates as latent heat storage materials. *Solar Energy Materials and Solar Cells* **1992**, *27*, 161-172.

(60) Koski, H. Calorimetric Study of Lithium Nitrate Trihydrate. . *Suomen Kemistilehti. B* **1972**, *45*, 135-141.

(61) Nedeljkovic, L. Fusion and Formation Enthalpies of Lithium Nitrate Trihydrate. *Z. Anorg. Allg. Chem* **1968**, *357*, 103-106.

(62) Shamberger, P. J.; O'Malley, M. J. Heterogeneous nucleation of thermal storage material LiNO3·3H2O from stable lattice-matched nucleation catalysts. *Acta Materialia* **2015**, *84*, 265-274.

(63) Wu, Y.; Wang, T. Preparation and characterization of hydrated salts/silica composite as shape-stabilized phase change material via sol–gel process. *Thermochimica Acta* **2014**, *591*, 10-15.

(64) Wu, Y.; Wang, T. Hydrated salts/expanded graphite composite with high thermal conductivity as a shape-stabilized phase change material for thermal energy storage. *Energy Conversion and Management* **2015**, *101*, 164-171.

(65) Wang, Y.; Libera, M.; Busscher, H. J.; van der Mei, H. C.: Mono-functional to multifunctional coatings: The changing paradigm to control biofilm formation on biomedical implants. In *Biofilms in Bioengineering*; Simoes, M., Mergulho, F., Eds.; Nova Science: Commack, 2012.

(66) Zhang, H.; Wang, X.; Wu, D. Silica encapsulation of n-octadecane via sol–gel process: a novel microencapsulated phase-change material with enhanced thermal

conductivity and performance. *Journal of colloid and interface science* **2010**, *343*, 246-255.

(67) Tang, B.; Cui, J.; Wang, Y.; Jia, C.; Zhang, S. Facile synthesis and performances of PEG/SiO2 composite form-stable phase change materials. *Solar Energy* **2013**, *97*, 484-492.

(68) Ward, M. A.; Georgiou, T. K. Thermoresponsive Polymers for Biomedical Applications. *Polymers* **2011**, *3*, 1215.

(69) Klouda, L.; Mikos, A. G. Thermoresponsive hydrogels in biomedical applications. *European Journal of Pharmaceutics and Biopharmaceutics* **2008**, *68*, 34-45.

(70) Malmsten, M.; Lindman, B. Self-assembly in aqueous block copolymer solutions. *Macromolecules* **1992**, *25*, 5440-5445.

(71) Pandit, N. K.; Kisaka, J. Loss of gelation ability of Pluronic® F127 in the presence of some salts. *International Journal of Pharmaceutics* **1996**, *145*, 129-136.

(72) Pandit, N. K.; Wang, D. Salt effects on the diffusion and release rate of propranolol from poloxamer 407 gels. *International Journal of Pharmaceutics* **1998**, *167*, 183-189.

(73) Trindade, J. R.; Visak, Z. P.; Blesic, M.; Marrucho, I. M.; Coutinho, J. A.; Canongia Lopes, J. N.; Rebelo, L. P. Salting-out effects in aqueous ionic liquid solutions: cloud-point temperature shifts. *The Journal of Physical Chemistry B* **2007**, *111*, 4737-4741.

(74) Winter, R.; Hua, D. W.; Song, X.; Mantulin, W.; Jonas, J. Structural and dynamical properties of the sol-gel transition. *The Journal of Physical Chemistry* **1990**, *94*, 2706-2713.

(75) Briscoe, B.; Luckham, P.; Zhu, S. The effects of hydrogen bonding upon the viscosity of aqueous poly(vinyl alcohol) solutions. *Polymer* **2000**, *41*, 3851-3860.

(76) Carnali, J. O. Gelation in physically associating biopolymer systems. *Rheologica Acta* **1992**, *31*, 399-412.

(77) Kobayashi, K.; Huang, C.-i.; Lodge, T. P. Thermoreversible gelation of aqueous methylcellulose solutions. *Macromolecules* **1999**, *32*, 7070-7077.

(78) Su, H.; Wang, X.; Du, M.; Song, Y.; Zheng, Q. Boundary lubricating properties of hydrophobically modified polyacrylamide. *RSC Advances* **2016**, *6*, 5695-5702.

(79) Manasco, J. L.; Tang, C.; Burns, N. A.; Saquing, C. D.; Khan, S. A. Rapidly dissolving poly (vinyl alcohol)/cyclodextrin electrospun nanofibrous membranes. *RSC Advances* **2014**, *4*, 13274-13279.

(80) Michelman-Ribeiro, A.; Horkay, F.; Nossal, R.; Boukari, H. Probe diffusion in aqueous poly (vinyl alcohol) solutions studied by fluorescence correlation spectroscopy. *Biomacromolecules* **2007**, *8*, 1595-1600.

(81) Wang, B.; Mukataka, S.; Kokufuta, E.; Ogiso, M.; Kodama, M. Viscometric, light scattering, and size-exclusion chromatography studies on the structural changes of aqueous poly (vinyl alcohol) induced by γ-ray irradiation. *Journal of Polymer Science Part B: Polymer Physics* **2000**, *38*, 214-221.

(82) Rajendran, S.; Sivakumar, M.; Subadevi, R. Li-ion conduction of plasticized PVA solid polymer electrolytes complexed with various lithium salts. *Solid State Ionics* **2004**, *167*, 335-339.

(83) Noor, I. S.; Majid, S. R.; Arof, A. K. Poly(vinyl alcohol)–LiBOB complexes for lithium–air cells. *Electrochimica Acta* **2013**, *102*, 149-160.

(84) Rajendran, S.; Sivakumar, M.; Subadevi, R.; Nirmala, M. Characterization of PVA–PVdF based solid polymer blend electrolytes. *Physica B: Condensed Matter* **2004**, *348*, 73-78.

(85) Krasovitski, E.; Cohen, Y.; Bianco-Peled, H. The effect of salts on the conformation and microstructure of poly(N-isopropylacrylamide) (PNIPA) in aqueous solution. *Journal of Polymer Science Part B: Polymer Physics* **2004**, *42*, 3713-3720.

(86) Muniz-Miranda, F.; Pagliai, M.; Cardini, G.; Righini, R. Bifurcated Hydrogen Bond in Lithium Nitrate Trihydrate Probed by ab Initio Molecular Dynamics. *The Journal of Physical Chemistry A* **2012**, *116*, 2147-2153.

(87) Goebbert, D. J.; Garand, E.; Wende, T.; Bergmann, R.; Meijer, G.; Asmis, K. R.; Neumark, D. M. Infrared Spectroscopy of the Microhydrated Nitrate Ions NO3−(H2O)1−6. *The Journal of Physical Chemistry A* **2009**, *113*, 7584-7592.

(88) Buslov, D.; Sushko, N.; Tretinnikov, O. IR Investigation of hydrogen bonds in weakly hydrated films of poly (vinyl alcohol). *Polymer Science Series A* **2011**, *53*, 1121-1127.

(89) Otsuka, E.; Suzuki, A. A simple method to obtain a swollen PVA gel crosslinked by hydrogen bonds. *Journal of applied polymer science* **2009**, *114*, 10-16.

(90) Mähler, J.; Persson, I. A study of the hydration of the alkali metal ions in aqueous solution. *Inorganic chemistry* **2011**, *51*, 425-438.

(91) Dawedeit, C.; Kim, S. H.; Braun, T.; Worsley, M. A.; Letts, S. A.; Wu, K. J.; Walton, C. C.; Chernov, A. A.; Satcher, J. H.; Hamza, A. V. Tuning the rheological properties of sols for low-density aerogel coating applications. *Soft Matter* **2012**, *8*, 3518-3521.

(92) Di Biase, M.; de Leonardis, P.; Castelletto, V.; Hamley, I. W.; Derby, B.; Tirelli, N. Photopolymerization of Pluronic F127 diacrylate: a colloid-templated polymerization. *Soft Matter* **2011**, *7*, 4928-4937.

(93) Ikkai, F.; Shibayama, M. Static Inhomogeneities in Thermoreversible Physical Gels. *Physical Review Letters* **1999**, *82*, 4946-4949.

(94) Martin, J. E.; Wilcoxon, J.; Odinek, J. Decay of density fluctuations in gels. *Physical Review A* **1991**, *43*, 858-872.

(95) Matsunaga, T.; Shibayama, M. Gel point determination of gelatin hydrogels by dynamic light scattering and rheological measurements. *Phys Rev E Stat Nonlin Soft Matter Phys* **2007**, *76*, 030401.

(96) Park, S. Y.; Han, D. K.; Kim, S. C. Synthesis and Characterization of Star-Shaped PLLA−PEO Block Copolymers with Temperature-Sensitive Sol−Gel Transition Behavior. *Macromolecules* **2001**, *34*, 8821-8824.

(97) Song, M. J.; Lee, D. S.; Ahn, J. H.; Kim, D. J.; Kim, S. C. Dielectric behavior during sol-gel transition of PEO-PPO-PEO triblock copolymer aqueous solution. *Polymer Bulletin* **2000**, *43*, 497-504.

(98) Lee, Y.; Chung, H. J.; Yeo, S.; Ahn, C.-H.; Lee, H.; Messersmith, P. B.; Park, T. G. Thermo-sensitive, injectable, and tissue adhesive sol–gel transition hyaluronic acid/pluronic composite hydrogels prepared from bio-inspired catechol-thiol reaction. *Soft Matter* **2010**, *6*, 977-983.

(99) Van Den Bulcke, A. I.; Bogdanov, B.; De Rooze, N.; Schacht, E. H.; Cornelissen, M.; Berghmans, H. Structural and Rheological Properties of Methacrylamide Modified Gelatin Hydrogels. *Biomacromolecules* **2000**, *1*, 31-38.

(100) Miyoshi, E.; Takaya, T.; Nishinari, K. Effects of glucose, mannose and konjac glucomannan on the gel–sol transition in gellan gum aqueous solutions by rheology and DSC. *Polymer Gels and Networks* **1998**, *6*, 273-290.

(101) Busato, A. P.; Reicher, F.; Domingues, R.; Silveira, J. L. M. Rheological properties of thermally xyloglucan gel from the seeds of Hymenaea courbaril. *Materials Science and Engineering: C* **2009**, *29*, 410-414.

(102) Dutta, S.; Shome, A.; Debnath, S.; Das, P. K. Counterion dependent hydrogelation of amino acid based amphiphiles: switching from non-gelators to gelators and facile synthesis of silver nanoparticles. *Soft Matter* **2009**, *5*, 1607-1620.

(103) Priestley, R. D.; Ellison, C. J.; Broadbelt, L. J.; Torkelson, J. M. Structural relaxation of polymer glasses at surfaces, interfaces, and in between. *Science* **2005**, *309*, 456-459.

(104) Reddy, N. K.; Zhang, Z.; Lettinga, M. P.; Dhont, J. K.; Vermant, J. Probing structure in colloidal gels of thermoreversible rodlike virus particles: Rheology and scattering. *Journal of Rheology (1978-present)* **2012**, *56*, 1153-1174.

(105) Kavanagh, G. M.; Ross-Murphy, S. B. Rheological characterisation of polymer gels. *Progress in Polymer Science* **1998**, *23*, 533-562.

(106) Gupta, P.; Vermani, K.; Garg, S. Hydrogels: from controlled release to pH-responsive drug delivery. *Drug Discovery Today* **2002**, *7*, 569-579.

(107) Appel, E. A.; del Barrio, J.; Loh, X. J.; Scherman, O. A. Supramolecular polymeric hydrogels. *Chemical Society Reviews* **2012**, *41*, 6195-6214.

(108) Ibrahim, M. M.; Hafez, S. A.; Mahdy, M. M. Organogels, hydrogels and bigels as transdermal delivery systems for diltiazem hydrochloride. *Asian Journal of Pharmaceutical Sciences* **2013**, *8*, 48-57.

(109) Zhao, Z.; Zhang, K.; Liu, Y.; Zhou, J.; Liu, M. Highly Stretchable, Shape Memory Organohydrogels Using Phase-Transition Microinclusions. *Advanced Materials* **2017**, *29*.

(110) Deng, G.; Tang, C.; Li, F.; Jiang, H.; Chen, Y. Covalent cross-linked polymer gels with reversible sol− gel transition and self-healing properties. *Macromolecules* **2010**, *43*, 1191-1194.

(111) Yang, Y.; Urban, M. W. Self-healing polymeric materials. *Chemical Society Reviews* **2013**, *42*, 7446-7467.

(112) Bromberg, L. E.; Ron, E. S. Temperature-responsive gels and thermogelling polymer matrices for protein and peptide delivery. *Advanced drug delivery reviews* **1998**, *31*, 197-221.

(113) Zhou, F.; Shu, W.; Welland, M. E.; Huck, W. T. Highly reversible and multi-stage cantilever actuation driven by polyelectrolyte brushes. *Journal of the American Chemical Society* **2006**, *128*, 5326-5327.

(114) Valiaev, A.; Abu-Lail, N. I.; Lim, D. W.; Chilkoti, A.; Zauscher, S. Microcantilever sensing and actuation with end-grafted stimulus-responsive elastin-like polypeptides. *Langmuir* **2007**, *23*, 339-344.

(115) Blanazs, A.; Armes, S. P.; Ryan, A. J. Self-assembled block copolymer aggregates: from micelles to vesicles and their biological applications. *Macromolecular rapid communications* **2009**, *30*, 267-277.

(116) Stuart, M. A. C.; Huck, W. T.; Genzer, J.; Müller, M.; Ober, C.; Stamm, M.; Sukhorukov, G. B.; Szleifer, I.; Tsukruk, V. V.; Urban, M. Emerging applications of stimuli-responsive polymer materials. *Nature materials* **2010**, *9*, 101-113.

(117) Appel, E. A.; Tibbitt, M. W.; Webber, M. J.; Mattix, B. A.; Veiseh, O.; Langer, R. Self-assembled hydrogels utilizing polymer–nanoparticle interactions. *Nature communications* **2015**, *6*.

(118) Lee, K. Y.; Mooney, D. J. Hydrogels for tissue engineering. *Chemical reviews* **2001**, *101*, 1869-1880.

(119) Puig, J.; dell' Erba, I. E.; Schroeder, W. F.; Hoppe, C. E.; Williams, R. J. J. Epoxy-Based Organogels for Thermally Reversible Light Scattering Films and Form-Stable Phase Change Materials. *ACS Applied Materials & Interfaces* **2017**, *9*, 11126-11133.

(120) Hale, D.; Hoover, M.; ONeill, M. Phase change materials handbook. **1971**.

(121) Hoover, M.; Grodzka, P. G.; Oneill, M. Space thermal control development. **1971**.

(122) Zhang, Y.; Wang, L.; Tang, B.; Lu, R.; Zhang, S. Form-stable phase change materials with high phase change enthalpy from the composite of paraffin and cross-linking phase change structure. *Applied Energy* **2016**, *184*, 241-246.

(123) Xie, Y.; Kim, W.; Kim, Y.; Kim, S.; Gonsalves, J.; BrightSky, M.; Lam, C.; Zhu, Y.; Cha, J. J. Self-Healing of a Confined Phase Change Memory Device with a Metallic Surfactant Layer. *Advanced Materials* **2018**, *30*.

(124) Markovic, N.; Dutta, N. K. Physical organogels: mechanism and kinetics of evaporation of the solvents entrapped within network scaffolding. *Thermochimica Acta* **2005**, *427*, 207-219.

(125) Singh, V. K.; Pal, K.; Pradhan, D. K.; Pramanik, K. Castor oil and sorbitan monopalmitate based organogel as a probable matrix for controlled drug delivery. *Journal of Applied Polymer Science* **2013**, *130*, 1503-1515.

(126) Shibayama, M.; Hiroyuki, Y.; Hidenobu, K.; Hiroshi, F.; Shunji, N. Sol-gel transition of poly (vinyl alcohol)-borate complex. *Polymer* **1988**, *29*, 2066-2071.

(127) Na, Y.-H.; Kurokawa, T.; Katsuyama, Y.; Tsukeshiba, H.; Gong, J. P.; Osada, Y.; Okabe, S.; Karino, T.; Shibayama, M. Structural characteristics of double network gels with extremely high mechanical strength. *Macromolecules* **2004**, *37*, 5370-5374.

(128) Huang, M.; Furukawa, H.; Tanaka, Y.; Nakajima, T.; Osada, Y.; Gong, J. P. Importance of Entanglement between First and Second Components in High-Strength Double Network Gels. *Macromolecules* **2007**, *40*, 6658-6664.

(129) Chen, X.; Zhang, Y.; Wang, H.; Wang, S.-W.; Liang, S.; Colby, R. H. Solution rheology of cellulose in 1-butyl-3-methyl imidazolium chloride. *Journal of Rheology* **2011**, *55*, 485-494.

(130) He, Y.; Boswell, P. G.; Bühlmann, P.; Lodge, T. P. Ion gels by self-assembly of a triblock copolymer in an ionic liquid. *The Journal of Physical Chemistry B* **2007**, *111*, 4645-4652.

(131) Yamada, Y.; Usui, K.; Sodeyama, K.; Ko, S.; Tateyama, Y.; Yamada, A. Hydrate-melt electrolytes for high-energy-density aqueous batteries. *Nature Energy* **2016**, *1*, 16129.

(132) Shamberger, P. J.; Reid, T. Thermophysical properties of potassium fluoride tetrahydrate from (243 to 348) K. *Journal of Chemical & Engineering Data* **2013**, *58*, 294-300.

(133) Wu, Y.; Wang, T. Preparation and characterization of hydrated salts/silica composite as shape-stabilized phase change material via sol–gel process. *Thermochimica Acta* **2014**, *591*, 10-15.

(134) Mohan, V.; Qiu, W.; Shen, J.; Chen, W. Electrical properties of poly (vinyl alcohol)(PVA) based on LiFePO4 complex polymer electrolyte films. *Journal of polymer research* **2010**, *17*, 143.

(135) Ricciardi, R.; Auriemma, F.; De Rosa, C.; Lauprêtre, F. X-ray Diffraction Analysis of Poly(vinyl alcohol) Hydrogels, Obtained by Freezing and Thawing Techniques. *Macromolecules* **2004**, *37*, 1921-1927.

(136) Li, L.; Aoki, Y. Rheological images of poly (vinyl chloride) gels. 1. The dependence of sol− gel transition on concentation. *Macromolecules* **1997**, *30*, 7835-7841.

(137) Michon, C.; Cuvelier, G.; Launay, B. Concentration dependence of the critical viscoelastic properties of gelatin at the gel point. *Rheologica Acta* **1993**, *32*, 94-103.

(138) Shibayama, M.; Hiroyuki, Y.; Hidenobu, K.; Hiroshi, F.; Shunji, N. Sol-gel transition of poly(vinyl alcohol)-borate complex. *Polymer* **1988**, *29*, 2066-2071.

(139) Winter, H. H.; Chambon, F. Analysis of linear viscoelasticity of a crosslinking polymer at the gel point. *Journal of rheology* **1986**, *30*, 367-382.

(140) Winter, H. Can the gel point of a cross-linking polymer be detected by the G′–G ″crossover? *Polymer Engineering & Science* **1987**, *27*, 1698-1702.

(141) Winter, H. H.; Mours, M.: Rheology of Polymers Near Liquid-Solid Transitions. In *Neutron Spin Echo Spectroscopy Viscoelasticity Rheology*; Springer Berlin Heidelberg: Berlin, Heidelberg, 1997; pp 165-234.

(142) Denisin, A. K.; Pruitt, B. L. Tuning the range of polyacrylamide gel stiffness for mechanobiology applications. *ACS applied materials & interfaces* **2016**, *8*, 21893-21902.

(143) De Rosa, M.; Winter, H. The effect of entanglements on the rheological behavior of polybutadiene critical gels. *Rheologica acta* **1994**, *33*, 220-237.

(144) Cohen, Y.; Ramon, O.; Kopelman, I.; Mizrahi, S. Characterization of inhomogeneous polyacrylamide hydrogels. *Journal of Polymer Science Part B: Polymer Physics* **1992**, *30*, 1055-1067.

(145) Baselga, J.; Hernandez-Fuentes, I.; Pierola, I.; Llorente, M. Elastic properties of highly crosslinked polyacrylamide gels. *Macromolecules* **1987**, *20*, 3060-3065.

(146) Flory, P. J.: *Principles of polymer chemistry*; Cornell University Press, 1953.

(147) Wang, Q.; Mynar, J. L.; Yoshida, M.; Lee, E.; Lee, M.; Okuro, K.; Kinbara, K.; Aida, T. High-water-content mouldable hydrogels by mixing clay and a dendritic molecular binder. *Nature* **2010**, *463*, 339-343.

(148) Ying, H.; Zhang, Y.; Cheng, J. Dynamic urea bond for the design of reversible and self-healing polymers. *Nature communications* **2014**, *5*, 3218.

(149) de Greef, T. F.; Meijer, E. Materials science: supramolecular polymers. *Nature* **2008**, *453*, 171-173.

(150) Zhao, Z.; Liu, Y.; Zhang, K.; Zhuo, S.; Fang, R.; Zhang, J.; Jiang, L.; Liu, M. Biphasic Synergistic Gel Materials with Switchable Mechanics and Self-Healing Capacity. *Angewandte Chemie International Edition* **2017**, *56*, 13464-13469.

(151) Zhang, H.; Xia, H.; Zhao, Y. Poly (vinyl alcohol) hydrogel can autonomously self-heal. *Acs Macro Letters* **2012**, *1*, 1233-1236.

(152) Han, J.; Lei, T.; Wu, Q. High-water-content mouldable polyvinyl alcohol-borax hydrogels reinforced by well-dispersed cellulose nanoparticles: Dynamic

rheological properties and hydrogel formation mechanism. *Carbohydrate Polymers* **2014**, *102*, 306-316.

(153) Li, G.; Zhang, H.; Fortin, D.; Xia, H.; Zhao, Y. Poly (vinyl alcohol)–Poly (ethylene glycol) Double-Network Hydrogel: A General Approach to Shape Memory and Self-Healing Functionalities. *Langmuir* **2015**, *31*, 11709-11716.

(154) Refojo, M. F. Hydrophobic interaction in poly (2-hydroxyethyl methacrylate) homogeneous hydrogel. *Journal of Polymer Science Part A-1: Polymer Chemistry* **1967**, *5*, 3103-3113.

(155) Tuncaboylu, D. C.; Sari, M.; Oppermann, W.; Okay, O. Tough and self-healing hydrogels formed via hydrophobic interactions. *Macromolecules* **2011**, *44*, 4997-5005.

(156) Suzuki, M.; Nakajima, Y.; Yumoto, M.; Kimura, M.; Shirai, H.; Hanabusa, K. Effects of hydrogen bonding and van der Waals interactions on organogelation using designed low-molecular-weight gelators and gel formation at room temperature. *Langmuir* **2003**, *19*, 8622-8624.

(157) Fullenkamp, D. E.; He, L.; Barrett, D. G.; Burghardt, W. R.; Messersmith, P. B. Mussel-inspired histidine-based transient network metal coordination hydrogels. *Macromolecules* **2013**, *46*, 1167-1174.

(158) Grindy, S. C.; Learsch, R.; Mozhdehi, D.; Cheng, J.; Barrett, D. G.; Guan, Z.; Messersmith, P. B.; Holten-Andersen, N. Control of hierarchical polymer mechanics with bioinspired metal-coordination dynamics. *Nature materials* **2015**, *14*, 1210.

(159) Guo, M.; Pitet, L. M.; Wyss, H. M.; Vos, M.; Dankers, P. Y.; Meijer, E. Tough stimuli-responsive supramolecular hydrogels with hydrogen-bonding network junctions. *Journal of the American Chemical Society* **2014**, *136*, 6969-6977.

(160) Hu, X.; Vatankhah-Varnoosfaderani, M.; Zhou, J.; Li, Q.; Sheiko, S. S. Weak hydrogen bonding enables hard, strong, tough, and elastic hydrogels. *Advanced materials* **2015**, *27*, 6899-6905.

(161) Zhang, Z.; Liu, C.; Cao, X.; Gao, L.; Chen, Q. Linear viscoelastic and dielectric properties of strongly hydrogen-bonded polymers near the sol–gel transition. *Macromolecules* **2016**, *49*, 9192-9202.

(162) Leibler, L.; Rubinstein, M.; Colby, R. H. Dynamics of reversible networks. *Macromolecules* **1991**, *24*, 4701-4707.

(163) Chen, Q.; Huang, C.; Weiss, R.; Colby, R. H. Viscoelasticity of reversible gelation for ionomers. *Macromolecules* **2015**, *48*, 1221-1230.

(164) Huang, C.; Chen, Q.; Weiss, R. Nonlinear Rheology of Random Sulfonated Polystyrene Ionomers: The Role of the Sol–Gel Transition. *Macromolecules* **2016**, *49*, 9203-9214.

(165) Huang, C.; Wang, C.; Chen, Q.; Colby, R. H.; Weiss, R. Reversible gelation model predictions of the linear viscoelasticity of oligomeric sulfonated polystyrene ionomer blends. *Macromolecules* **2016**, *49*, 3936-3947.

(166) Budtova, T.; Navard, P. Viscosity-temperature dependence and activation energy of cellulose solutions. *Nordic Pulp & Paper Research Journal* **2015**, *30*, 99-104.

(167) Porter, R. S.; Johnson, J. F. In *Tilte*1967; Wiley Online Library.

(168) Feldman, K. E.; Kade, M. J.; Meijer, E.; Hawker, C. J.; Kramer, E. J. Model transient networks from strongly hydrogen-bonded polymers. *Macromolecules* **2009**, *42*, 9072-9081.

(169) Baeza, G. P.; Dessi, C.; Costanzo, S.; Zhao, D.; Gong, S.; Alegria, A.; Colby, R. H.; Rubinstein, M.; Vlassopoulos, D.; Kumar, S. K. Network dynamics in nanofilled polymers. *Nature Communications* **2016**, *7*, 11368.

(170) Tierney, N. K.; Register, R. A. Ion hopping in ethylene− methacrylic acid ionomer melts as probed by rheometry and cation diffusion measurements. *Macromolecules* **2002**, *35*, 2358-2364.

(171) Weiss, R.; Zhao, H. Rheological behavior of oligomeric ionomers. *Journal of Rheology* **2009**, *53*, 191-213.

(172) Koike, A.; Nemoto, N.; Inoue, T.; Osaki, K. Dynamic light scattering and dynamic viscoelasticity of poly (vinyl alcohol) in aqueous borax solutions. 1. Concentration effect. *Macromolecules* **1995**, *28*, 2339-2344.

(173) Brochard, F.; De Gennes, P. Dynamical scaling for polymers in theta solvents. *Macromolecules* **1977**, *10*, 1157-1161.

(174) Li, J.; Ngai, T.; Wu, C. The slow relaxation mode: from solutions to gel networks. *Polymer journal* **2010**, *42*, 609.

(175) Doi, M.; Onuki, A. Dynamic coupling between stress and composition in polymer solutions and blends. *Journal de Physique II* **1992**, *2*, 1631-1656.

(176) Brochard, F. Gel-like modes. of polymer solutions in «θ» solvents. *Journal de Physique* **1983**, *44*, 39-43.

(177) Zhang, E.; Zhao, Y.; Yang, W.; Chen, H.; Liu, W.; Dai, X.; Qiu, X.; Ji, X. Viscoelastic behaviour and relaxation modes of one polyamic acid organogel studied by rheometers and dynamic light scattering. *Soft matter* **2018**, *14*, 73-82.

(178) Ramos, L.; Cipelletti, L. Ultraslow dynamics and stress relaxation in the aging of a soft glassy system. *Physical review letters* **2001**, *87*, 245503.

(179) Tuncaboylu, D. C.; Sahin, M.; Argun, A.; Oppermann, W.; Okay, O. Dynamics and large strain behavior of self-healing hydrogels with and without surfactants. *Macromolecules* **2012**, *45*, 1991-2000.

(180) Nicolai, T.; Brown, W.; Hvidt, S.; Heller, K. A comparison of relaxation time distributions obtained from dynamic light scattering and dynamic mechanical measurements for high-molecular-weight polystyrene in entangled solutions. *Macromolecules* **1990**, *23*, 5088-5096.

(181) Hu, X.; Zhou, J.; Daniel, W. F.; Vatankhah-Varnoosfaderani, M.; Dobrynin, A. V.; Sheiko, S. S. Dynamics of dual networks: strain rate and temperature effects in hydrogels with reversible H-bonds. *Macromolecules* **2017**, *50*, 652-659.

(182) Bomboi, F.; Romano, F.; Leo, M.; Fernandez-Castanon, J.; Cerbino, R.; Bellini, T.; Bordi, F.; Filetici, P.; Sciortino, F. Re-entrant DNA gels. *Nature communications* **2016**, *7*, 13191.

(183) Bomboi, F.; Biffi, S.; Cerbino, R.; Bellini, T.; Bordi, F.; Sciortino, F. Equilibrium gels of trivalent DNA-nanostars: effect of the ionic strength on the dynamics. *The European Physical Journal E* **2015**, *38*, 64.

(184) Biffi, S.; Cerbino, R.; Bomboi, F.; Paraboschi, E. M.; Asselta, R.; Sciortino, F.; Bellini, T. Phase behavior and critical activated dynamics of limited-valence DNA nanostars. *Proceedings of the National Academy of Sciences* **2013**, *110*, 15633-15637.

(185) Karimineghlani, P.; Palanisamy, A.; Sukhishvili, S. A. Self-Healing Phase Change Salogels with Tunable Gelation Temperature. *ACS Applied Materials & Interfaces* **2018**, *10*, 14786-14795.

(186) Bosman, d. A.; Janssen, H.; Meijer, E. About dendrimers: structure, physical properties, and applications. *Chemical reviews* **1999**, *99*, 1665-1688.

(187) Love, C. S.; Hirst, A. R.; Chechik, V.; Smith, D. K.; Ashworth, I.; Brennan, C. One-component gels based on peptidic dendrimers: Dendritic effects on materials properties. *Langmuir* **2004**, *20*, 6580-6585.

(188) Tamesue, S.; Ohtani, M.; Yamada, K.; Ishida, Y.; Spruell, J. M.; Lynd, N. A.; Hawker, C. J.; Aida, T. Linear versus dendritic molecular binders for hydrogel network formation with clay nanosheets: studies with ABA triblock copolyethers carrying guanidinium ion pendants. *Journal of the American Chemical Society* **2013**, *135*, 15650-15655.

(189) Okamoto, M.; Norisuye, T.; Shibayama, M. Time-Resolved Dynamic Light Scattering Study on Gelation and Gel-Melting Processes of Gelatin Gels. *Macromolecules* **2001**, *34*, 8496-8502.

(190) Titantah, J. T.; Karttunen, M. Water dynamics: Relation between hydrogen bond bifurcations, molecular jumps, local density & hydrophobicity. *Scientific reports* **2013**, *3*, 2991.

(191) Zhao, X.; Huebsch, N.; Mooney, D. J.; Suo, Z. Stress-relaxation behavior in gels with ionic and covalent crosslinks. *Journal of applied physics* **2010**, *107*, 063509.

(192) Chaudhuri, O.; Gu, L.; Klumpers, D.; Darnell, M.; Bencherif, S. A.; Weaver, J. C.; Huebsch, N.; Lee, H.-p.; Lippens, E.; Duda, G. N. Hydrogels with tunable stress relaxation regulate stem cell fate and activity. *Nature materials* **2016**, *15*, 326.

(193) Drzal, P. L.; Shull, K. R. Origins of Mechanical Strength and Elasticity in Thermally Reversible, Acrylic Triblock Copolymer Gels. *Macromolecules* **2003**, *36*, 2000-2008.

(194) Zabet, M.; Mishra, S.; Kundu, S. Effect of graphene on the self-assembly and rheological behavior of a triblock copolymer gel. *RSC Advances* **2015**, *5*, 83936-83944.

(195) Han, Y.; Li, J.; Zhang, Z.; Liu, Y.; Li, Y.; Chen, Q. Linear viscoelasticity of poly (acrylic acid) complexed with ferric ion. *Rheologica Acta* **2019**, 1-11.

(196) Nemoto, N.; Koike, A.; Osaki, K. Dynamic light scattering and dynamic viscoelasticity of poly (vinyl alcohol) in aqueous borax solutions. 2. Polymer concentration and molecular weight effects. *Macromolecules* **1996**, *29*, 1445-1451.

(197) Narita, T.; Mayumi, K.; Ducouret, G.; Hébraud, P. Viscoelastic properties of poly (vinyl alcohol) hydrogels having permanent and transient cross-links studied by

microrheology, classical rheometry, and dynamic light scattering. *Macromolecules* **2013**, *46*, 4174-4183.

(198) Fuchs, T.; Richtering, W.; Burchard, W.; Kajiwara, K.; Kitamura, S. Gel point in physical gels: rheology and light scattering from thermoreversibly gelling schizophyllan. *Polymer Gels and Networks* **1998**, *5*, 541-559.

(199) Lin, H.-L.; Liu, Y.-F.; Yu, T. L.; Liu, W.-H.; Rwei, S.-P. Light scattering and viscoelasticity study of poly (vinyl alcohol)–borax aqueous solutions and gels. *Polymer* **2005**, *46*, 5541-5549.

(200) Zainuddin; Cooper-White, J. J.; Hill, D. J. Viscoelasticity of radiation-formed PVA/PVP hydrogel. *Journal of Biomaterials Science, Polymer Edition* **2002**, *13*, 1007-1020.

(201) Lin, H.-L.; Liu, W.-H.; Shen, K.-S.; Yu, T. L.; Cheng, C.-H. Weak gel behaviour of poly (vinyl alcohol)-borax aqueous solutions. *Journal of Polymer Research* **2003**, *10*, 171-179.

(202) Zhou, D.; Zhao, C.-Y.; Tian, Y. Review on thermal energy storage with phase change materials (PCMs) in building applications. *Applied energy* **2012**, *92*, 593-605.

(203) Mohamed, S. A.; Al-Sulaiman, F. A.; Ibrahim, N. I.; Zahir, M. H.; Al-Ahmed, A.; Saidur, R.; Yılbaş, B.; Sahin, A. A review on current status and challenges of inorganic phase change materials for thermal energy storage systems. *Renewable and Sustainable Energy Reviews* **2017**, *70*, 1072-1089.

(204) Kumar, N.; Hirschey, J.; LaClair, T. J.; Gluesenkamp, K. R.; Graham, S. Review of stability and thermal conductivity enhancements for salt hydrates. *Journal of Energy Storage* **2019**, *24*, 100794.

(205) Karimineghlani, P.; Sukhishvili, S. A. Activation Energy for Dissociation of Hydrogen-Bonding Crosslinkers in Phase-Change Salogels: Dynamic Light Scattering versus Rheological Studies. *Macromolecular Chemistry and Physics* **2019**, *220*, 1900329.

(206) Tsujimoto, M.; Shibayama, M. Dynamic Light Scattering Study on Reentrant Sol− Gel Transition of Poly (vinyl alcohol)− Congo Red Complex in Aqueous Media. *Macromolecules* **2002**, *35*, 1342-1347.

(207) Gao, L.; Guo, G.; Liu, M.; Tang, Z.; Xie, L.; Huo, Y. Multi-responsive, bidirectional, and large deformation bending actuators based on borax cross-linked polyvinyl alcohol derivative hydrogel. *RSC Advances* **2017**, *7*, 40005-40014.

(208) Ochiai, H.; Kurita, Y.; Murakami, I. Viscosity behavior of the polyelectrolyte poly (vinyl alcohol) having some intrachain crosslinks. *Die Makromolekulare Chemie: Macromolecular Chemistry and Physics* **1984**, *185*, 167-172.

(209) Li, J.; Zhang, Z.; Cao, X.; Liu, Y.; Chen, Q. The role of electrostatic repulsion in the gelation of poly (vinyl alcohol)/borax aqueous solutions. *Soft matter* **2018**, *14*, 6767-6773.

(210) Shibayama, M.; Adachi, M.; Ikkai, F.; Kurokawa, H.; Sakurai, S.; Nomura, S. Gelation of poly (vinyl alcohol)-vanadate aqueous solutions. *Macromolecules* **1993**, *26*, 623-627.

(211) Kharel, A.; Lodge, T. P. Effect of Ionic Liquid Components on the Coil Dimensions of PEO. *Macromolecules* **2019**, *52*, 3123-3130.

(212) Lee, H.-N.; Lodge, T. P. Lower Critical Solution Temperature (LCST) Phase Behavior of Poly(ethylene oxide) in Ionic Liquids. *The Journal of Physical Chemistry Letters* **2010**, *1*, 1962-1966.

(213) Lee, H.-N.; Newell, N.; Bai, Z.; Lodge, T. P. Unusual lower critical solution temperature phase behavior of poly (ethylene oxide) in ionic liquids. *Macromolecules* **2012**, *45*, 3627-3633.

(214) Mondal, J.; Choi, E.; Yethiraj, A. Atomistic Simulations of Poly(ethylene oxide) in Water and an Ionic Liquid at Room Temperature. *Macromolecules* **2014**, *47*, 438-446.

(215) Wang, Z.; Wu, P. Spectral Insights into Gelation Microdynamics of PNIPAM in an Ionic Liquid. *The Journal of Physical Chemistry B* **2011**, *115*, 10604-10614.

(216) Chen, G.; Chen, N.; Li, L.; Wang, Q.; Duan, W. Ionic liquid modified poly (vinyl alcohol) with improved thermal processability and excellent electrical conductivity. *Industrial & Engineering Chemistry Research* **2018**, *57*, 5472-5481.

(217) Chremos, A.; Douglas, J. F. The Influence of Polymer and Ion Solvation on the Conformational Properties of Flexible Polyelectrolytes. *Gels (Basel, Switzerland)* **2018**, *4*, 20.

(218) Zettl, U.; Hoffmann, S. T.; Koberling, F.; Krausch, G.; Enderlein, J. r.; Harnau, L.; Ballauff, M. Self-diffusion and cooperative diffusion in semidilute polymer

solutions as measured by fluorescence correlation spectroscopy. *Macromolecules* **2009**, *42*, 9537-9547.

(219) Phillies, G. D. Chain architecture in the hydrodynamic scaling picture for polymer dynamics. *Macromolecules* **1990**, *23*, 2742-2748.

(220) Zhou, P.; Brown, W. Static and dynamic properties of poly (ethylene oxide) in methanol. *Macromolecules* **1990**, *23*, 1131-1139.

(221) Chamignon, C.; Duret, D.; Charreyre, M. T.; Favier, A. 1H DOSY NMR Determination of the Molecular Weight and the Solution Properties of Poly (N-acryloylmorpholine) in Various Solvents. *Macromolecular Chemistry and Physics* **2016**, *217*, 2286-2293.

(222) Douglas, J. F.; Freed, K. F. Influence of draining and excluded volume on the translational diffusion coefficient of flexible polymers. *Macromolecules* **1984**, *17*, 2354-2364.

(223) Douglas, J. F.; Freed, K. F. Competition between Hydrodynamic Screening (" Draining") and Excluded Volume Interactions in an Isolated Polymer Chain. *Macromolecules* **1994**, *27*, 6088-6099.

(224) Wang, S. Q.; Douglas, J. F.; Freed, K. F. Influence of variable draining and excluded volume on hydrodynamic radius within Kirkwood–Riseman model: Dynamical renormalization group description to order ε2. *The Journal of chemical physics* **1987**, *87*, 1346-1354.

(225) Mansfield, M. L.; Douglas, J. F. Influence of variable hydrodynamic interaction strength on the transport properties of coiled polymers. *Physical Review E* **2010**, *81*, 021803.

(226) Mansfield, M. L.; Tsortos, A.; Douglas, J. F. Persistent draining crossover in DNA and other semi-flexible polymers: Evidence from hydrodynamic models and extensive measurements on DNA solutions. *The Journal of chemical physics* **2015**, *143*, 124903.

(227) Liu, R.; Gao, X.; Adams, J.; Oppermann, W. A fluorescence correlation spectroscopy study on the self-diffusion of polystyrene chains in dilute and semidilute solution. *Macromolecules* **2005**, *38*, 8845-8849.

(228) Sukhishvili, S. A.; Chen, Y.; Müller, J. D.; Gratton, E.; Schweizer, K. S.; Granick, S. Surface Diffusion of Poly(ethylene glycol). *Macromolecules* **2002**, *35*, 1776-1784.

(229) Zettl, H.; Zettl, U.; Krausch, G.; Enderlein, J.; Ballauff, M. Direct observation of single molecule mobility in semidilute polymer solutions. *Physical Review E* **2007**, *75*, 061804.

(230) Rogers, R. D.; Seddon, K. R. Ionic Liquids--Solvents of the Future? *Science* **2003**, *302*, 792-793.

(231) Andreev, M.; de Pablo, J. J.; Chremos, A.; Douglas, J. F. Influence of Ion Solvation on the Properties of Electrolyte Solutions. *The Journal of Physical Chemistry B* **2018**, *122*, 4029-4034.

(232) Paţachia, S.; Friedrich, C.; Florea, C.; Croitoru, C. Study of the PVA hydrogel behaviour in 1-butyl-3-methylimidazolium tetrafluoroborate ionic liquid. *Express Polymer Letters* **2011**, *5*.

(233) Spinks, G. M.; Lee, C. K.; Wallace, G. G.; Kim, S. I.; Kim, S. J. Swelling behavior of chitosan hydrogels in ionic liquid− water binary systems. *Langmuir* **2006**, *22*, 9375-9379.

(234) Schlenoff, J. B.; Rmaile, A. H.; Bucur, C. B. Hydration contributions to association in polyelectrolyte multilayers and complexes: Visualizing hydrophobicity. *Journal of the American Chemical Society* **2008**, *130*, 13589-13597.

(235) Wernet, P.; Nordlund, D.; Bergmann, U.; Cavalleri, M.; Odelius, M.; Ogasawara, H.; Näslund, L.-Å.; Hirsch, T.; Ojamäe, L.; Glatzel, P. The structure of the first coordination shell in liquid water. *Science* **2004**, *304*, 995-999.

(236) Sun, Q. The Raman OH stretching bands of liquid water. *Vibrational Spectroscopy* **2009**, *51*, 213-217.

(237) Fong, K. D.; Self, J.; Diederichsen, K. M.; Wood, B. M.; McCloskey, B. D.; Persson, K. A. Ion Transport and the True Transference Number in Nonaqueous Polyelectrolyte Solutions for Lithium Ion Batteries. *ACS Central Science* **2019**, *5*, 1250-1260.

(238) Ganguly, R.; Aswal, V. Improved Micellar Hydration and Gelation Characteristics of PEO− PPO− PEO Triblock Copolymer Solutions in the Presence of LiCl. *The Journal of Physical Chemistry B* **2008**, *112*, 7726-7731.

(239) Hanghofer, I.; Brinek, M.; Eisbacher, S.; Bitschnau, B.; Volck, M.; Hennige, V.; Hanzu, I.; Rettenwander, D.; Wilkening, H. Substitutional disorder: structure and ion dynamics of the argyrodites Li 6 PS 5 Cl, Li 6 PS 5 Br and Li 6 PS 5 I. *Physical Chemistry Chemical Physics* **2019**, *21*, 8489-8507.

(240) Bloembergen, N.; Purcell, E. M.; Pound, R. V. Relaxation effects in nuclear magnetic resonance absorption. *Physical review* **1948**, *73*, 679.

(241) Adebahr, J.; Forsyth, M.; Macfarlane, D. R.; Gavelin, P.; Jacobsson, P. Lithium coordination and mobility in gel electrolytes based on an acrylate polymer with ethylene oxide side chains. *Journal of Materials Chemistry* **2003**, *13*, 814-817.

(242) De Gennes, P.-G.; Gennes, P.-G.: *Scaling concepts in polymer physics*; Cornell university press, 1979.

(243) Budhlall, B.; Landfester, K.; Sudol, E.; Dimonie, V.; Klein, A.; El-Aasser, M. Characterization of partially hydrolyzed poly (vinyl alcohol). Effect of poly (vinyl alcohol) molecular architecture on aqueous phase conformation. *Macromolecules* **2003**, *36*, 9477-9484.

(244) Bercea, M.; Morariu, S.; Rusu, D. In situ gelation of aqueous solutions of entangled poly (vinyl alcohol). *Soft Matter* **2013**, *9*, 1244-1253.

(245) Flory, P.; Krigbaum, W. Statistical mechanics of dilute polymer solutions. II. *The Journal of Chemical Physics* **1950**, *18*, 1086-1094.

(246) Kirkwood, J. G.; Riseman, J. The intrinsic viscosities and diffusion constants of flexible macromolecules in solution. *The Journal of Chemical Physics* **1948**, *16*, 565-573.

(247) Dondos, A. Denaturated proteins: Draining effect and molecular dimensions. *Physica B: Condensed Matter* **2010**, *405*, 3572-3575.

(248) Dondos, A. Treating any polymer dissolved in water as polymer presenting a draining effect. *Polymer bulletin* **2011**, *67*, 333-342.

(249) Woodley, D.; Dam, C.; Lam, H.; LeCave, M.; Devanand, K.; Selser, J. Draining and long-ranged interactions in the poly (ethylene oxide)/water good solvent system. *Macromolecules* **1992**, *25*, 5283-5286.

(250) Lodge, T.; Rotstein, N.; Prager, S. Dynamics of entangled polymer liquids: Do linear chains reptate? *Advances in chemical physics* **1992**, *79*, 1-1.

(251) De Gennes, P. Dynamics of entangled polymer solutions. I. The Rouse model. *Macromolecules* **1976**, *9*, 587-593.

(252) Colby, R. H.; Rubinstein, M. Two-parameter scaling for polymers in θ solvents. *Macromolecules* **1990**, *23*, 2753-2757.

(253) Colby, R. H. Structure and linear viscoelasticity of flexible polymer solutions: comparison of polyelectrolyte and neutral polymer solutions. *Rheologica Acta* **2010**, *49*, 425-442.

(254) Hong, P.-D.; Chou, C.-M.; He, C.-H. Solvent effects on aggregation behavior of polyvinyl alcohol solutions. *Polymer* **2001**, *42*, 6105-6112.

APPENDIX A

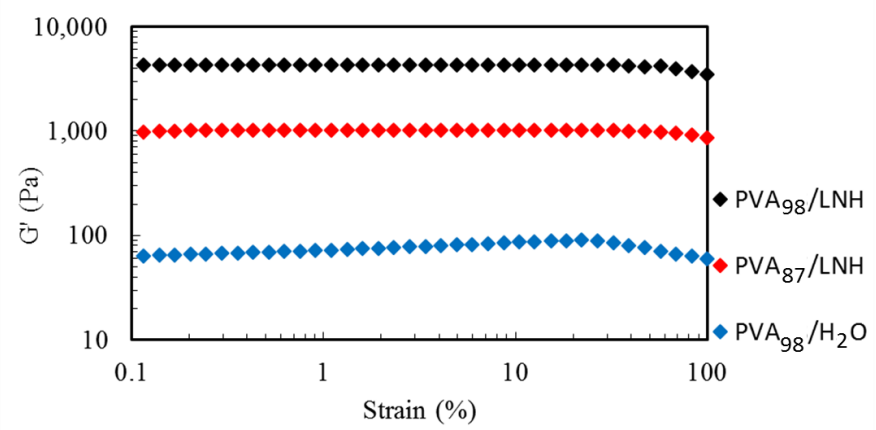

Figure A-1. Strain-dependent G' for 15 wt% PVA solutions in LNH and H_2O for 87% and 98% degrees of PVA hydrolysis. Testing was conducted at a temperature of 25°C with an angular frequency of 10 rad/s. Reprinted from [10] with permission from the Royal Society of Chemistry.

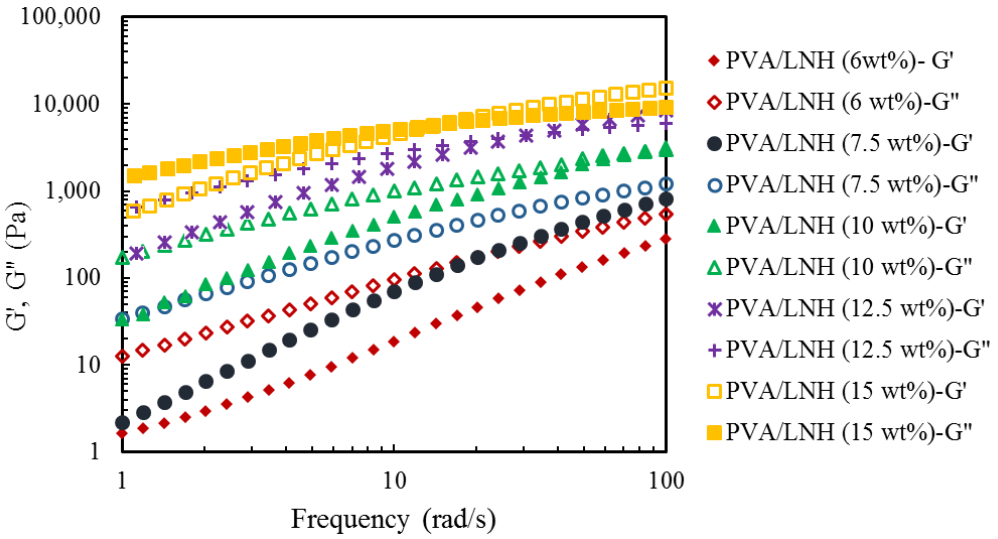

Figure A-2. Frequency dependencies of G' and G" in PVA_{98}/LNH system at different polymer concentrations. Temperature was 25°C. The measurement was performed at γ_L = 1%. Reprinted from [10] with permission from the Royal Society of Chemistry.

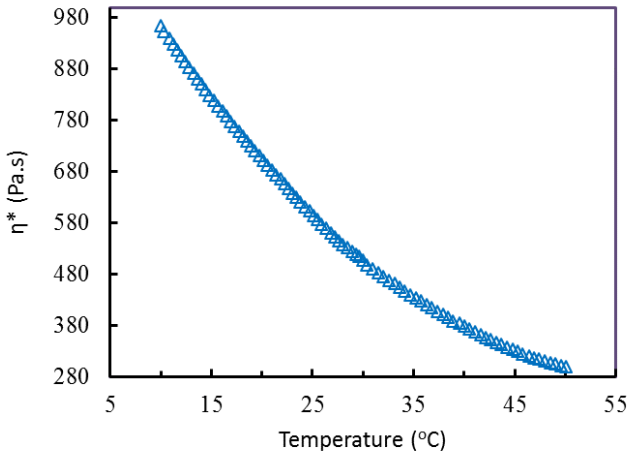

Figure A-3. Complex viscosity of PVA/LNH gels measured versus temperature during cooling. Testing was conducted at an angular frequency of 10 rad/s and γ_L = 10%. Reprinted from [10] with permission from the Royal Society of Chemistry.

APPENDIX B

Figure B-1 shows the log-log plots of specific viscosity *versus* PVA concentration measured in LNH solutions at 23 °C. For the entangled regime, a dependence of $\eta \sim c^{4.7}$ for the θ-solvent conditions was previously reported.[129,252-254]

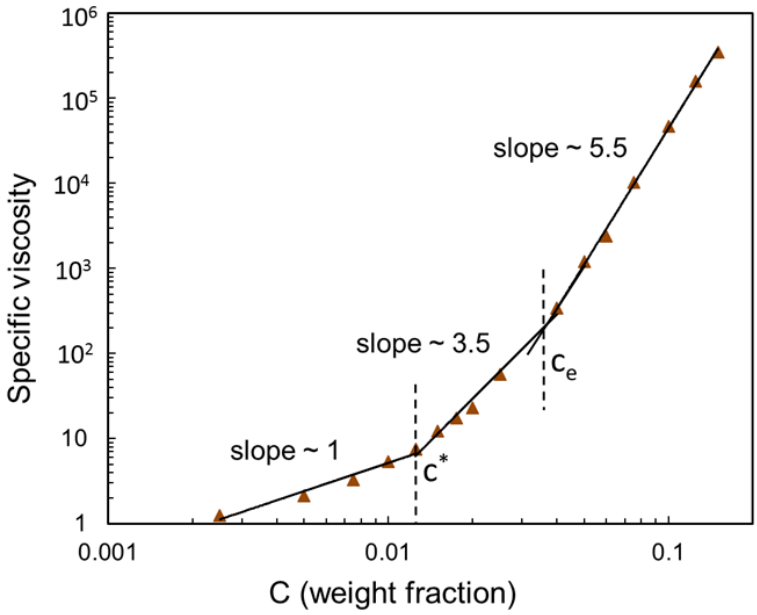

Figure B-1. Specific viscosity of PVA/LNH solutions as a function of PVA concentration. Temperature was 23 °C. Reprinted from [185] with permission from American Chemical Society.

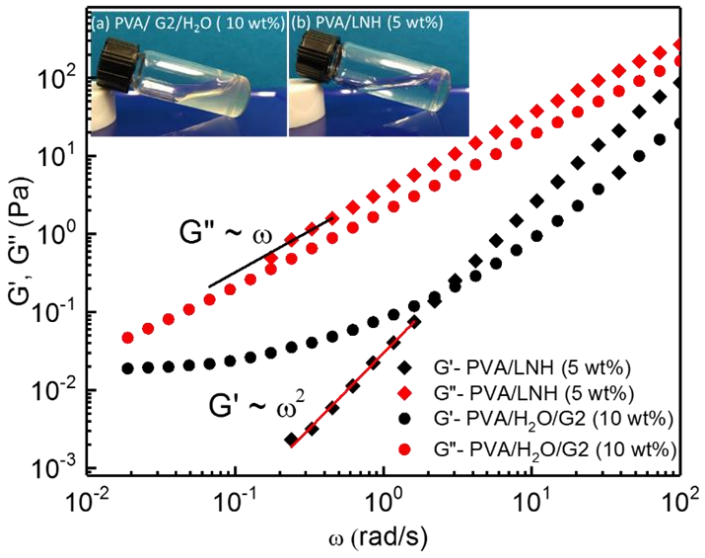

Figure B-2. Frequency dependences of *G'* and *G"* in the PVA/LNH (5 wt% polymer concentration, no crosslinker) and PVA/G2/H_2O (10 wt% polymer concentration, 2 wt% G2) systems at 25°C. Measurements were performed at a strain γ_L of 1%. Reprinted from [185] with permission from American Chemical Society.

Figure B-3a shows a set of infrared spectra of PVA/G2/D_2O/LND system at a wide range of wavenumbers. The strongest absorption peaks occurred in the following regions: (a) 2000-2800 cm^{-1} associated with *-OD* stretching vibrations; (b) 3000-3600 cm^{-1} due to the stretching vibrations of *-OH* groups of PVA; and (c) 1328 cm^{-1} due to the antisymmetric stretching vibrations of nitrate ions.[10,86,87] No vibrational features associated with G2 are seen in the spectra because of a low content (1 wt%) of the dendrimer in the system. As shown in Figure B-3a, at higher weight fractions of LND, the shape of the 2000-2800 cm^{-1} band significantly changed its shape, and the contributions of higher-energy intensities to this band increased, as shown by spectral deconvolution in Figure B-3b and c. At the

same time, the shape and position of the nitrate ion vibrational band at 1328 cm^{-1} did not change with the solvent composition (D_2O/LND ratio), suggesting negligible contribution of these ions to gelation.

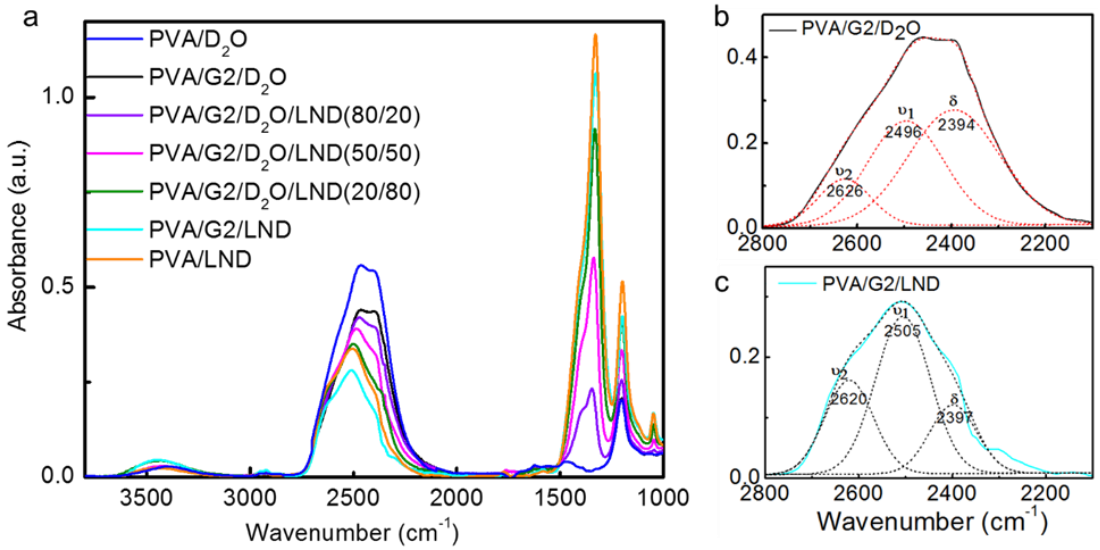

Figure B-3. (a) ATR-FTIR spectra of PVA dissolved in D_2O, LND and their mixtures with G2. (b, c) Spectral deconvolution of -*OD* stretching vibration peaks performed for PVA/G2/D_2O and PVA/G2/LND systems. Reprinted from [185] with permission from American Chemical Society.

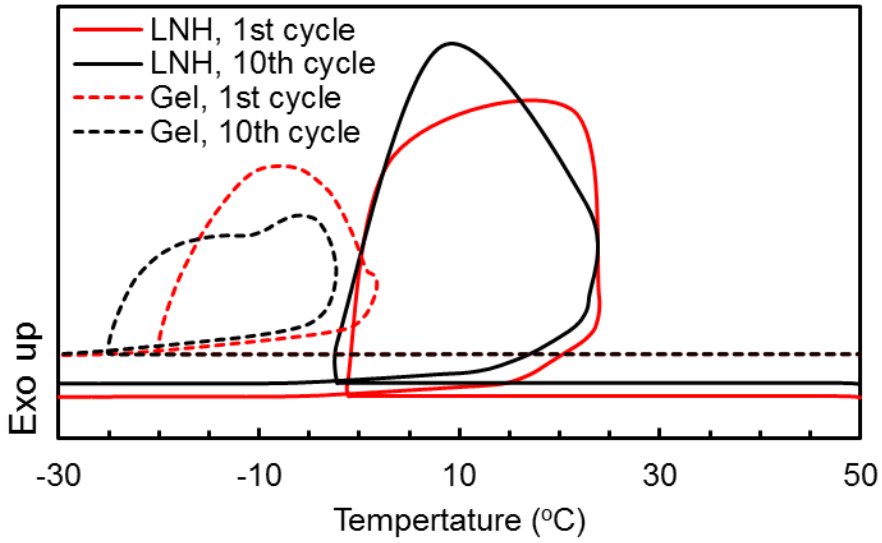

Figure B-4. DSC studies of temperature transitions in LNH and PVA/G3/LNH salogel upon cooling at a rate of 10 °C min^{-1} under a nitrogen atmosphere. Concentrations of PVA and G3 were 5 and 1 wt%, respectively. Reprinted from [185] with permission from American Chemical Society.

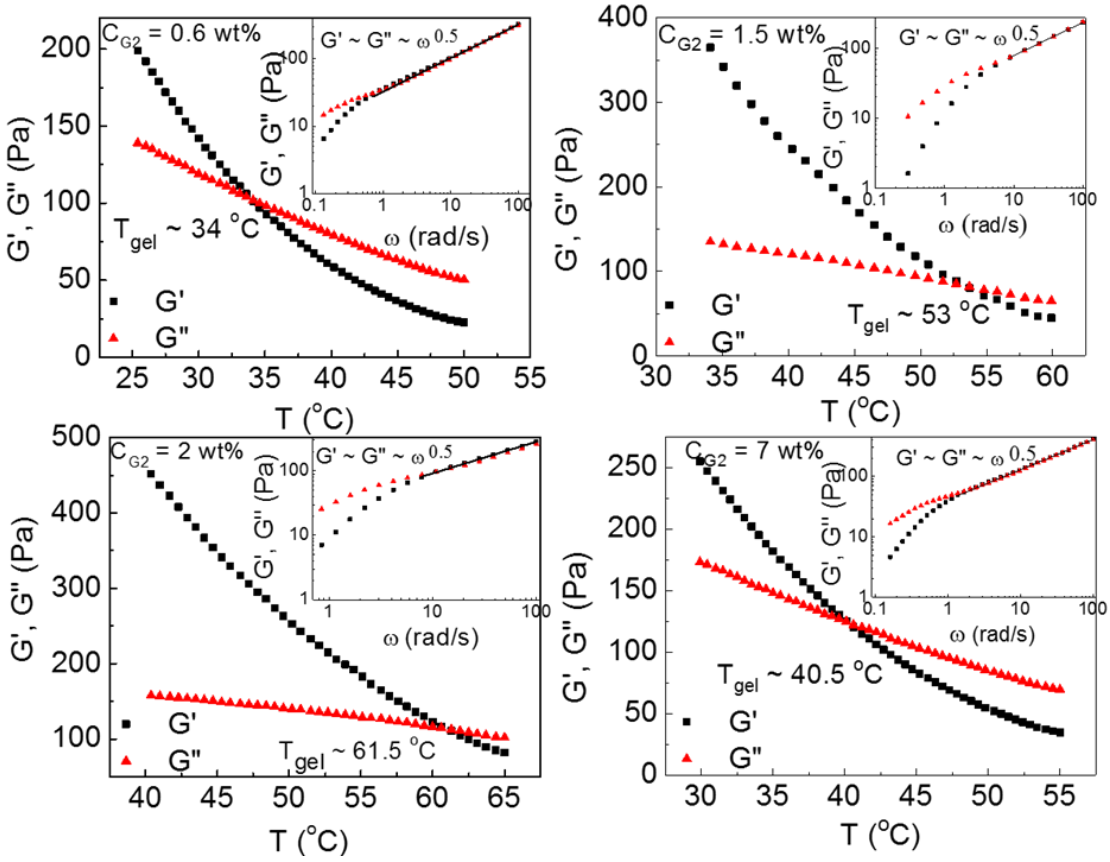

Figure B-5. Rheological measurements of the gelation temperature, T_{gel}, with PVA/G3/LNH salogels at various concentrations of G3 (0.6, 1.5, 2 and 7 wt%) conducted at a strain γ_L of 10%. Insets show the oscillation shear moduli versus frequency measured at the corresponding T_{gel} for each G3 concentration. Reprinted from [185] with permission from American Chemical Society.

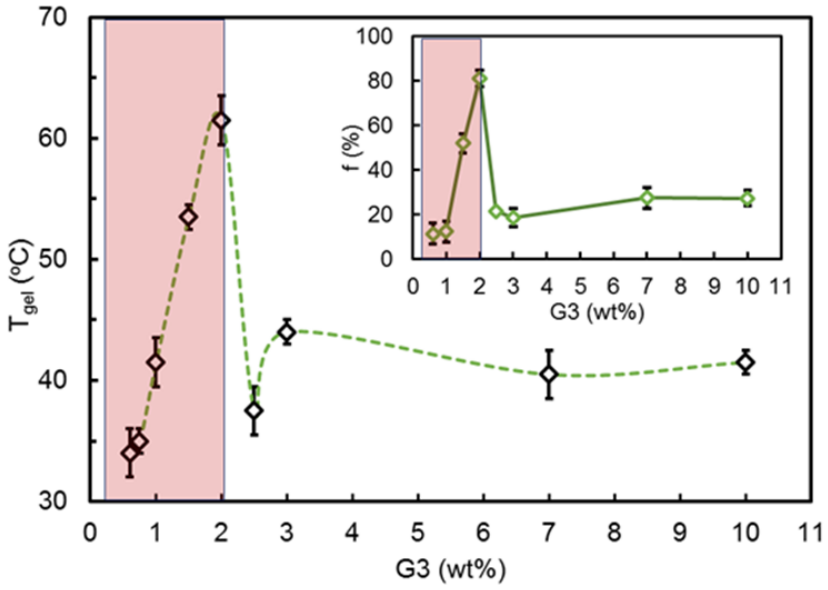

Figure B-6. The effect of dendrimer concentration on the gel-sol transition temperature (T_{gel}) for PVA/G3/LNH salogels (main panel), as well as fraction of elastically effective chains (inset) determined based on rheological measurements performed at 25 °C and a frequency of 10 rad s^{-1}. Reprinted from [185] with permission from American Chemical Society.

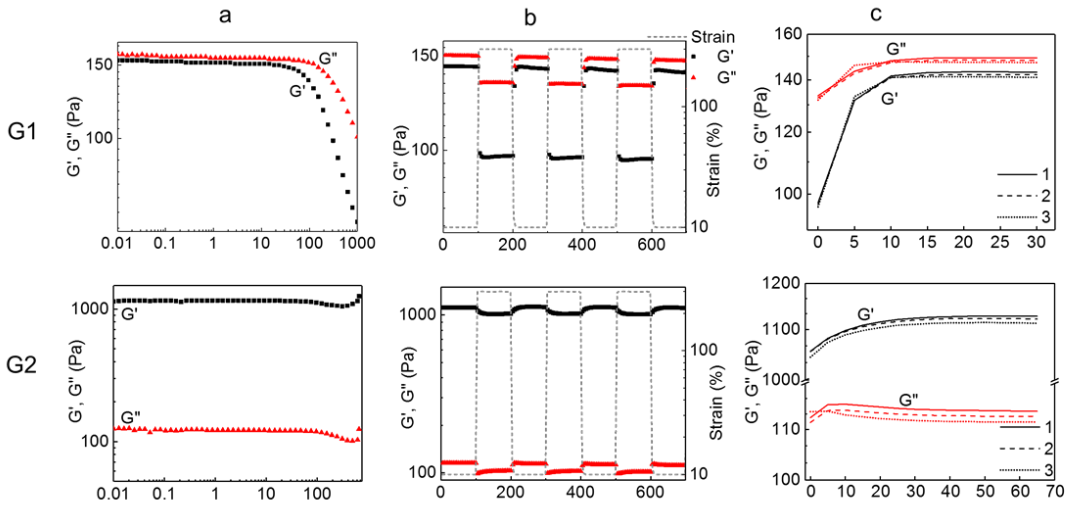

Figure B-7. Rheological experiments that demonstrate self-healing capability of PVA/GX/LNH salogels (ω =10 rad s^{-1}, 25 °C): (a, b) strain amplitude sweep and corresponding step-strain measurements performed with salogels prepared with G1, G2 (top and bottom, respectively); (c) the recovery rate of *G'* and *G''* after three repeated cycles of salogel breaking and recovery. In all experiments, the total number of $–NH_2$ groups in systems containing G1 or G2 was matched. Reprinted from [185] with permission from American Chemical Society.

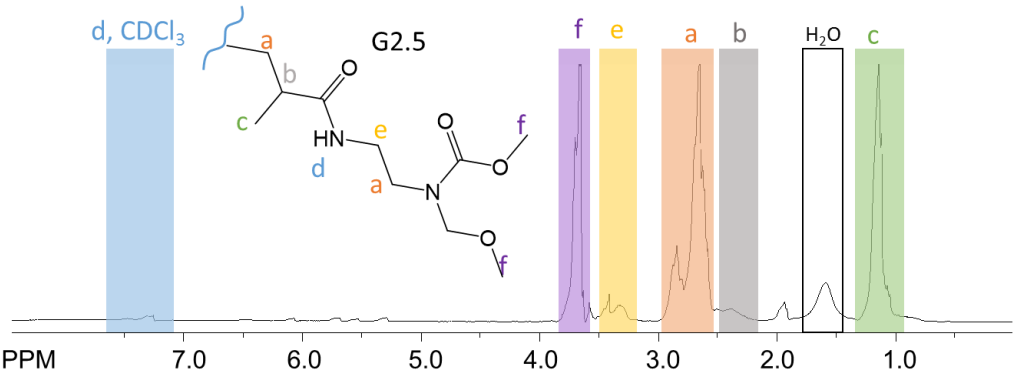

Figure B-8. ^{1}H NMR of G2.5 dendrimer in $CDCl_3$. Reprinted from [185] with permission from American Chemical Society.

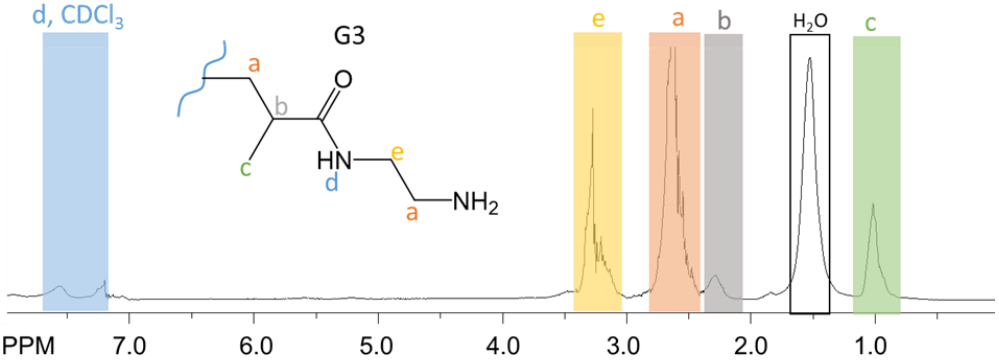

Figure B-9. ^{1}H NMR of G3 dendrimer in $CDCl_3$. Reprinted from [185] with permission from American Chemical Society.

APPENDIX C

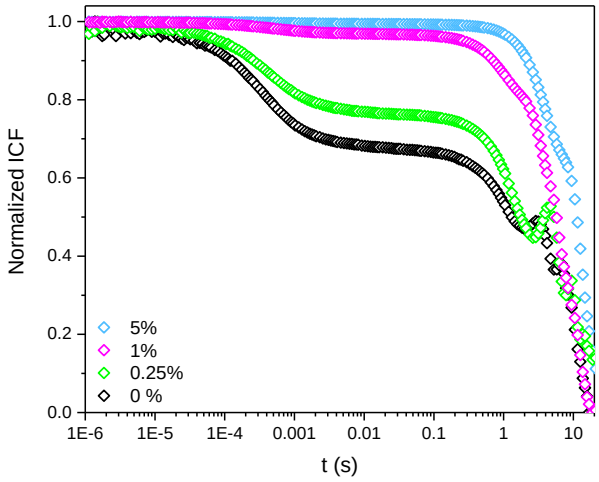

Figure C-1. DLS intensity correlation functions for DETA-based salogels with different crosslinker concentrations. Reprinted from [205] with permission from the Wiley.

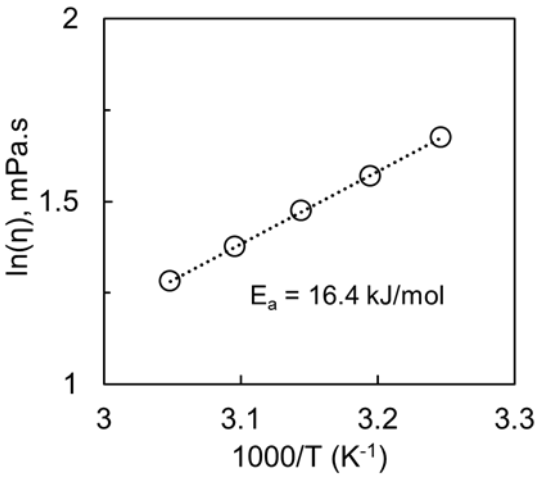

Figure C-2. Temperature dependence of LNH dynamic viscosity. Reprinted from [205] with permission from the Wiley.

APPENDIX D

GPC was performed using a TOSOH GPC system equipped with refractive index and UV detectors at ambient temperature. A TSK-GEL Super MultiporePW-M column with a particle size of 5 μm and different pore sizes was used for the characterization of 4 mg mL^{-1} polymer solutions. Water was used as an eluent for the characterization of polymers. All solutions were eluted at a rate of 0.3 mL min−1, at ambient temperature.

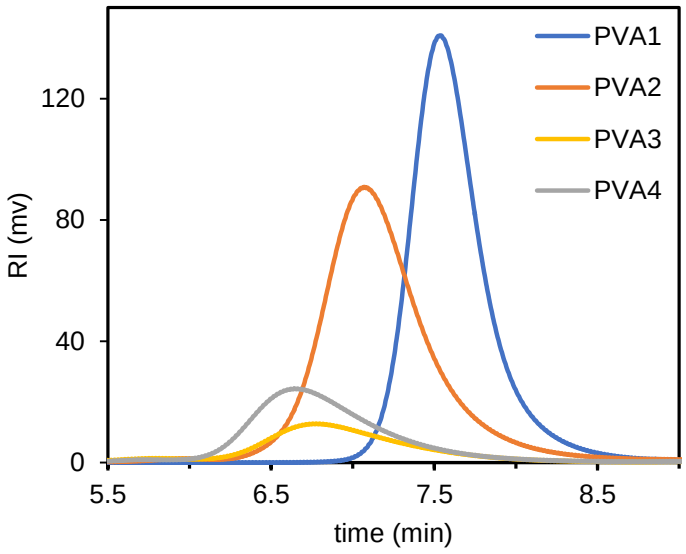

Figure D-1. GPC traces of 4 mg/ml aqueous solutions of PVA with different molecular weights.

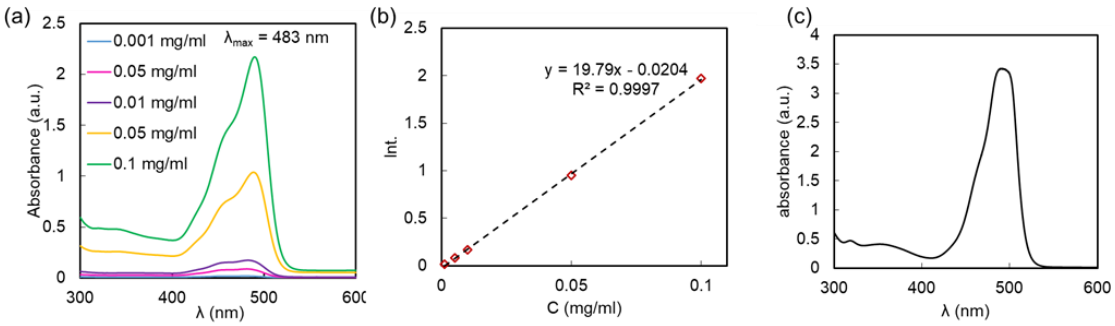

Figure D-2. UV-vis calibration curves and determination of the labeling degree of PVA* with FITC: (a) UV-vis absorbances of aqueous solutions of FITC of known concentrations (pH =11); (b) the calibration curve for determining FITC concentration and (c) a UV-vis spectrum of 1 mg/ml aqueous solution of PVA3* after extensive dialysis. Only PVA3* results are shown here as an example.

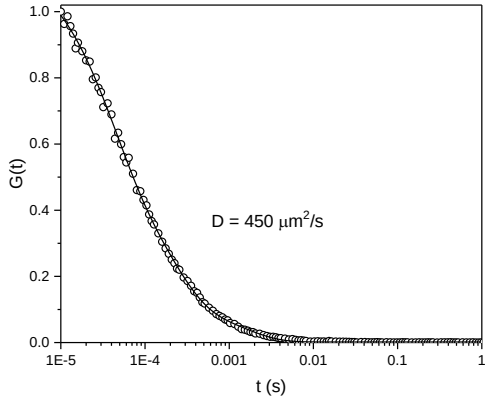

Figure D-3. FCS autocorrelation function and diffusion coefficient of FITC in aqueous solutions used for calibration of the excitation volume of the FCS setup. Temperature was 22 ^{o}C.

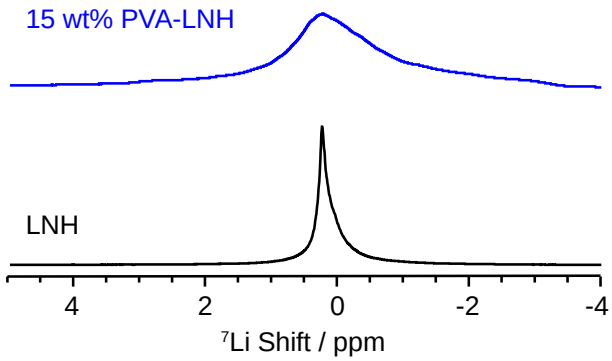

Figure D-4. ^{7}Li NMR spectra of a15 wt% solution of PVA in LNH, along with the spectra of LNH solvent.

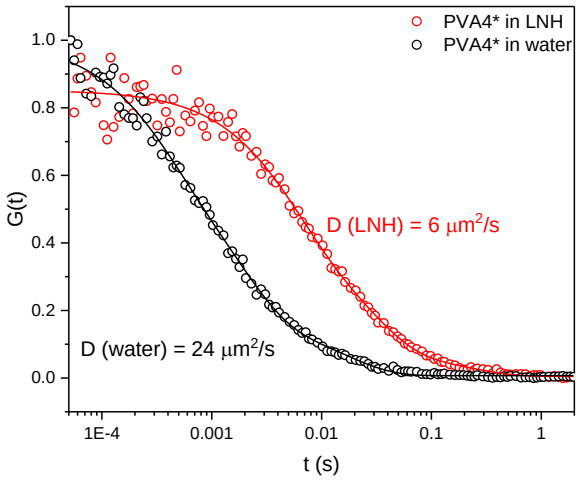

Figure D-5. FCS autocorrelation functions and diffusion coefficients of 10^{-4} mg/ml PVA4* solutions in water and LNH. Temperature was 22 ^{o}C.

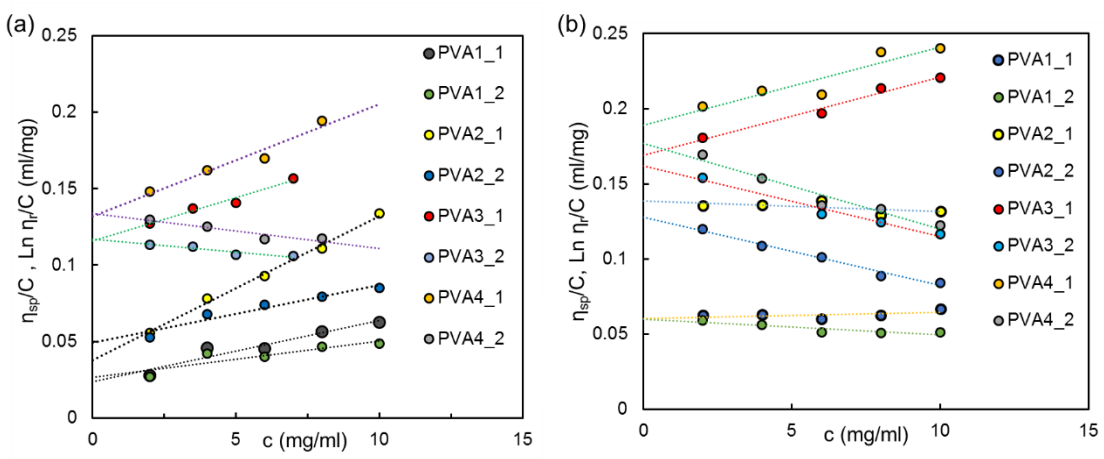

Figure D-6. Intrinsic viscosity measurements for PVA in (a) LNH, and (b) aqueous solutions at a temperature of 35 ^{o}C. “H” and “K” refer to fitting using the Huggins and Kraemer equations, respectively.